International Journal of Polymer Science

Biodegradable Polymers for Medical Applications

Guest Editors: Anezka Lengalova, Alenka Vesel, Yakai Feng, and Vitor Sencadas

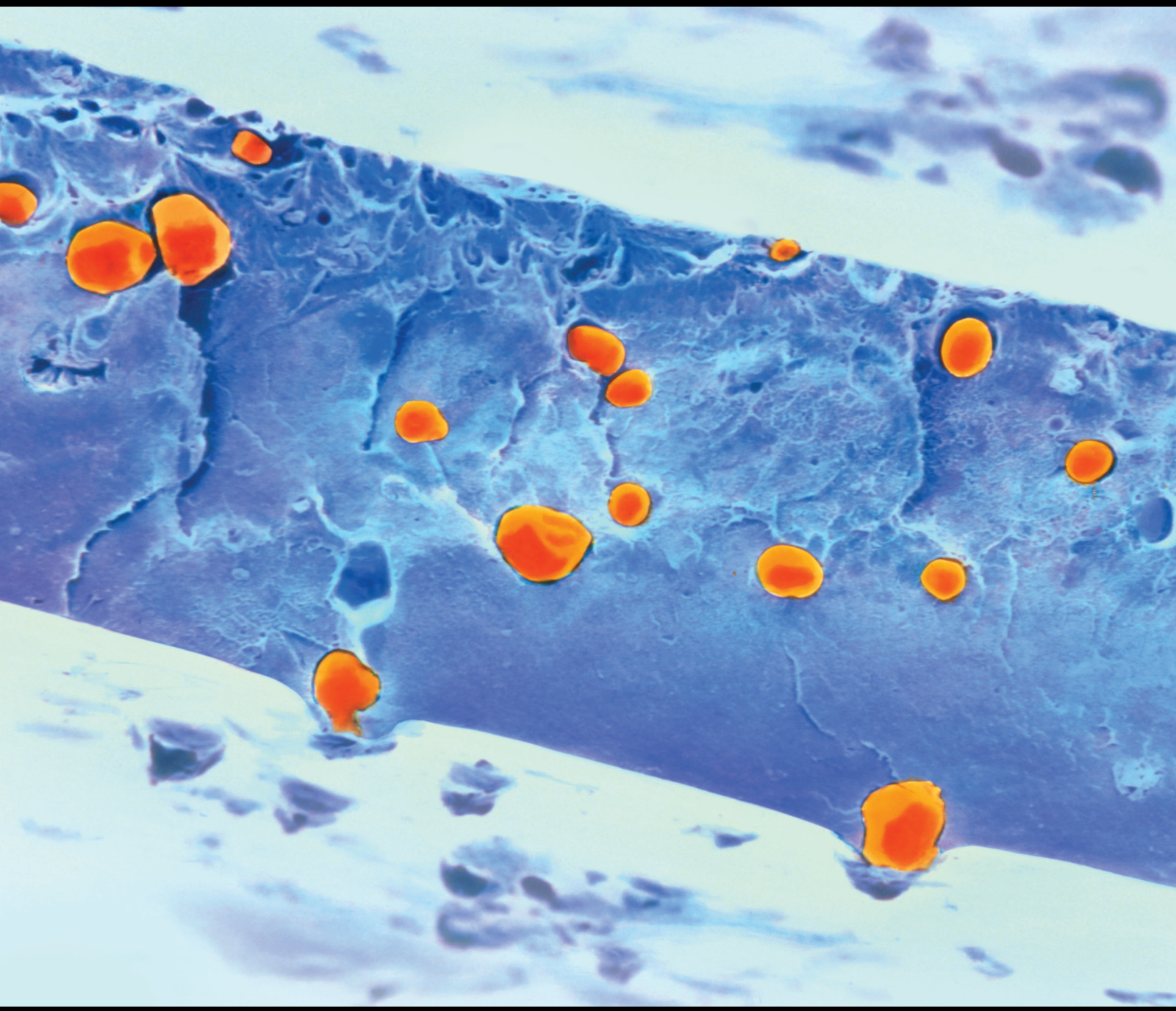

Biodegradable Polymers for Medical Applications

International Journal of Polymer Science

Biodegradable Polymers for Medical Applications

Guest Editors: Anezka Lengalova, Alenka Vesel, Yakai Feng, and Vitor Sencadas

Editorial Board

Contents

Hindawi Publishing Corporation
International Journal of Polymer Science
Volume 2016, Article ID 6047284, 2 pages
http://dx.doi.org/10.1155/2016/6047284

Editorial

Biodegradable Polymers for Medical Applications

Anezka Lengalova,[1] Alenka Vesel,[2] Yakai Feng,[3] and Vitor Sencadas[4]

[1]*Centre of Polymer Systems, Tomas Bata University in Zlín, 760 01 Zlín, Czech Republic*
[2]*Jozef Stefan Institute, SI-1000 Ljubljana, Slovenia*
[3]*School of Chemical Engineering and Technology, Tianjin University, Tianjin 300072, China*
[4]*School of Mechanical, Materials and Mechatronics Engineering, University of Wollongong, Wollongong, NSW 2522, Australia*

Correspondence should be addressed to Anezka Lengalova; lengalova@fhs.utb.cz

Received 5 April 2016; Accepted 6 April 2016

Biodegradable polymers have a long history which, however, is difficult to be traced as some of them are natural products. The concept of synthetic biodegradable polymers, the topic of this special issue, was introduced in the 1980s. Since then the field has experienced a steady and stable growth as its outcomes are potentially relevant to the majority of population. This interdisciplinary field encompasses elements of materials science, biology, chemistry, medicine, tissue engineering, and others.

The advantage of polymers in this area is that they can be tailored from the viewpoint of their chemical, physical, and surface properties, so as to enable good cell adhesion and proliferation *in vivo*, maintenance of their properties for a given time, and then degradation with no harmful effects in the body. They are suitable for a variety of applications, but their priority application is in tissue engineering and drug delivery. This reflects also in the present special issue; the articles cover various views on biodegradable polymers.

The paper "Cell Adhesion on Polycaprolactone Modified by Plasma Treatment" shows how plasma treatment of polycaprolactone fibrous membrane surface can affect adhesion and proliferation of human cells. Thus this material with improved biocompatibility can be more effectively used as scaffolds in the body.

Scaffolds are also dealt with in the paper "Designing of Collagen Based Poly(3-hydroxybutyrate-*co*-4-hydroxybutyrate) Scaffolds for Tissue Engineering." With the aim of enhancing the hydrophilicity for application of P(3HB-co-4HB) copolymer in tissue engineering, collagen was incorporated in the surface. At the optimum conditions the material showed significant cell adhesion and proliferation on the surface, so its ability to be used for biopurposes increased. Hence surface modification by blending biomacromolecules proved to enhance the biocompatibility of the original polymeric material.

Similarly to the first one, also the paper "Haemostatic Response of Polyethylene Terephthalate Treated by Oxygen and Nitrogen Plasma Afterglows" is connected with plasma treatment, in this case plasma afterglow. Afterglow was used to alter haemostatic response of PET polymer and binding of anticoagulant heparin. The study shows improved biocompatibility of plasma-treated PET with and without heparin coating in contact with fresh blood. Although it was still lower than that of the PET with covalently bonded heparin, it is another promising direction of research.

The fact that hydrogels are materials with a great potential is demonstrated in two papers. One of them, "Direct Synthesis of Hyperbranched Poly(acrylic acid-co-3-hydroxypropionate)," presents the stage of the material preparation. The produced hyperbranched PAcHP exhibits hydrogel properties and thus can be considered as a biodegradable polymer matrix for drug delivery or hydrogel scaffold for tissue engineering applications. The other paper, "Effect of Sodium Salicylate on the Viscoelastic Properties and Stability of Polyacrylate-Based Hydrogels for Medical Applications," goes a step further; it studies long term stability, an important aspect for practical medical use, of polyacrylate-based hydrogel. The presence of sodium salicylate noticeably influences hydrogel neutralization,

rheological and antimicrobial properties, and has a positive effect on aging.

The paper "Antiepileptic Effects of Lacosamide Loaded Polymers Implanted Subdurally in GAERS" concentrates on the possibility of using targeted drug delivery for the treatment of long-lasting seizure remission from epilepsy, which can be a hope for patients in future. The biodegradable polymer involved here was poly(D,L-lactide-co-glycolide) in the form of electrospun mats and it was loaded with lacosamide. This was implanted with skull electrodes to a special strain of rats. In comparison with blanks the material showed a partial sustained antiepileptic effect, which is a good start for further development of the method.

We hope that the readers of this special issue will consider it not only as a source of information, but also as an inspiration for their further research, for example, in cooperation of researchers from different institutions or even different countries.

Acknowledgments

We would like to thank all authors who sent their papers for the review in this special issue. We paid large attention to the selection, so not all of them could be published, for either the reasons of unsuitable topics, or unsatisfactory quality. However, all the effort is appreciated.

Anezka Lengalova
Alenka Vesel
Yakai Feng
Vitor Sencadas

Hindawi Publishing Corporation
International Journal of Polymer Science
Volume 2016, Article ID 7354396, 9 pages
http://dx.doi.org/10.1155/2016/7354396

Research Article

Cell Adhesion on Polycaprolactone Modified by Plasma Treatment

Nina Recek,[1] Matic Resnik,[1,2] Helena Motaln,[3] Tamara Lah-Turnšek,[3] Robin Augustine,[4,5] Nandakumar Kalarikkal,[4,6] Sabu Thomas,[4,7] and Miran Mozetič[1]

[1]*Jozef Stefan Institute, Jamova Cesta 39, 1000 Ljubljana, Slovenia*
[2]*Jozef Stefan International Postgraduate School, Jamova Cesta 39, 1000 Ljubljana, Slovenia*
[3]*National Institute of Biology, Večna Pot 111, 1000 Ljubljana, Slovenia*
[4]*International and Inter University Centre for Nanoscience and Nanotechnology, Mahatma Gandhi University, Kottayam, Kerala 686560, India*
[5]*Department of Materials Science and Engineering, Technion-Israel Institute of Technology, De-Jur Building, Technion City, 3200003 Haifa, Israel*
[6]*School of Pure and Applied Physics, Mahatma Gandhi University, Kottayam, Kerala 686560, India*
[7]*School of Chemical Sciences, Mahatma Gandhi University, Kottayam, Kerala 686560, India*

Correspondence should be addressed to Nina Recek; nina.recek@ijs.si

Received 19 October 2015; Revised 19 March 2016; Accepted 28 March 2016

Academic Editor: Anezka Lengalova

We have investigated the influence of various plasma treatments of electrospun polycaprolactone (PCL) scaffolds on the adhesion and proliferation of human umbilical endothelial cells (HUVEC). The PCL scaffolds were treated in plasmas created in O_2, NH_3 or SO_2 gas at identical conditions. Surface functionalization of plasma-treated samples was determined using X-ray photoelectron spectroscopy. Cell adhesion and morphology were investigated by scanning electron microscopy and the influence of plasma treatment on cell adhesion and viability was evaluated with cell viability assay (MTT assay). The results showed the highest metabolic activity of HUVEC on PCL samples treated with O_2 and NH_3 plasma. Accordingly, the cells reflected the best adhesion and morphology on O_2 and NH_3 plasma-treated PCL samples already at 3 h. Moreover, treatment with O_2 and NH_3 plasma even stimulated endothelial cell proliferation on PCL surfaces by 60% as measured at 24 h, showing significant improvement in endothelialization of this material. Contrarily, SO_2 plasma appeared to be less promising in comparison with O_2 and NH_3 plasma; however, it was still better than without any plasma treatment. Thus, our results importantly contribute to the biocompatibility improvement of the PCL polymer, commonly used for scaffolds in tissue engineering.

1. Introduction

Polymeric materials are nowadays frequently used in various medical applications including artificial implants, tissue engineering scaffolds, wound dressings, and drug delivery systems [1–4]. Many of such applications usually require modification of surface properties of the polymer to improve its biocompatibility, cell adhesion and proliferation, and attachment of bioactive functional groups [5–8]. Various methods like plasma treatment, grafting of polymer brushes, or applying different coatings can be used for polymer surface modification.

For the past few decades, nanofibers have gained much importance due to the potential applications in broad areas of technological applications. Many of the potential uses of nanofibrous membranes are related to high porosity, large surface area, and small pore distribution. There are many methods for the fabrication of nanofibrous membranes; however, the most successful method is the electrospinning. Electrospinning can produce continuous nanofibers from submicron diameter scale down to nanometer diameter scale through an electrically charged jet of polymer solution [9, 10].

Electrospun three-dimensional polymeric scaffolds are becoming important in tissue engineering applications,

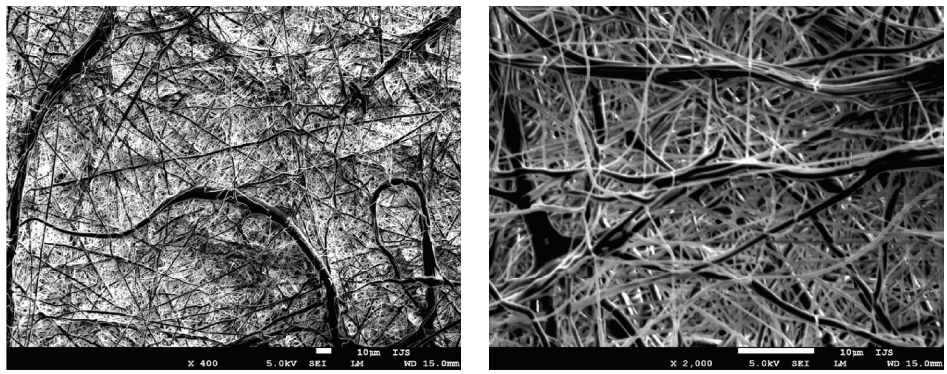

(a) (b)

Figure 1: SEM image of electrospun PCL membranes at two different magnifications: (a) 400x magnification and (b) 2,000x magnification.

especially in bone regeneration [11, 12] and skin reconstruction [13, 14]. When cells attach to the scaffold, the scaffold has to offer optimal support and conditions for cell growth that leads to the formation of a new tissue. Tissue engineering scaffolds are often made of polymers like polycaprolactone (PCL) or polylactic acid (PLA) [15, 16]. Such polymeric scaffolds are biocompatible and biodegradable, which means that it is not necessary to remove them from the human body after implantation, because *in vivo* they slowly degrade to nontoxic products [17]. However, such scaffolds require surface modification to improve cell adhesion and proliferation [18]. Plasma treatment is one of the most useful techniques, because it allows for incorporation of different functional groups on the surface of the treated polymer. By proper choice of gas it is possible to manipulate these functional groups and change their nature, this way altering their surface wettability and surface energy, which both have a drastic impact on protein and cell adhesion [19–21].

Some authors have used oxygen or air plasma for surface modification of PCL and found increased surface hydrophilicity, surface energy, surface roughness, and total amount of oxygen functional groups on PCL surface [22, 23]. They have also observed better attachment and proliferation of osteoblast cells [18, 24, 25]. Wulf et al. have used ammonia plasma and found that modified surface did not affect the mouse fibroblast cell viability [26]. Helium and argon plasma were used as well. Both plasmas led to incorporation of oxygen functional groups to PCL. In case of helium, the nitrogen functional groups were found on the surface of treated PCL as well. Unfortunately, the biological cell response to modified PCL was not tested [22].

Because different plasmas can influence cell adhesion differently and, furthermore, different cells can behave differently on the same surface [27], more systematic research of modified polymer surfaces is needed. In the present investigation we investigated the surface modifications of PCL polymer induced by oxygen (O_2), ammonia (NH_3), or sulphur dioxide (SO_2) plasma treatment. NH_3 plasma was chosen to introduce amino groups which are important in many biological processes. For SO_2 plasma there is a lack of scientific literature, although it is known that sulphate groups can play an important role in antithrombogenicity of the surface [28, 29], whereas O_2 plasma was used as a control, because it is usually very efficient for achieving good endothelialization [27]. Therefore, we have tested the effect of these modifications on cell adhesion and proliferation of human umbilical vein endothelial cells (HUVEC).

2. Material and Methods

2.1. Fabrication of Electrospun PCL Scaffolds. Electrospinning was carried out using PCL solutions with a polymer concentration of 15 wt.% which were prepared in acetone. The clear solution without any turbidity was taken in a 15 mL plastic syringe with 20-gauge blunt tip needle and electrospun at a high direct current (DC) voltage of 18 kV, a flow rate of 1 mL/h, and a tip to collector distance of 15 cm. A thin aluminum sheet with an approximate dimension of 10 cm × 7 cm was used as the collector. Upon applying a high DC voltage using a high-voltage power supply, a fluid jet was ejaculated from the tip of the needle. As the jet accelerated toward the target, the solvent evaporated and polymer nanofibers get deposited on the aluminum sheet as a fibrous membrane. All the electrospinning process was carried out at a temperature of 28°C and a relative humidity of 60%.

Scanning electron microscopic (SEM) images of the fabricated electrospun PCL membranes are shown in Figure 1.

2.2. Plasma Treatment. PCL samples were treated in a discharge tube made from Pyrex glass, 80 cm long and 4 cm in diameter. The tube was pumped with a rotary pump operating at a nominal pumping speed of 80 $m^3 h^{-1}$. A coil of 6 turns was mounted in the centre of the tube. Plasma was created by an RF generator coupled to the coil via a matching network. The generator operated at the standard frequency of 13.56 MHz and its nominal power was set to 150 W. The plasma was ignited in the capacitive mode (E-mode). Samples were treated in plasmas created in different gasses: oxygen (O_2), ammonia (NH_3), or sulphur dioxide (SO_2). The pressure was set to 50 Pa. Samples were treated in the afterglow 20 cm away from the coil. Treatment time was 10 s.

Table 1: Surface composition of plasma-treated samples.

	C	N	O	S	O/C	N/C	S/C
Untreated	77.8		22.2		0.29		
Treated in O_2	68.0		32.0		0.47		
Treated in NH_3	81.0	3.8	15.2		0.19	0.05	
Treated in SO_2	65.9	1.6	28.5	4.0	0.43		0.06

2.3. Surface Characterization. Surface functionalization of plasma-treated samples was determined by X-ray photoelectron spectroscopy (XPS). XPS characterization was performed using an XPS (TFA XPS, Physical Electronics, Munich, Germany). The samples were excited with monochromatic Al K$\alpha_{1,2}$ radiation at 1486.6 eV over an area with a diameter of 400 μm. Photoelectrons were detected with a hemispherical analyser positioned at an angle of 45° with respect to the normal of the sample surface. XPS survey spectra were measured at a pass energy of 187 eV using an energy step of 0.4 eV, whereas high-resolution spectra were measured at a pass energy of 23.5 eV using an energy step of 0.1 eV. An additional electron gun was used for surface neutralization during XPS measurements. All spectra were referenced to the main C1s peak of the carbon atoms, which was assigned a value of 284.8 eV. The measured spectra were analyzed using MultiPak v8.1c software (Ulvac-Phi Inc., Kanagawa, Japan, 2006) from Physical Electronics, which was supplied with the spectrometer.

2.4. Cell Adhesion and Morphology Studies. Human umbilical endothelial cells (HUVEC, ATTC, Manassas, VA, USA) were cultured in MEM medium (Sigma-Aldrich, USA) supplemented with 10% fetal bovine serum (FBS; Sigma-Aldrich, USA), 100 U penicillin, 1000 U streptomycin, and 2 mM L-glutamine and plated at density of 3000 cells/cm^2. For the cell adhesion and morphology investigations, the cells were seeded at a density of 2×10^4 cells in 100 μL drop of medium on the upper side of the polymers (concentration: 2.55×10^4 cells/cm^2) and left for 3 h and 24 h to attach at 37°C in a humidified atmosphere of 5% CO_2. Cells were seeded onto modified polymer in duplicate for each time and plasma treatment condition. Cells were seeded to the plasma-treated polymer samples within 30 minutes, after plasma treatment.

Cell adhesion and morphology were assessed only after 3 and 24 hours of incubation to see differences in adhesion of cells in the first few hours after incubation, because after 24 h cells normally already adapt to different surface conditions and differences are not that pronounced anymore.

Cell adhesion and morphology were investigated by scanning electron microscopy (SEM). Briefly, the polymer samples with the attached cells were fixed in 2% glutaraldehyde (Sigma-Aldrich, USA) in phosphate buffer solution for 5 minutes, followed by dehydration through an increasing gradient of ethanol and then vacuum-dried by the critical point method. Finally the samples were covered by a thin layer of gold and analyzed by SEM. For gold evaporation PECS instrument (Model 682) from Gatan GmbH (Munich, Germany) was used. SEM analyses were performed using a JEOL JSM-840 Scanning Electron Microscope (JEOL, Tokyo, Japan).

2.4.1. MTT Assay. HUVEC were seeded and cultured in the same manner as for the cell adhesion and morphology investigation by SEM. The MTT-related colorimetric assay (EZ4U; Biomedica, Austria) was used to determine cell growth and viability, according to the manufacturer's instructions. The method is based on the fact that living cells are capable of reducing less colored tetrazolium salts into intensely colored formazan derivatives. This reduction process requires functional mitochondria, which are inactivated within a few minutes after cell death. Briefly, after 3 and 24 hours of HUVEC culture on the differently modified polymer surfaces the medium was removed and the polymer samples were rinsed with phosphate buffer saline to remove for all nonattached cells. Then 200 μL of fresh Hanks' Balanced Salt Solution (HBSS) mixed with the tetrazolium agent was added to each well with the polymer sample of the 24-well plate. After 3 and 24 h of incubation, supernatants were transferred into 96-well plates and the absorbance was measured at OD 570/690 nm with Synergy™ HT Microplate Reader (Bio-Tech Instruments, Inc., USA).

2.5. Statistical Analysis. All the above experiments were performed in duplicate and independently repeated at least three times, unless otherwise stated. The results obtained are shown as the mean ± SE for duplicates of cultures. Student's t-test was used to test the effect different plasma modifications of PCL have on the adhesion and metabolic activity of HUVEC and a value of $p < 0.05$ was considered significant.

3. Results and Discussion

3.1. Surface Characterization of Plasma-Treated PCL. Surface composition of various plasma-treated samples as deduced from XPS survey spectra is shown in Table 1. Each gas used for plasma treatment of the polymer caused different modification of the surface. Oxygen plasma treatment caused oxidation of the PCL surface, where the concentration of oxygen increased from 22 atomic % to 32 atomic %. Contrarily, NH_3 plasma treatment of the PCL samples caused reduction of the amount of oxygen as oxygen concentration decreased to only 15 atomic %. This is due to dissociation of NH_3 in plasma to hydrogen atoms that react with oxygen from the polymer. NH_3 plasma treatment also caused incorporation of nearly 4 atomic % of nitrogen to the polymer surface.

Oxygen concentration on the surface of plasma-treated PCL sample also increased upon SO_2 plasma treatment.

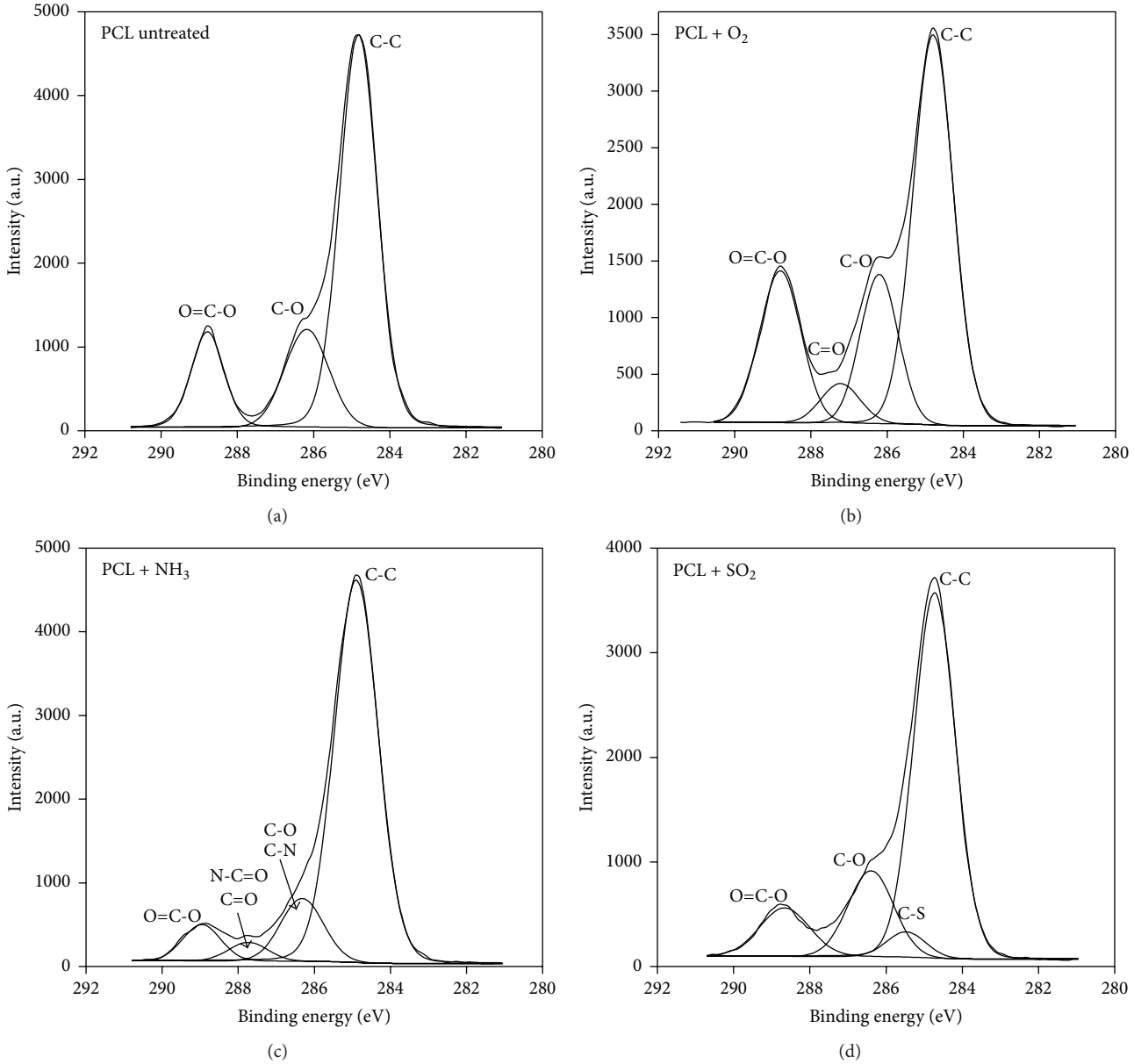

Figure 2: Carbon high-resolution peaks for various plasma-treated PCL samples.

Furthermore, 4 atomic % of sulphur was found incorporated to the PCL surface. Oxygen found on the surface of SO_2 plasma-treated PCL sample was bound to sulphur groups rather than carbon atoms as explained later in the text. Additionally, small concentrations of nitrogen were found on the surface of the SO_2 plasma-treated PCL sample. This is not unusual, because many authors have found small amounts of nitrogen on SO_2 plasma-treated surfaces and its presence was explained by traces of nitrogen in the residual atmosphere [30, 31]. Collaud Coen et al. proposed stabilization of newly formed sulfur group via a hydrogen bond with amine group which can be formed in plasma [30], whereas Holländer and Kröpke proposed reaction (deactivation) of surface radicals with NO which is also formed in the plasma [31].

To get more details regarding surface functional groups induced by various plasma-treatment procedures, we performed deconvolution of high-resolution carbon peaks (Figure 2). Concentration of different chemical groups is shown in Table 2. For untreated PCL polymer (Figure 2(a)) we can found C-C (284.8 eV) as well as C-O (286.3 eV) and O=C-O groups (288.8 eV). Concentration of these oxygen-containing functional groups has increased after O_2 plasma treatment and a new peak at 287.3 eV due to C=O groups appeared as well, whereas the C-C peak decreased (Figure 2(b)).

For the case of NH_3 plasma treatment (Figure 2(c)) the intensity of the C-C peak increased, whereas the intensity of other peaks associated with oxygen decreased, which is in correlation with quite low oxygen concentration shown in

Table 2: Concentration of different functional groups for various plasma treated samples (∗ in the case of NH_3 treatment).

	C-C	C-S	C-O C-N*	C=O O=C-N*	O=C-O
Untreated	66.7		18.8		14.5
Treated in O_2	54.3		19.2	5.3	21.2
Treated in NH_3	78.4		12.1	3.3	6.2
Treated in SO_2	67.8	4.3	17.1		10.8

Table 1. Furthermore, a new peak at 287.7 eV appeared, which is attributed to amide groups O=C-N; however C=O groups can be present as well. C-N groups appear close to C-O peak; therefore, the peak at approximately 286.3 eV was attributed to both C-O and C-N functional groups.

SO_2 plasma treatment (Figure 2(d)) gave rise to a new C-S peak at approximately 285.5 eV. Since concentration of carbon-oxygen functional groups did not change much or it even slightly decreased (Table 2), it is clear that increased oxygen concentration observed in Table 1 is due to the formation of oxygen rich sulphur groups such as C-SO_3 or C-SO_4. Namely, sulphur S2p peak appeared at approximately 168.6 eV, which is typical for highly oxidized sulphur groups [28].

Because plasma treatment and related surface modification can have significant influence on the surface wettability, we measured water contact angle on different plasma-treated PCL polymers. The contact angle of untreated sample was approximately 110°. The contact angle slightly increased in NH_3 plasma, whereas in oxygen and SO_2 plasma it decreased significantly and reached approximately 20°. This means that surface treated in oxygen and SO_2 plasma was very hydrophilic, while the one treated in NH_3 plasma was very hydrophobic.

3.2. Cell Adhesion Studies. Morphology and adhesion of HUVEC on different plasma-treated PCL polymers were investigated with SEM at two time intervals: after 3 and 24 hours (Figure 3). The SEM image after 3 hours of incubation was taken to capture the initial appearance of the cells getting adhered and adapted to the surface. Figure 3 shows that, already after 3 hours, the HUVEC were observed to best adhere to NH_3- and O_2-plasma-treated PCL samples, whereas there was nearly no difference between untreated and SO_2 plasma-treated PCL samples. Later, after 24 hours the cells already fully adhered to the surface and the substantial difference in the number of the adherent cells between the untreated sample and plasma-treated samples was observed. Again, the highest number of HUVEC was present on a PCL surface that has been treated with NH_3 and O_2 plasma, which both allowed for significant increase in cell adhesion and likely triggered different cellular signalling pathways, consequently resulting in improved metabolic activity and growth of HUVEC.

Moreover, similar morphology of the PCL samples treated with O_2 and NH_3 plasma, consisting of porous fibrous structure with very thin crisscrossed fibers, was observed by SEM. It is well known that polymer sample morphology plays a crucial role in cell-surface adhesion process [32]. Another important effect on cell adhesion has a chemical composition of the surface and surface functional groups, created by plasma treatment [33]. Based on the SEM and XPS analyses, the conditions created by O_2 and NH_3 plasma on PCL surface represent optimal condition for cell adhesion and proliferation. Cells exhibit long protrusions, for spreading all over the fibrous surface to cover the maximum surface area for sufficient attachment, which would signal them then to proceed with their proliferation to form the tissue. Thus, great adhesion was achieved after O_2 and NH_3 plasma treatment. The integrity of endothelialization depends on cell-matrix adhesion and the transmembrane proteins called integrins play a crucial role in this process [34].

On the SO_2 plasma-treated PCL samples, the surface morphology changed significantly after plasma treatment. The fibers became denser and thicker, and the surface of the PCL samples appeared less porous. This could be the potential reason for the impaired anchoring of the integrins and subsequently reduced adhesion of cells to the SO_2 treated PCL surface.

With SO_2 plasma treatment sulphur functional groups were introduced to the surface. As reported in the literature by various authors [28, 29], sulphur functional groups display antithrombogenic effect by reducing adhesion and activation of platelets. This is extremely important for the production of the prosthetic implants such as synthetic vascular grafts, which are always in direct contact with the blood. However, adhesion of cells to polymer surfaces containing sulphur functional groups does not appear promising, because the SEM images showed poor and impaired adhesion of the cells, although it appears that once the cell is attached to the surface it grows normally. This is supported by the relatively high signal of MTT assay obtained for the SO_2 plasma-treated PCL samples, as explained later in the text.

On the untreated polymer most of the HUVEC appeared shrunken and rounded, with the morphology not typical for HUVEC. Furthermore, a very few attached cells observed on the untreated PCL surface indicate adhesion problems of this surface, which per se possibly represents unfavourable environment for cells. Cells on the untreated PCL surface were not firmly attached to the surface; their morphology changed significantly because of the PLC fibres, which were twisted or captured in between them.

To get additional data on the metabolic activity of the adhered cells and their proliferation on plasma-treated PCL samples, the MTT assay was performed (Figure 4). Three hours after HUVEC seeding no difference in their metabolic

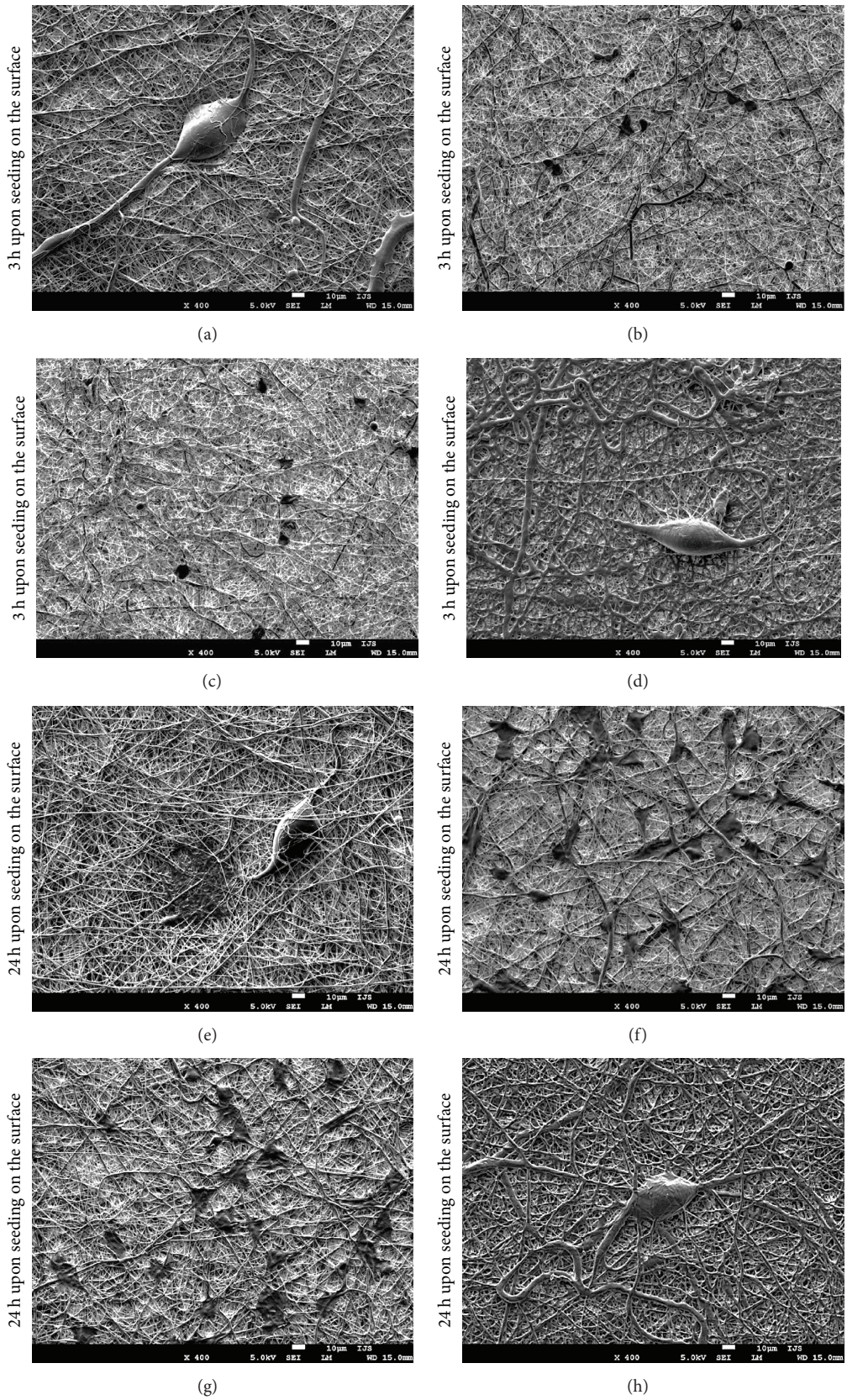

Figure 3: SEM images of plasma-treated PCL samples with adhered HUVEC 3 and 24 h upon seeding: (a, e) untreated, (b, f) treated in O_2 plasma, (c, g) treated in NH_3 plasma, and (f, h) treated in SO_2 plasma.

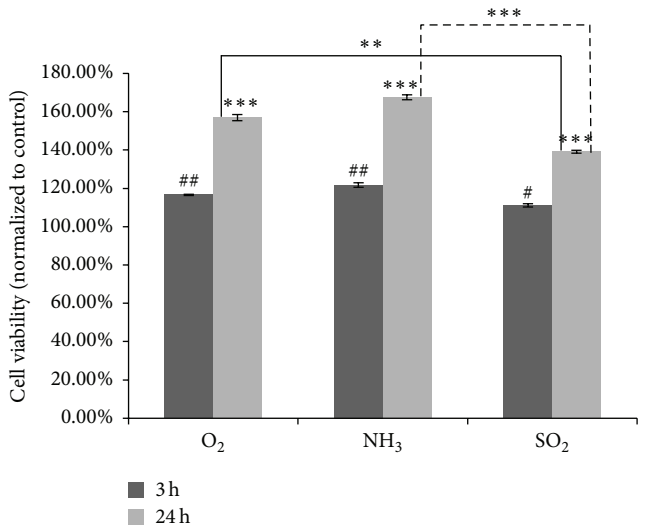

Figure 4: Effect of chemical surface composition on HUVEC proliferation. Proliferation of HUVEC on plasma untreated and treated PCL polymers determined by MTT assay. Student's t-test was used to check the statistical significance. $^{\#}$Statistically significant at $p < 0.05$ for 3 hours compared with control. $^{\#\#}$Statistically significant at $p < 0.01$ for 3 hours compared with control. **Statistically significant at $p < 0.01$ for 24 hours compared between O_2 and SO_2 plasma treated samples. ***Statistically significant at $p < 0.001$ for 24 hours compared with control and/or between NH_3 and SO_2 treated samples. Mean values (±SE) for the respective duplicates are given.

activity was observed for SO_2 plasma-treated PCL samples as compared to the untreated one. However, after 3 hours the significant increase of metabolic activity was already observed for O_2 and NH_3 plasma-treated PCL surfaces, compared to control ($p < 0.05$). After 24 hours, proliferation of HUVEC on these two surfaces increased by more than 60% in comparison to the untreated sample ($p < 0.05$). Interestingly, polymers treated with SO_2 plasma also showed 40% increase in cell viability as compared to the untreated sample, although SEM images showed poor adhesion of HUVEC to these surfaces.

Moreover, after 24 hours the significant differences in cell viability can also be observed in between different plasma-treated samples. One can observe decrease in cell viability on PCL surfaces treated with SO_2 plasma, when compared to NH_3 and O_2 plasma-treated surfaces ($p < 0.01$).

To summarize, our results clearly show that plasma treatment has an important effect on cell adhesion and viability, as well as cell morphology. NH_3 and O_2 treatment led to strong HUVEC adhesion and viability. HUVEC did also adhere to SO_2 plasma treated-surface; however, their adhesion was poorer and aggravated. Yet, once the cells managed to adhere to the surface they were capable of growing and proliferating further normally. Contrarily, untreated PCL sample represents the least suitable environment for HUVEC adhesion and growth. Enhanced cell proliferation in the case of NH_3 and O_2 plasma treatment was explained by the presence of functional groups that are beneficial for cell proliferation and by different surface morphology.

4. Conclusions

PLC polymer was treated with NH_3, O_2, and SO_2 plasma in order to change surface properties of the sample (i.e., morphology, chemistry, and roughness). We were seeking for the best modification of the PCL surface that would allow for the best cell adhesion and proliferation. Plasma treatment led to changes in surface chemical composition and morphology as well as related hydrophobicity of the polymer, reflecting different adhesion characteristics of cells to the polymer surface. According to literature, the best cell proliferation is normally observed at moderate hydrophobic polymers. Our results show that surface morphology and surface chemistry can be even more important than surface hydrophobicity, because none of our plasma-treated surfaces was moderately hydrophobic. Using various plasmas allowed for incorporation of different functionalities to the surface: various carbon-oxygen functional groups after O_2 plasma treatment, formation of nitrogen groups after NH_3 plasma treatment, and oxidized sulphur groups after SO_2 plasma treatment. MTT assay showed that modification of polymers with O_2 and NH_3 plasmas significantly increased cell adhesion and viability as compared to the untreated polymer, proving that the characteristics of NH_3 and O_2 plasma-treated surfaces are the most favourable for cell adhesion and proliferation. Interestingly, increased viability of HUVEC was also observed on SO_2 plasma-treated surfaces; however, SEM images of SO_2 plasma-treated surfaces showed unfavourable conditions for HUVEC adhesion. Lower cell adhesion can be attributed to changed fibrous morphology of the PCL samples, after treatment in SO_2 plasma. Nevertheless, once the cells managed to adhere to this surface, they were capable of growing and proliferating further normally that indicated the high signal of our MTT assay for SO_2 plasma-treated PCL surfaces.

Competing Interests

The authors declare that they have no competing interests.

Authors' Contributions

Robin Augustine fabricated electrospun PCL scaffolds, Matic Resnik carried out plasma treatment, Nina Recek carried out XPS analysis, and Nina Recek, Helena Motaln, and Tamara Lah-Turnšek evaluated the cell viability and cell proliferation after plasma modification. Robin Augustine, Miran Mozetič, Nandakumar Kalarikkal, and Sabu Thomas were involved in the discussions to outline and implement the work. Nina Recek and Miran Mozetič wrote the paper. All authors have read and made necessary modifications before submission of the paper.

Acknowledgments

This research was financially supported by the Slovenian Research Agency ARRS (Project L7-6782).

References

[1] S. D. Bruck, "Medical applications of polymeric materials," *Medical Progress through Technology*, vol. 9, no. 1, pp. 1–16, 1982.

[2] J. Jagur-Grodzinski, "Polymers for tissue engineering, medical devices, and regenerative medicine. Concise general review of recent studies," *Polymers for Advanced Technologies*, vol. 17, no. 6, pp. 395–418, 2006.

[3] R. Augustine, N. Kalarikkal, and S. Thomas, "Advancement of wound care from grafts to bioengineered smart skin substitutes," *Progress in Biomaterials*, vol. 3, no. 2, pp. 103–113, 2014.

[4] R. Augustine, E. A. Dominic, I. Reju, B. Kaimal, N. Kalarikkal, and S. Thomas, "Electrospun poly(ε-caprolactone)-based skin substitutes: in vivo evaluation of wound healing and the mechanism of cell proliferation," *Journal of Biomedical Materials Research Part B Applied Biomaterials*, vol. 103, no. 7, pp. 1445–1454, 2015.

[5] M. Modic, I. Junkar, A. Vesel, and M. Mozetic, "Aging of plasma treated surfaces and their effects on platelet adhesion and activation," *Surface and Coatings Technology*, vol. 213, pp. 98–104, 2012.

[6] J. L. García, A. Asadinezhad, J. Pacherník et al., "Cell proliferation of HaCaT keratinocytes on collagen films modified by argon plasma treatment," *Molecules*, vol. 15, no. 4, pp. 2845–2856, 2010.

[7] P. Ferreira, P. Alves, P. Coimbra, and M. H. Gil, "Improving polymeric surfaces for biomedical applications: a review," *Journal of Coatings Technology Research*, vol. 12, pp. 463–475, 2015.

[8] R. Augustine, A. Saha, V. P. Jayachandran, S. Thomas, and N. Kalarikkal, "Dose-dependent effects of gamma irradiation on the materials properties and cell proliferation of electrospun polycaprolactone tissue engineering scaffolds," *International Journal of Polymeric Materials and Polymeric Biomaterials*, vol. 64, no. 10, pp. 526–533, 2015.

[9] R. Augustine, N. Kalarikkal, and S. Thomas, "Electrospun PCL membranes incorporated with biosynthesized silver nanoparticles as antibacterial wound dressings," *Applied Nanoscience*, vol. 6, no. 3, pp. 337–344, 2016.

[10] R. Augustine, N. Kalarikkal, and S. Thomas, "Clogging free electrospinning of polycaprolactone using acetic acid/acetone mixture," *Polymer-Plastics Technology and Engineering*, vol. 55, no. 5, pp. 518–529, 2015.

[11] G. Tetteh, A. S. Khan, R. M. Delaine-Smith, G. C. Reilly, and I. U. Rehman, "Electrospun polyurethane/hydroxyapatite bioactive Scaffolds for bone tissue engineering: the role of solvent and hydroxyapatite particles," *Journal of the Mechanical Behavior of Biomedical Materials*, vol. 39, pp. 95–110, 2014.

[12] I. K. Shim, M. R. Jung, K. H. Kim et al., "Novel three-dimensional scaffolds of poly(L -lactic acid) microfibers using electrospinning and mechanical expansion: fabrication and bone regeneration," *Journal of Biomedical Materials Research—Part B: Applied Biomaterials*, vol. 95, no. 1, pp. 150–160, 2010.

[13] R. Augustine, E. A. Dominic, I. Reju, B. Kaimal, N. Kalarikkal, and S. Thomas, "Electrospun polycaprolactone membranes incorporated with ZnO nanoparticles as skin substitutes with enhanced fibroblast proliferation and wound healing," *RSC Advances*, vol. 4, no. 47, pp. 24777–24785, 2014.

[14] R. Augustine, N. Kalarikkal, and S. Thomas, "An in vitro method for the determination of microbial barrier property (MBP) of porous polymeric membranes for skin substitute and wound dressing applications," *Tissue Engineering and Regenerative Medicine*, vol. 12, no. 1, pp. 12–19, 2015.

[15] R. Morent, N. De Geyter, T. Desmet, P. Dubruel, and C. Leys, "Plasma surface modification of biodegradable polymers: a review," *Plasma Processes and Polymers*, vol. 8, no. 3, pp. 171–190, 2011.

[16] K. Hamad, M. Kaseem, H. W. Yang, F. Deri, and Y. G. Ko, "Properties and medical applications of polylactic acid: a review," *Express Polymer Letters*, vol. 9, no. 5, pp. 435–455, 2015.

[17] R. Augustine, N. Kalarikkal, and S. Thomas, "Effect of zinc oxide nanoparticles on the in vitro degradation of electrospun polycaprolactone membranes in simulated body fluid," *International Journal of Polymeric Materials and Polymeric Biomaterials*, vol. 65, no. 1, pp. 28–37, 2016.

[18] E. D. Yildirim, H. Ayan, V. N. Vasilets, A. Fridman, S. Guceri, and W. Sun, "Effect of dielectric barrier discharge plasma on the attachment and proliferation of osteoblasts cultured over poly(ε-caprolactone) scaffolds," *Plasma Processes and Polymers*, vol. 5, no. 1, pp. 58–66, 2008.

[19] N. Recek and A. Vesel, "Surface modification of polymer polyethylene terephthalate with plasmas created in different gases," *Materiali in Tehnologije*, vol. 48, no. 6, pp. 893–897, 2014.

[20] M. Jaganjac, A. Vesel, L. Milkovic et al., "Oxygen-rich coating promotes binding of proteins and endothelialization of polyethylene terephthalate polymers," *Journal of Biomedical Materials Research—Part A*, vol. 102, no. 7, pp. 2305–2314, 2014.

[21] N. Recek, M. Jaganjac, M. Kolar et al., "Protein adsorption on various plasma-treated polyethylene terephthalate substrates," *Molecules*, vol. 18, no. 10, pp. 12441–12463, 2013.

[22] T. Jacobs, N. De Geyter, R. Morent, T. Desmet, P. Dubruel, and C. Leys, "Plasma treatment of polycaprolactone at medium pressure," *Surface & Coatings Technology*, vol. 205, no. 2, pp. S543–S547, 2011.

[23] N. De Geyter, A. Sarani, T. Jacobs, A. Y. Nikiforov, T. Desmet, and P. Dubruel, "Surface modification of poly-ε-caprolactone with an atmospheric pressure plasma jet," *Plasma Chemistry and Plasma Processing*, vol. 33, no. 1, pp. 165–175, 2013.

[24] E. D. Yildirim, D. Pappas, S. Güçeri, and W. Sun, "Enhanced cellular functions on polycaprolactone tissue scaffolds by O_2 plasma surface modification," *Plasma Processes and Polymers*, vol. 8, no. 3, pp. 256–267, 2011.

[25] S. Siri, P. Wadbua, V. Amornkitbamrung, N. Kampa, and S. Maensiri, "Surface modification of electrospun PCL scaffolds by plasma treatment and addition of adhesive protein to promote fibroblast cell adhesion," *Materials Science and Technology*, vol. 26, no. 11, pp. 1292–1297, 2010.

[26] K. Wulf, M. Teske, M. Löbler, F. Luderer, K.-P. Schmitz, and K. Sternberg, "Surface functionalization of poly(ε-caprolactone) improves its biocompatibility as scaffold material for bioartificial vessel prostheses," *Journal of Biomedical Materials Research Part B Applied Biomaterials*, vol. 98, no. 1, pp. 89–100, 2011.

[27] T. Jacobs, R. Morent, N. De Geyter, P. Dubruel, and C. Leys, "Plasma surface modification of biomedical polymers: influence on cell-material interaction," *Plasma Chemistry and Plasma Processing*, vol. 32, no. 5, pp. 1039–1073, 2012.

[28] K. S. Siow, L. Britcher, S. Kumar, and H. J. Griesser, "Plasma methods for the generation of chemically reactive surfaces for biomolecule immobilization and cell colonization—a review," *Plasma Processes and Polymers*, vol. 3, no. 6-7, pp. 392–418, 2006.

[29] K. S. Siow, L. Britcher, S. Kumar, and H. J. Griesser, "Sulfonated surfaces by sulfur dioxide plasma surface treatment of plasma polymer films," *Plasma Processes and Polymers*, vol. 6, no. 9, pp. 583–592, 2009.

[30] M. Collaud Coen, B. Keller, P. Groening, and L. Schlapbach, "Functionalization of graphite, glassy carbon, and polymer surfaces with highly oxidized sulfur species by plasma treatments," *Journal of Applied Physics*, vol. 92, no. 9, pp. 5077–5083, 2002.

[31] A. Holländer and S. Kröpke, "Polymer surface treatment with SO_2-containing plasmas," *Plasma Processes and Polymers*, vol. 7, no. 5, pp. 390–402, 2010.

[32] H. Cui and P. J. Sinko, "The role of crystallinity on differential attachment/proliferation of osteoblasts and fibroblasts on poly (caprolactone-co-glycolide) polymeric surfaces," *Frontiers of Materials Science*, vol. 6, no. 1, pp. 47–59, 2012.

[33] I. Junkar, U. Cvelbar, A. Vesel, N. Hauptman, and M. Mozetič, "The role of crystallinity on polymer interaction with oxygen plasma," *Plasma Processes and Polymers*, vol. 6, no. 10, pp. 667–675, 2009.

[34] H. Song, M.-J. Cha, B.-W. Song et al., "Reactive oxygen species inhibit adhesion of mesenchymal stem cells implanted into ischemic myocardium via interference of focal adhesion complex," *Stem Cells*, vol. 28, no. 3, pp. 555–563, 2010.

Hindawi Publishing Corporation
International Journal of Polymer Science
Volume 2016, Article ID 5614687, 6 pages
http://dx.doi.org/10.1155/2016/5614687

Research Article

Effect of Sodium Salicylate on the Viscoelastic Properties and Stability of Polyacrylate-Based Hydrogels for Medical Applications

Zuzana Kolarova Raskova, Martina Hrabalikova, and Vladimir Sedlarik

Centre of Polymer Systems, University Institute, Tomas Bata University in Zlin, Trida T. Bati 5678, 76001 Zlín, Czech Republic

Correspondence should be addressed to Vladimir Sedlarik; sedlarik@ft.utb.cz

Received 13 December 2015; Revised 19 January 2016; Accepted 31 January 2016

Academic Editor: Yakai Feng

Investigation was made into the effect exerted by the presence of sodium salicylate (0–2 wt.%), in Carbomer-based hydrogel systems, on processing conditions, rheological and antimicrobial properties in tests against Gram-positive (*Staphylococcus aureus*) and Gram-negative (*Escherichia coli*) bacterial strains, and examples of yeast (*Candida albicans*) and mould (*Aspergillus niger*). In addition, the work presents an examination of long-term stability by means of aging over one year the given hydrogels at 8°C and 25°C. The results show that 0.5 wt.% NaSal demonstrated a noticeable effect on the hydrogel neutralization process, viscosity, and antimicrobial properties against all of the tested microorganisms. The long-term stability studies revealed that hydrogels can maintain antimicrobial activity as well as viscosity to a degree that would be sufficient for practical use.

1. Introduction

Hydrogels are in use in various applications, including foodstuffs, pharmaceuticals, cosmetics, and medicine, due to the convenient physical properties they boast, their compatibility with a wide range of active ingredients, and the nontoxicity and biocompatibility they demonstrate [1]. The biodegradability and/or bioresorbability of certain developed hydrogels represent favourable characteristics for tissue engineering applications [2]. Indeed, some of the hydrogel systems exhibit an effective response to external physical (temperature) or chemical (pH, ionic strength) factors, in terms of rapid change in volume (swelling or shrinking) which is important for controlled delivery of an active substance or for biosensors construction [3].

Crosslinked polymers and copolymers of acrylic acid are compounds frequently utilized in the preparation of hydrogels, and they have been the object of both scientific and commercial interest. Such materials are known as Carbomers, which have proven applicable as additives (thickeners) or bases for incorporating cosmetically or medically active substances [4, 5].

A promising use of Carbomer is in dermatology as a hydrating agent for photorejuvenation therapy, involving intense pulsed light or laser treatments [6]. Carbomer hydrogels are applied prior to the laser treatment itself in order to hasten the passage of light. The expectation is for a synergetic effect to occur through combining the hydrogel, active substances, and therapeutic laser [7].

The active substances applicable in the hydrogels, for instance, pertain to antioxidants, aromatics, or antimicrobial agents that can, however, exert significant influence on the rheological properties, stability, and therapeutic effect of the hydrogel system [5, 8].

Sodium salt of salicylic acid (NaSal) is an interesting bioactive substance that has been primarily used as a preserving agent. Additionally, its anti-inflammatory properties lend it perspective with regard to therapeutic effects. Furthermore, salicylates have been studied as components for skin care creams and in dermatology as a keratolytic and antifungal agent; hence relevant safety data are already available for potential producers [9, 10]. Indeed, the connection of the Carbomer and NaSal has therapeutic potential.

Nevertheless, it is known that monovalent ions, including Na^{+1}, crucially affect the stability of hydrogel systems [11]. While low NaSal content fails to trigger the necessary preservation effect, high concentration can cause hydrogel systems to collapse. Despite this, the effect of NaSal concentration in Carbomer-based hydrogel on its processability, antimicrobial activity, and stability has yet to be studied in detail, and no concentration limits have been optimized.

The work presented herein describes the effect of NaSal at concentration (0–2 wt.%) on the rheological and antimicrobial properties of Carbomer-based hydrogel systems. In addition, elaboration of a long-term stability (1 year) assessment is given. The characteristics studied were observed on a rotary rheometer. The antimicrobial activities of the hydrogels were determined by the agar diffusion technique against Gram-positive and Gram-negative bacterial strains, as well as examples of a yeast and mould.

2. Experimental Section

2.1. Materials. Carbomer (Carbopol® 940 Polymer) was the product of Lubrizol Advanced Materials, Inc. (Cleveland, USA). Glycerol, sodium hydroxide (NaOH), and sodium salicylate (NaSal) (all analytical grade) were purchased from Penta (Prague, Czech Republic). Triethanolamine (TEA) (analytical grade) was supplied by P-Lab (Prague, Czech Republic).

The microbial cultures *Escherichia coli* (CCM 4517), *Staphylococcus aureus* (CCM 4516), *Candida albicans* (CCM 8355), *Aspergillus niger* (CCM 8222), and *Pseudomonas aeruginosa* (CCM 478) were obtained from the Czech Collection of Microorganisms, Masaryk University (Brno, Czech Republic).

2.2. Methods

2.2.1. Hydrogel Preparation. Carbomer resin (powder, 0.8 wt.%) was dispersed in deionized water (23°C) and an appropriate amount of NaSal was added subsequently; the composition of said samples is shown in Table 1. Following this, the dispersion of Carbomer and NaSal was maintained to enable swelling at the temperature of 8°C for various time periods—from 3 to 120 hours. The mixture was neutralized with 10 wt.% NaOH aqueous solution under gentle stirring at 23°C. Optimal swelling time and supplementation with NaOH were investigated (see later in the text). Finally, the hydrogels were left to stabilize for 24 hours at 23°C. The samples were stored in the dark at 8°C. All the samples were conditioned for 6 hours at 23°C prior to further analyses.

2.2.2. Rheological Measurements. The viscoelastic properties of the hydrogel samples were investigated on a rotational viscometer (ARES 2000, Rheometrics Scientific, USA) equipped with the *RSI Orchestrator* software package. A 25 mm diameter parallel plate, which measured geometry with a gap of approximately 2 mm under slight strain (1%), was used to maintain measurements within the linear viscoelastic region. The samples were spread on the lower plate and upper one was moved down to make a required gap. Generally, at least 10 min waiting time to allow the hydrogel to reach the equilibrium temperature with the measuring system was kept before each measurement. Dynamic frequency sweep tests were carried out at the temperature of 29°C to determine storage (G') and loss (G'') moduli as a function of frequency, ω, from 0.1 to 100 rad·s^{-1} in dynamic frequency mode (angular frequency ω ranging from 0.1 to 100 rad·s^{-1}). Viscoelastic properties were also described by the complex viscosity (η^*) parameter calculated according to the following equation:

$$\eta^* = \sqrt{\left(\frac{G'}{\omega}\right)^2 + \left(\frac{G''}{\omega}\right)^2}. \quad (1)$$

Dynamic yield stress (τ_0) values were determined by extrapolating flow curves to zero shear rate and from the complex shear modulus, respectively, [12, 13].

A relative gel strength was defined as a function of G' value (at 0.4 rad·s^{-1}) and NaSal concentration [14].

Table 1: Compositions of the investigated hydrogel systems.

Sample designation	Carbomer (wt.%)	NaSal* (wt.%)
G1	0.8	0
G2		0.3
G3		0.5
G4		1
G5		1.5
G6		2

∗ related to 100 g of Carbomer (0.8 wt.%) and water mixture.

2.2.3. Stability Study. Investigation was made into the effect of NaSal concentration on gel stability in addition to antimicrobial properties. The aforementioned long-term stability tests were carried out in real time during product storage under recommended conditions (8°C and/or 25°C, in a dark place). The samples were kept at room temperature for 6 hours prior to taking measurements in order to maintain identical conditions during tests for viscosity and pH.

The viscosities of the samples in the stability study were measured on a Viscotester 6+ Haake device (Thermoelectron GmbH, Germany). The viscosity of the samples was measured in the glass beaker with diameter and height of 5 and 9 cm, respectively. A spindle type R6 (20 rpm) was used for the measurement in all cases. The pH measurements were gauged on a GPH014GL pH meter (Greisinger Electronic GmbH, Germany).

2.2.4. Antibacterial Properties and Microbial Stability Assay. Antibacterial properties pertaining to NaSal content were determined by an agar diffusion test [15]. Mueller Hinton Agar (MHA) was used in plates of 90 mm diameter and 4 mm depth. The following organisms were tested: *Escherichia coli* CCM 4517 at the concentration 10^7–10^8 CFU/mL, *Staphylococcus aureus* CCM 4516 (10^7–10^8 CFU/mL), *Candida albicans* CCM 8355 (10^6–10^7 CFU/mL), and *Aspergillus niger* CCM 8222 (10^6–10^7 CFU/mL). The bacterial suspension was

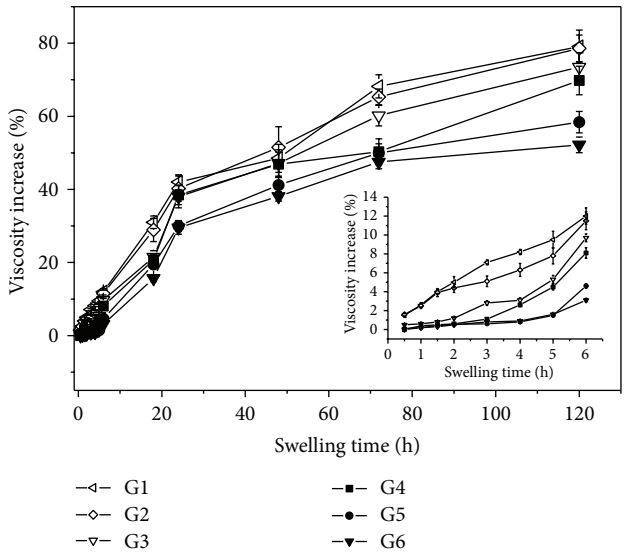

Figure 1: Swelling course of the hydrogels. The inserted figure shows the initial part of the swelling process.

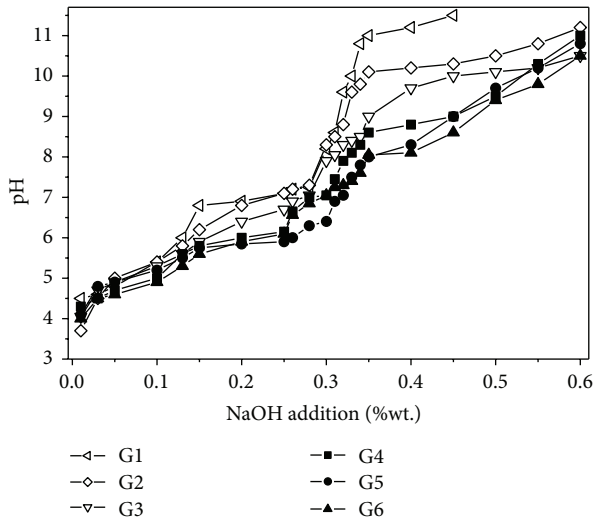

Figure 2: The pH of the hydrogels versus concentration of the neutralizer NaOH.

inoculated on the entire surface of MHA with a sterile cotton-tipped swab to enable it to form. Two holes of 8 mm diameter were made into each plate and these were filled with gel containing an active agent. Incubation time was 18–24 hours, while incubation temperature equalled 35°C for *S. aureus* and 37°C for *E. coli*. The representatives of yeast (*C. albicans*) and fungus (*A. niger*) were incubated at 25°C for 75 hours.

3. Results and Discussion

The swelling behaviour of the investigated compositions (G1–G6, see Table 1) expressed as the dependence of relative increase in hydrogel viscosity on duration of swelling is depicted in Figure 1. Said Figure 1 shows the initial swelling period (1–6 hours). The increase in viscosity is represented by the fraction for viscosity of hydrogel at a given time (η_t) over initial viscosity (η_0), according to

$$\text{viscosity increase}\,(\%) = \frac{\eta_t}{\eta_0} \times 100. \quad (2)$$

It is noticeable that interaction between water molecules and polymer chains is significantly reduced during the initial stage of the swelling process. In particular, compositions supplemented with NaSal at content above 1% (G4–G6) demonstrate no increase in viscosity after the first 3 hours. Generally, the assumption is that the higher the content of NaSal, the lesser the extent of swelling. Sodium and other multivalent salts are known to exert a negative effect on the viscosity and stability of Carbomer-based hydrogels. Thus, the viscosity of the hydrogel samples is limited by the presence of NaSal. Viscosity values continue to rise even after 120 hours; however, optimal processing parameters could be defined at 48 hours due to technological reasons. Herein, the swelling time of 48 hours was selected as the reference time for all samples presented further.

The stability of a Carbomer-based hydrogel is also strongly dependent on pH, which is usually adjusted by NaOH to the figure for pH in the range 7–8.5 that provides the most stabile hydrogel structure [11, 12]. This pH value makes it suitable for dermatological applications. A dependence of pH on supplementation with NaOH (expressed as the content of NaOH related to 100 g of hydrogel compositions G1–G6) is presented in Figure 2. Initially, adding the neutralizer (NaOH) triggered a slight increase in pH followed by a steep rise in pH, in the range 0.25–0.35 wt.%. The behaviour of the samples at higher contents of the neutralizer (0.36–0.6 wt.%) can be split into two groups. While the pH for compositions with NaSal concentrations at 0, 0.3, and 0.5 wt.% (G1, G2, and G3) did not change much, compositions with NaSal content at 1, 1.5, and 2 wt.% were characterized by intense rise in pH values. In parallel with the swelling experiment (Figure 1), Figure 2 clearly displays the effect of increasing NaSal concentration. Samples containing NaSal possess lower pH at the same level of addition of neutralizer in comparison with the composition without NaSal (G1).

The pH of hydrogels, influenced by adding the neutralizer, is linked with viscosity, as presented in Figure 3. The results clearly demonstrate the noticeable effect of NaSal on reducing the viscosity of the resultant hydrogel system. Furthermore, pH adjustment does not exert a positive influence on increase in viscosity, as is usual for NaSal-free composition (G1).

The thickening mechanism of the neutralizer is based on alteration of coiled polymer chains into an uncoiled form through transforming acidic Carbomer into a salt through the action of a neutralizing agent, NaOH. An alternative neutralizer, such as triethanolamine, is also known to be effective [16]. When an additive in ionized form is used to modify the Carbomer system, a negative effect can occur. Monovalent ions cause diminished thickening. However, multivalent ions (Ca^{2+}, Al^{3+}) potentially cause insoluble precipitate to form, with subsequent collapse of the hydrogel systems [11].

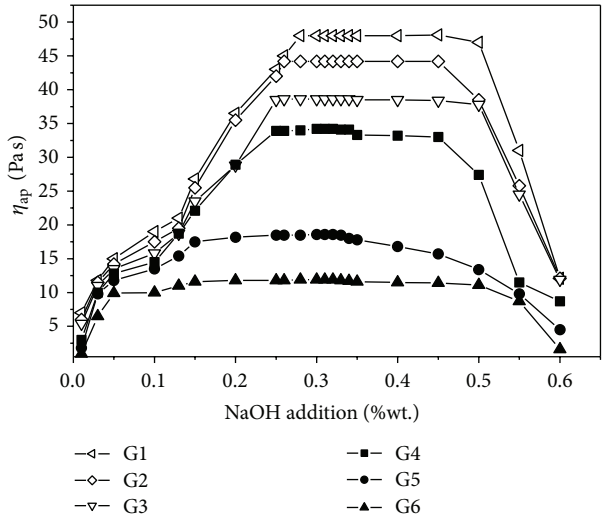

Figure 3: Apparent viscosity of the hydrogels versus concentration of the neutralizer NaOH.

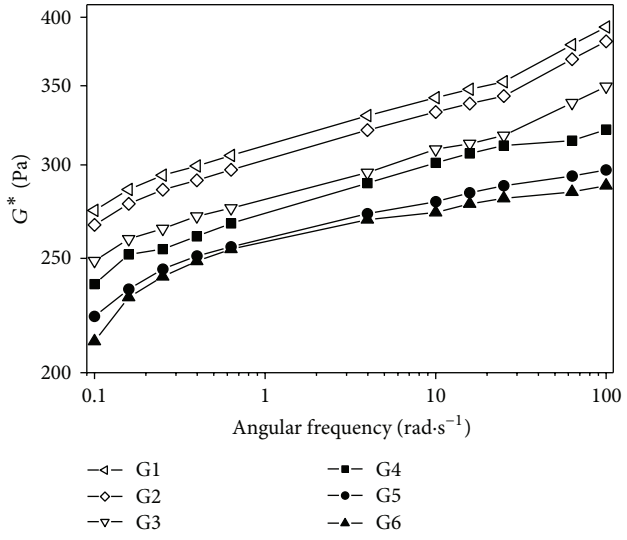

Figure 4: Complex shear modulus (G^*) versus angular frequency dependence of the hydrogels.

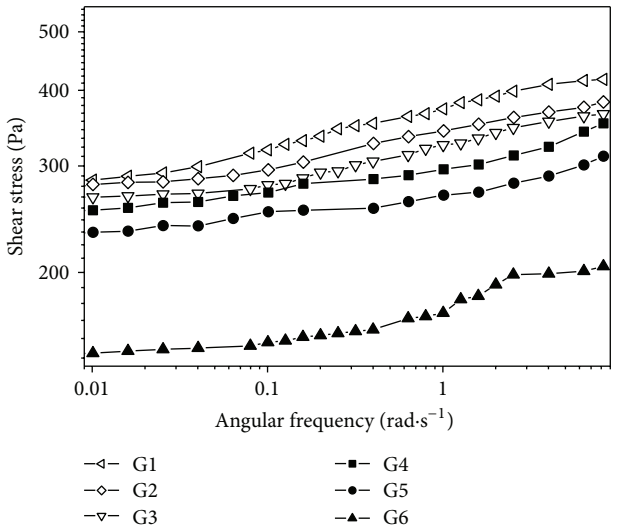

Figure 5: Shear stress versus angular frequency dependence of the hydrogels.

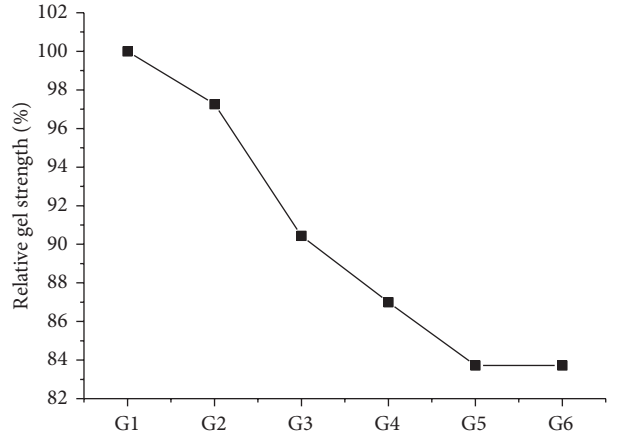

Figure 6: Relative gel strength as a function of the hydrogel composition and NaSal content.

Table 2: Dynamic yield stress and gel strength of the hydrogels.

Sample	Dynamic yield stress (Pa)
G1	283 ± 5
G2	271 ± 4
G3	265 ± 5
G4	252 ± 5
G5	232 ± 3
G6	145 ± 5

The effect of NaSal concentration on Carbomer hydrogels, specifically their rheological properties, is shown in Figures 4 and 5, which depict dependencies of complex shear modulus (G^*) versus angular frequency and shear stress versus the same, respectively. The parallel increase in shear stress with shear rate reveals the characteristics of Bingham fluid with yield stress, as presented in Table 2 together with the characteristics of gel strength. In accordance with the results presented above, NaSal degrades the rheological properties of hydrogels.

Increasing content of NaSal in the systems leads to reduction of the observed rheological characteristics including the dynamic yield stress. These reductions are relatively small up to 0,5 wt.% NaSal (6.3% yield stress reduction in comparison to pure hydrogel, G1). On the contrary 2 wt.% of NaSal (G6) caused significant drop of the dynamic yield stress (about 49% decrease).

Similar effect of NaSal can be observed in relative gel strength parameter that is depicted as a function of NaSal content in Figure 6. Small additions of NaSal (G3) cause its reduction up to 10%. Hydrogels with 1 and 2 wt.% of NaSal (G5 and G6) showed relative gel strength decrease above 15%. These results have reverse trend compared to work of Farres

Table 3: Antimicrobial activity of freshly prepared samples G1–G6 expressed as inhibition zone diameter (mm).

Sample	*Escherichia coli*	*Pseudomonas aeruginosa*	*Candida albicans*	*Staphylococcus aureus*	*Aspergillus niger*
G1	No inhibition	No inhibition	No inhibition	No inhibition	No inhibition
G2	0.5 ± 0.0	1.0 ± 0.3	0.5 ± 0.0	4.5 ± 0.5	0.5 ± 0.3
G3	1.0 ± 0.3	1.5 ± 0.3	1.0 ± 0.5	6.5 ± 0.5	0.5 ± 0.3
G4	1.5 ± 0.3	2.0 ± 0.5	1.5 ± 0.3	9.0 ± 1.0	1.0 ± 0.3
G5	3.5 ± 0.3	4.5 ± 0.5	2.0 ± 0.3	11.5 ± 1.0	1.5 ± 0.3
G6	5.5 ± 0.5	6.0 ± 0.5	2.5 ± 0.3	15.0 ± 1.0	2.0 ± 0.3

Table 4: Antimicrobial activity of samples G1–G6 after 1 year of storage at 8°C expressed as inhibition zone diameter (mm).

Sample	*Escherichia coli*	*Pseudomonas aeruginosa*	*Candida albicans*	*Staphylococcus aureus*	*Aspergillus niger*
G1	No inhibition	No inhibition	No inhibition	No inhibition	No inhibition
G2	No inhibition	0.5 ± 0.3	No inhibition	1.0 ± 0.5	No inhibition
G3	No inhibition	0.5 ± 0.3	No inhibition	2.5 ± 0.5	No inhibition
G4	1.0 ± 0.3	1.5 ± 0.5	1.0 ± 0.3	3.5 ± 1.0	0.5 ± 0.3
G5	2.0 ± 0.3	3.0 ± 0.5	1.0 ± 0.3	7.5 ± 1.0	1.0 ± 0.3
G6	4.0 ± 0.5	3.5 ± 0.5	2.5 ± 0.3	8.0 ± 1.0	1.5 ± 0.3

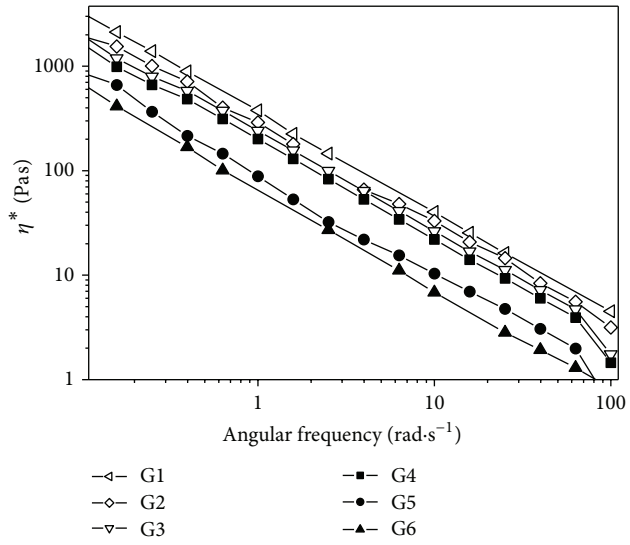

Figure 7: Complex viscosity versus angular frequency dependence of the hydrogel systems.

et al. who reported rheology of alginate fluid gels produced by in-situ calcium release. Specific interactions of calcium are caused of calcium junction into calcium chelates.

The viscoelastic properties of the compositions tested are presented in Figure 7 as the dependence of complex viscosity (η^*) on angular frequency, where a significantly decreasing trend is observable for samples G1–G6. Nevertheless, the increase in Na^+ ions concentration, originating from the presence of NaSal, brought about reduction in η^* alongside a rise in angular frequency (ω). This behaviour is typical for physically crosslinked polymer networks where, after a certain yield, stress is achieved.

The antimicrobial activity of the prepared compositions, observed by measuring inhibition zones, is presented in Table 3 for freshly prepared hydrogels and in Table 4 for those after 1 year of storage at 8°C. NaSal is known to be an effective antimicrobial agent against Gram-positive and Gram-negative bacterial strains, yeasts, and moulds. The results for freshly prepared hydrogels indicate that even 0.3 wt.% of NaSal exerts some effect against all the tested microorganisms. Indeed, composition G2 (0.5 wt.% NaSal) previously demonstrated its proven antimicrobial properties. The hydrogels stored for one year at 25°C had noticeably diminished antimicrobial activity (Table 5). However, sample G4 (1 wt.% NaSal) continued to show relatively suitable antimicrobial activity even after a year from its preparation.

Table 5: Changes of pH, viscosity, and NaSal concentration of the hydrogels after 1 year of storage at 8 and 25°C.

	G1	G2	G3	G4	G5	G6
$\Delta pH_{25°C}$ (%)	−27	−34	−35	−36	−45	−46
$\Delta pH_{8°C}$ (%)	−17	−18	−20	−24	−31	−38
$\Delta\eta_{25°C}$ (%)	−97	−36	−45	−56	−65	−75
$\Delta\eta_{8°C}$ (%)	−70	−21	−28	−43	−58	−64
$\Delta C_{NaSal,25°C}$ (%)	−54	−55	−52	−54	−54	−55
$\Delta C_{NaSal,8°C}$ (%)	−39	−38	−39	−39	−39	−38

Besides antimicrobial activity, the aging of the given hydrogel compositions was tested as regards pH and η and dependence on storage temperature (8°C and 25°C for 1 year). Since NaSal was expected to be deactivated by reacting with either of the components of the hydrogel systems (polymer, neutralizer), its concentration in the hydrogel samples was also subjected to study. The NaSal was determined by applying UV-VIS spectrometry at a fixed 515 nm wavelength using 5 mM $Fe(NO_3)_3$ in 12 mM H_2SO_4 and a colouring agent [17].

The results expressed as negative changes to the relevant characteristics are shown in Table 5. Indeed, the effect of storage temperature is noticeable. Storage at ambient temperature can completely eradicate all important characteristics, for

example, pH, η, and NaSal content, while loss of antimicrobial activity might also be anticipated. Despite reducing the characteristics studied, storage at 8°C could be considered sufficient for maintaining the quality of the hydrogel over the long term. Nevertheless, greater NaSal content (up to 1 wt.%) in the hydrogel composition brings about parallel reduction in the parameters studied. Supplementing the hydrogel systems with more NaSal (above 1 wt.%) does not bring further enhancement of properties.

4. Conclusions

This study investigated the effect exerted on rheological and antimicrobial properties through the presence of sodium salicylate (NaSal, 0–2 wt.%), in a hydrogel matrix based on a chemically crosslinked copolymer of acrylic acid (Carbomer). The results show that even small concentrations of NaSal noticeably affected hydrogel neutralization, viscosity, and antimicrobial properties against Gram-positive and Gram-negative bacterial strains, yeasts, and moulds. Long-term stability studies (1 year) revealed that hydrogels can maintain antimicrobial activity as well as viscosity at a level potentially sufficient for practical use, despite diminishment in the all properties observed. It was also found that NaSal reduced the effects of aging.

In addition to NaSal representing a potential active agent for cosmetic or medical applications, description was given on its contribution to the processing, final properties, and stability of the given hydrogel systems. Its optimal concentration in the Carbomer matrix was determined as 1 wt.% as a three-way compromise between the necessary therapeutic (antimicrobial) effect, hydrogel properties (pH and viscosity), and stability requirements.

Conflict of Interests

The authors declare that there is no conflict of interests regarding the publication of this paper.

Acknowledgments

This work was cofunded by the Ministry of Agriculture of the Czech Republic (Project no. QJ1310254) and the Ministry of Education, Youth and Sports of the Czech Republic (Project no. LO1504).

References

[1] N. Kayaman-Apohan and E. Akyürek, "Synthesis and drug-release properties of biodegradable hydrogels having β-cyclodextrin," *Polymer Bulletin*, vol. 70, no. 8, pp. 2151–2167, 2013.

[2] F. Rossi, G. Perale, G. Storti, and M. Masi, "A library of tunable agarose carbomer-based hydrogels for tissue engineering applications: the role of cross-linkers," *Journal of Applied Polymer Science*, vol. 123, no. 4, pp. 2211–2221, 2012.

[3] E. M. Ahmed, "Hydrogel: preparation, characterization, and applications," *Journal of Advanced Research*, vol. 6, no. 2, pp. 105–121, 2015.

[4] T. Kristmundsdóttir, P. Sigurdsson, and H. Thormar, "Effect of buffers on the properties of microbicidal hydrogels containing monoglyceride as the active ingredient," *Drug Development and Industrial Pharmacy*, vol. 29, no. 2, pp. 121–129, 2003.

[5] D. Mou, H. Chen, D. Du et al., "Hydrogel-thickened nanoemulsion system for topical delivery of lipophilic drugs," *International Journal of Pharmaceutics*, vol. 353, no. 1-2, pp. 270–276, 2008.

[6] M. O. Bodendorf, S. Grunewald, J. C. Simon, and U. Paasch, "Efficacy and cosmetic results of contact gel cooling of the skin during non-ablative laser procedures," *Journal der Deutschen Dermatologischen Gesellschaft*, vol. 6, no. 8, pp. 647–652, 2008.

[7] D. S. C. Lam, R. W. K. Law, A. S. Y. Ng et al., "Randomized double-masked controlled trial comparing pain scores with and without the use of supplementary 2% lidocaine gel in LASIK," *American Journal of Ophthalmology*, vol. 153, no. 4, pp. 627–631, 2012.

[8] K. Pramod, S. Shanavas, S. H. Ansari et al., "Sol-gel behavior of a novel nanodroplet biomaterial for drug delivery," *Journal of Sol-Gel Science and Technology*, vol. 61, no. 1, pp. 161–168, 2012.

[9] M. M. Rady and G. F. Mohamed, "Modulation of salt stress effects on the growth, physio-chemical attributes and yields of *Phaseolus vulgaris* L. plants by the combined application of salicylic acid and *Moringa oleifera* leaf extract," *Scientia Horticulturae*, vol. 193, pp. 105–113, 2015.

[10] E. Marengo, V. Gianotti, S. Angioi, and M. C. Gennaro, "Optimization by experimental design and artificial neural networks of the ion-interaction reversed-phase liquid chromatographic separation of twenty cosmetic preservatives," *Journal of Chromatography A*, vol. 1029, no. 1-2, pp. 57–65, 2004.

[11] Lubrizol Advanced Materials, "Viscosity of Carbopol® polymers in aqueous systems," Technical Data Sheet TDS-730 Edition, 2010.

[12] M. T. Islam, N. Rodríguez-Hornedo, S. Ciotti, and C. Ackermann, "Rheological characterization of topical carbomer gels neutralized to different pH," *Pharmaceutical Research*, vol. 21, no. 7, pp. 1192–1199, 2004.

[13] H. Y. Kim and H. J. Choi, "Core–shell structured poly(2-ethylaniline) coated crosslinked poly(methyl methacrylate) nanoparticles by graft polymerization and their electrorheology," *RSC Advances*, vol. 4, no. 54, pp. 28511–28518, 2014.

[14] I. Fernández Farrés and I. T. Norton, "Formation kinetics and rheology of alginate fluid gels produced by in-situ calcium release," *Food Hydrocolloids*, vol. 40, pp. 76–84, 2014.

[15] L. M. L. Dasilva, Mm. Filho, K. Bonifacio et al., "In vitro evaluation of antimicrobial activity of sealers and pastes used in endodontics," *Journal of Endodontics*, vol. 26, no. 7, pp. 391–394, 2000.

[16] M. Todica, C. V. Pop, L. Udrescu et al., "Rheological behavior of some aqueous gels of carbopol with pharmaceutical applications," *Chinese Physics Letters*, vol. 27, no. 1, Article ID 018301, 4 pages, 2010.

[17] J. T. Mitchell-Koch, K. R. Reid, and M. E. Meyerhoff, "Salicylate detection by complexation with iron(III) and optical absorbance spectroscopy. An undergraduate quantitative analysis experiment," *Journal of Chemical Education*, vol. 85, no. 12, pp. 1658–1659, 2008.

Hindawi Publishing Corporation
International Journal of Polymer Science
Volume 2016, Article ID 1749285, 7 pages
http://dx.doi.org/10.1155/2016/1749285

Research Article

Haemostatic Response of Polyethylene Terephthalate Treated by Oxygen and Nitrogen Plasma Afterglows

Metod Kolar[1] and Gregor Primc[2]

[1]*Centre of Excellence, PoliMat, Tehnološki Park 24, 1000 Ljubljana, Slovenia*
[2]*Plasmadis d.o.o., Teslova 30, 1000 Ljubljana, Slovenia*

Correspondence should be addressed to Gregor Primc; gregor.primc@plasmadis.com

Received 13 November 2015; Accepted 24 December 2015

Academic Editor: Yakai Feng

Samples of polymer polyethylene terephthalate were coated with heparin and the haemostatic response has been determined by optical imaging of samples after incubation with fresh blood from a healthy donor. Prior to coating the samples were treated by neutral reactive particles of the oxygen or nitrogen plasma flowing afterglow. X-ray photoelectron spectroscopy analysis showed intensive functionalization of the polymer foils upon treatment with afterglows; however, the concentration of sulphur from heparin remained below the detection limit. The optical imaging showed densely distributed blood platelets in highly activated forms on untreated samples, whereas treatment with both afterglows revealed improved hemocompatibility. Best results were obtained for oxygen-functionalized polymer, whereas additional coating with heparin caused moderate loss of hemocompatibility, that was explained by deactivation of surface functional groups upon incubation with heparin.

1. Introduction

Polymer materials are widely used for manufacturing products that come to contact with body tissues and liquids [1, 2]. The biological response depends enormously on the type of polymer as well as its surface finish. In many cases the biological response is not adequate so the products should be covered with thin coatings of materials of better biocompatibility [3, 4]. Examples of particular interest are products that come into contact with human blood, such as artificial blood vessels, fistulae, vascular stents, and heart valves. Such products are made from a limited number of polymers such as polytetrafluoroethylene (PTFE), polyurethane (PU), and polyethylene terephthalate (PET) [5–7]. The type of polymer is chosen according to mechanical properties and chemical stability, whereas the biocompatibility should be reasonably good. As-synthesized polymers never exhibit excellent biocompatibility when in contact with human blood, so many commercial cardiovascular implants are covered with different coatings (i.e., heparin) in order to improve the hemocompatibility [6, 7]. The coatings, however, do not always persist after prolonged incubation with human blood. They either can interact chemically with blood constituents or are just dissolved and washed away. Although numerous attempts have been made to stabilize such coatings on polymer surfaces, the results are still not optimal [6, 8].

An alternative to coating of polymer materials that come into contact with human blood is nanostructuring and functionalization [3, 9–14]. Such treatments are often performed in gaseous plasma [15]. Gaseous plasma definitely causes rich functionalization of polymer surfaces with desired functional groups [16]; however, on the other hand it also causes modification of subsurface properties of polymer materials. Namely, gaseous plasma is rich in charged particles and neutral reactive particles that may be excited to metastables of high potential energy. Such particles, when deexcited, radiate in the entire spectrum from IR to VUV [17]. Oxygen plasma, for example, is a source of VUV radiation that comes from radiative transition of neutral oxygen atoms. On the other hand, nitrogen plasma exhibits UV radiation from different transitions of both neutral and positively charged nitrogen molecules. Such radiation is absorbed in the subsurface film of polymer and causes bond scissions which in turn cause modification of chemical and mechanical

properties of polymers treated by such plasma [18]. In order to avoid this effect but still enable functionalization with specific functional groups, it is often better to use flowing afterglow of appropriate gaseous plasma. Such an approach has been also adopted in our case and the results show excellent hemocompatibility at practically no modification of subsurface polymer film.

2. Experimental Setup

2.1. Plasma Treatment. Samples of semicrystalline polymer PET (Goodfellow Ltd.) were treated in the experimental system presented schematically in Figure 1. Samples were placed into the treatment chamber which was made from borosilicate glass. Neutral reactive particles were leaked into the treatment chamber through a rather narrow quartz tube of an inner diameter 6 mm. The quartz tube was mounted into a microwave (MW) cavity where plasma was created. The cavity was powered with a MW generator of a standard frequency 2.45 GHz and an adjustable power up to 300 W. Due to continuous leakage of gas through the flow controller on one side of the quartz tube and pumping of the treatment chamber on the other side, there was a pressure gradient along the tube which allowed for fast drifting of gas from the plasma to the treatment chamber. The sample was placed in such a manner that any radiation from gaseous plasma could not reach the samples. The samples were treated in oxygen and nitrogen plasma. The concentration of neutral gaseous atoms in the treatment chamber was estimated with a catalytic probe, which was mounted onto the treatment chamber as shown schematically in Figure 1. Plasma was created at the MW power of 150 W and gas flow of 140 sccm. In such conditions the pressure in the treatment chamber was 50 Pa. In case the working gas was oxygen, the concentration of neutral oxygen atoms in the ground state at the position next to the sample was approximately 7×10^{20} m^{-3} [19], whereas, in the case of nitrogen, the dissociation fraction was somehow lower and the N-atom density was only approximately 4×10^{20} m^{-3}. The treatment time for both cases was 30 s.

2.2. XPS Surface Characterization. The samples were characterized with X-ray photoelectron spectroscopy (XPS) within a few minutes after the treatment. XPS characterization was performed using an XPS (TFA XPS Physical Electronics, Münich, Germany). The samples were excited with monochromatic Al K$\alpha_{1,2}$ radiation at 1486.6 eV over an area with a diameter of 400 μm. Photoelectrons were detected with a hemispherical analyser positioned at an angle of 45° with respect to the normal of the sample surface. XPS survey spectra were measured at pass energy of 187 eV using an energy step of 0.4 eV, whereas high-resolution spectra were measured at pass energy of 23.5 eV using an energy step of 0.1 eV. An additional electron gun was used for surface neutralization during XPS measurements. All spectra were referenced to the main C1s peak of the carbon atoms, which was assigned a value of 284.8 eV. The measured spectra were analysed using MultiPak v8.1c software (Ulvac-Phi, Inc., Kanagawa, Japan, 2006) from Physical Electronics, which was supplied with the spectrometer.

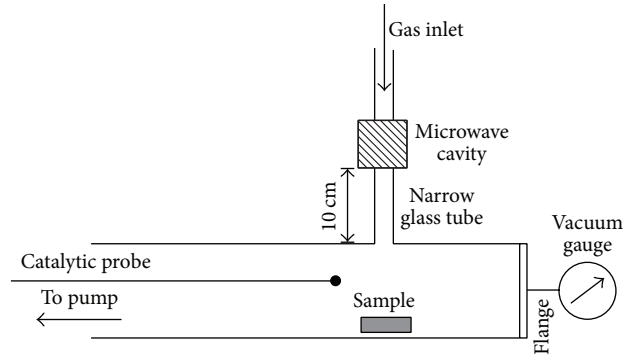

Figure 1: The experimental setup.

2.3. Coating with Heparin. Selected samples were incubated in a solution containing 1% heparin in 50 mM MES buffer. In order to facilitate covalent binding of heparin to the polymer surface treated in nitrogen plasma, a crosslinking agent was added at the concentration of 6 mM. The agent was 1-ethyl-3-(3-dimethylaminopropyl)carbodiimide hydroxide (EDC). EDC is used for coupling of amino groups on the nitrogen plasma-treated polymer surface with carboxyl groups of heparin [20, 21]. The binding was stabilized using N-hydroxysulfosuccinimide (NHS) at the concentration of 3.5 mM. The samples were left in the solution for at least 4 hours. Then they were rinsed thoroughly, first with 3 M water solution of NaCl and then by Milli-Q water. Samples were then dried in ambient conditions. For the polymer treated in oxygen plasma we used an anchoring agent polyethylenimine (PEI) which is rich in amino groups that are coupled to the oxygen plasma-treated surfaces by electrostatic interactions [21]. All reagents were purchased from Sigma Aldrich.

2.4. Platelet Adhesion and Characterization. Both plasma-treated and heparin coated samples were incubated with fresh blood from a healthy donor, which was supplied from the Blood Transfusion Centre of Slovenia. Blood was withdrawn with 21-gauge needle into evacuated tube containing 3.2% sodium citrate as anticoagulant. Samples were incubated with 1 mL of fresh whole human blood in 24-well cell culture plate with shaking at 250 RPM for 1 h at 37°C. After incubation the samples were rinsed several times with phosphate buffer saline (1x PBS) in order to remove blood residues and treated with 2.5% glutaraldehyde. After fixation the samples were rinsed with deionized water and left to air-dry. All experiments were performed in triplicate. The adhesion of platelets on samples was observed by confocal microscopy. A high-resolution Axio CSM 700 (Carl Zeiss, Jena, Germany) confocal light microscope was used.

3. Results and Discussion

Treatment of polymer samples with neutral reactive particles created in plasma caused activation of the sample surface due

Table 1: XPS surface composition of PET samples coated with heparin (in at.%).

Number	Sample	C	O	N	S
#0	Pure untreated PET	75.1	24.9	/	/
#1	Untreated + heparin	73.1	26.9	/	/
#2	Treated in O_2 plasma	59.5	40.5	/	/
#3	Treated in O_2 plasma + heparin	62.5	35.6	1.9	/
#4	Treated in N_2 plasma	66.2	30.2	3.6	/
#5	Treated in N_2 plasma + heparin	61.3	35.5	3.2	/

to functionalization with specific functional groups. Figure 2 reveals XPS spectra of the samples treated by either oxygen or nitrogen atoms in the treatment chamber presented in Figure 1 and incubated with heparin. The peaks corresponding to different elements in the surface film of samples changed upon the treatment and a small peak corresponding to nitrogen is observable at the binding energy of 400 eV. The spectra presented in Figure 2 allow for determination of elemental composition in the surface film of thickness of several nanometres. The results are summarized in Table 1. The composition for uncoated samples is added for comparison. The concentration of oxygen on untreated PET incubated with heparin (sample #1) is slightly larger than for pure PET (sample #0) that is explained by a high concentration of oxygen in the polysaccharide. The difference, however, is not dramatic: instead of 25 at.% typical for pure PET the concentration of oxygen for the untreated polymer incubated with heparin is 27 at.%. Furthermore, the concentration of both nitrogen and sulphur which should be present in heparin is below the detection limit of XPS. Such results indicate that heparin did not adhere well to the surface of untreated PET and was rather washed away upon preparation procedure.

The concentration of oxygen on polymer treated with neutral oxygen atoms (sample #2) is much larger than on pure untreated PET material (sample #0). This result is expected because neutral oxygen atoms interact extensively with polymer materials placed into the treatment chamber for time as long as 30 s [16]. In fact, functionalization of aromatic polymers in oxygen plasma afterglow is even better than in glowing plasma itself [22]. Because the O-atom density is approximately 7×10^{20} m^{-3}, the corresponding flux of O-atoms is approximately 10^{23} m^{-2}s^{-1} and the fluence 10^{24} m^{-2}. This is a huge value taking into account the surface density of atoms in the solid material which is of the order of 10^{19} m^{-2}. More interesting is the concentration of oxygen on the surface of the sample first treated with oxygen atoms and then incubated with heparin (sample #3). The concentration is approximately 35 at.% that is somehow lower than for the oxygen-treated sample (#2), but well above the untreated sample (#0). Such a large concentration can be explained either by polymer functionalization with O-rich functional groups upon treatment with neutral oxygen atoms or by presence of heparin or both. Due to the fact that the concentration of nitrogen on this sample is measurably high, one can speculate that the excessive oxygen on this sample is

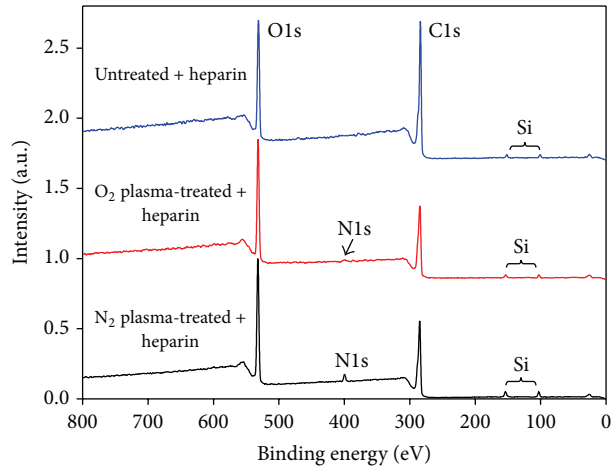

Figure 2: XPS survey spectra of PET samples coated with heparin.

at least partly due to the presence of heparin on the polymer, which was pretreated by neutral oxygen atoms.

Such a speculation is supported from the composition of the sample which was pretreated by nitrogen atoms and incubated with heparin (sample #5). Namely, in this case the concentration of oxygen is nearly identical as on the sample treated by oxygen atoms and incubated with heparin (sample #3). Because the pretreatment of this sample was performed in nitrogen atmosphere, it is clearly not possible that the increased concentration of oxygen is a result of pretreatment, but it is rather due to the presence of heparin on such a surface.

Modifications of surface composition between polymer materials with different pretreatment are reflected in the ability for blood platelets to adhere to and activate on the polymer surface. Figures 3–7 show both low and high magnification optical images of the samples after incubation with human blood. One can observe huge differences which will be discussed below. An untreated sample incubated with heparin (Figure 3) is nearly entirely covered with blood platelets. The high magnification image reveals some details about the morphological shape. Numerous flakes observed in the image are blood platelets in highly activated (often called "fully spread") form [23]. The sample which was not plasma pretreated is therefore as thrombogenic as any other polymer material, although it has been incubated with heparin. This result is sound with the result obtained by XPS. Namely, XPS showed only a marginal increase of oxygen on heparin-incubated sample and no nitrogen, so it was possible to speculate that any heparin was washed away even before incubation with human blood. The polymers without any antithrombogenic surface finish therefore adhere blood platelets and cause their activation as observed in Figure 3.

Figure 4 represents optical images of the sample treated by oxygen atoms only and not incubated with heparin. The treatment obviously causes a dramatic improvement of the polymer hemocompatibility. Low magnification image reveals sparsely distributed dots which are actually individual blood platelets that becomes apparent after viewing the high-resolution image. The treatment of PET material by

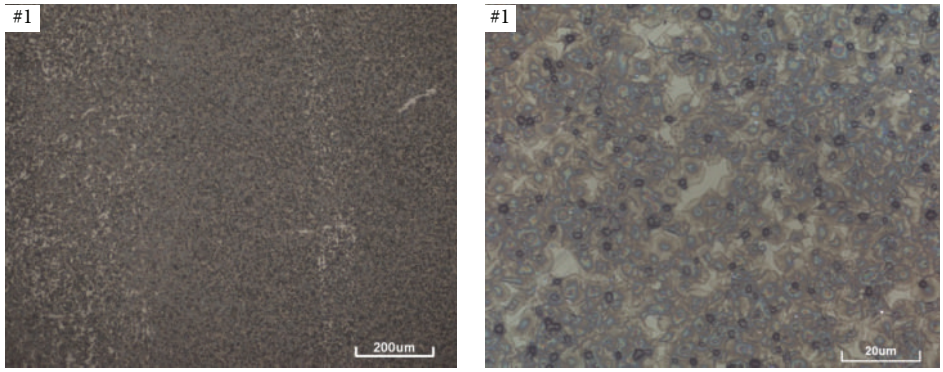

(a) (b)

Figure 3: Optical image of platelets on surface of untreated polymer PET (#1) coated with heparin after incubation with fresh blood at two different magnifications ((a) and (b)).

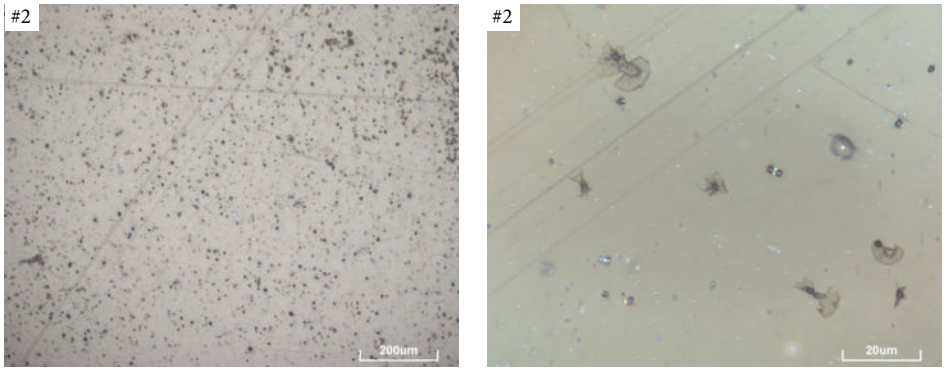

(a) (b)

Figure 4: Optical image of platelets on surface of PET polymer treated in oxygen plasma (#2) after incubation with fresh blood at two different magnifications ((a) and (b)).

neutral oxygen atoms is therefore beneficial and results are similar to those obtained by treatment of this polymer in oxygen plasma [24, 25]. The poor ability for adhesion of blood platelets on oxygen-functionalized materials has been explained by different conformation of blood proteins that adhere to the surface of PET polymer in a fraction of a second after incubating with fresh blood, so well before any platelet adheres and activates [26].

Incubation of the sample treated by oxygen atoms with heparin does not modify the hemocompatibility of this sample much. This is obvious from Figure 5 which is very similar to Figure 4. The only difference is in the high-resolution images. Whereas in Figure 4(a) one can observe only separate platelets, Figure 5(a) reveals clusters. Clusters contain both highly and weakly activated platelets. As mentioned above the activation degree is revealed from the morphology of the platelet. Almost spherical platelets are not activated, whereas flakes of rather large diameter indicate platelets in the final state of activation. In between there are flakes in dendritic or spread dendritic forms. The incubation of oxygen-treated polymer with heparin, therefore, does not improve hemocompatibility of the samples. An appealing explanation is that the majority of heparin (which is presented on the polymer before incubating with fresh blood; see Table 1) is removed upon incubation. Namely, bonded heparin always prevents any adhesion and activation of blood platelets on the surface of PET polymer [8]. It is interesting that the concentration of blood platelets on the surface of samples treated by O-atoms and subsequently incubated with heparin appears to be even larger than on the samples treated only by oxygen atoms. A possible explanation of this observation may be deactivation of surface functional groups on the oxygen-treated polymer during incubation with heparin.

Haemostatic response of the PET samples treated by nitrogen atoms (#4) is similar to that of samples treated by oxygen atoms (#2). Figure 6 represents images of a sample treated by nitrogen atoms and then incubated with fresh blood, whereas Figure 7 represents those which were also coated with heparin (#5). The lateral dimension of the spots on the polymer samples is now larger than for samples treated in oxygen plasma afterglow. High magnification images of Figures 6 and 7 also indicate almost complete activation of the adhered blood platelets. Comparison of high-resolution images of Figures 5 and 7 reveals much higher degree of platelet activation for the case of N-atom pretreatment of the sample. The active spots on the nitrogen-functionalized polymer therefore stimulate rapid activation of the blood platelets. Taking into account huge fluence of

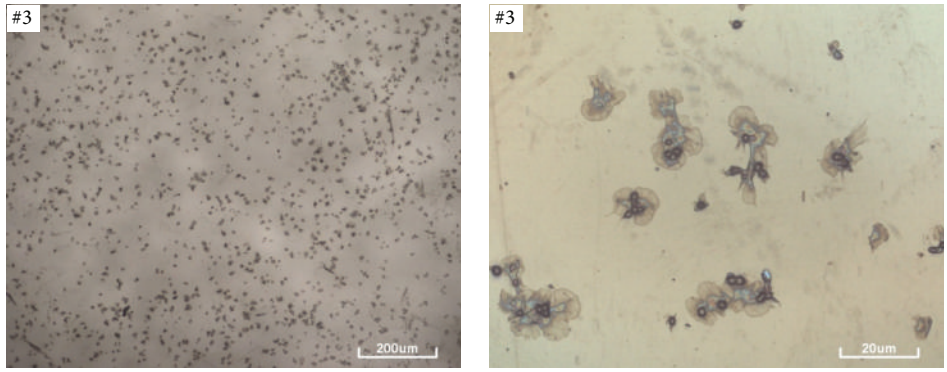

(a) (b)

Figure 5: Optical image of platelets on surface of PET polymer treated in oxygen plasma and coated with heparin (#3) after incubation with fresh blood at two different magnifications ((a) and (b)).

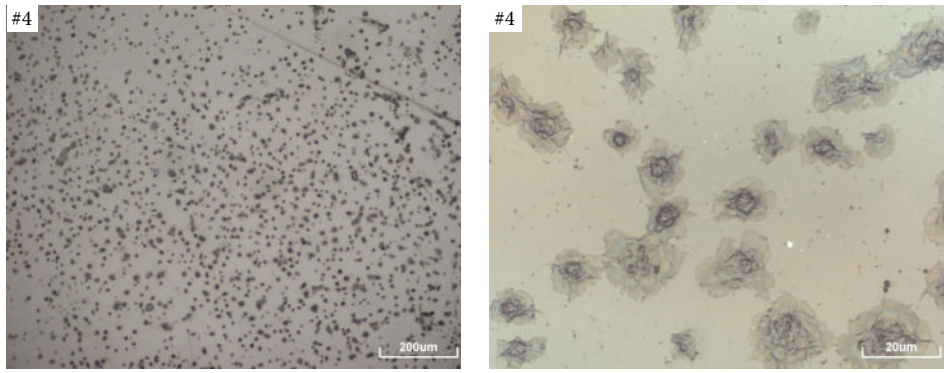

(a) (b)

Figure 6: Optical image of platelets on surface of PET polymer treated in nitrogen plasma (#4) after incubation with fresh blood at two different magnifications ((a) and (b)).

nitrogen atoms it is unlikely to explain rapid activation of blood platelets observed in Figure 6 by lack of nitrogen-containing functional groups. The available analytical techniques, unfortunately, do not allow for high lateral resolution and thus determination of any laterally inhomogeneous distribution of surface functionalities. It is interesting enough that the haemostatic response of the nitrogen-treated sample incubated with heparin (#5) does not seem to be any better than for the same samples without heparin (#4). Table 1 doubtfully confirms presence of heparin on such samples. The antithrombogenic coating must be either inhomogeneously distributed onto the sample surface after incubating with fresh blood or removed completely. Taking into account high similarity of images presented in Figures 6 and 7, it is more likely that the heparin was just removed from the polymer surface during incubation with blood. Unfortunately, any surface characterization of polymer after incubation with blood would not give satisfactory information, because blood proteins adhere to the polymer surface and remain bonded well; thus they screen any heparin that may persist at the interface between polymer and protein film.

Finally, let us mention a possible cytotoxic effect of EDC/NHS crosslinker. According to literature, EDC/NHS crosslinker was found to be toxic when added directly to the cell culture medium, because it reacted with the cell DNA [27]. However, cytotoxicity was not observed when EDC/NHS was used as a crosslinker to bind a coating to the surface of implants. Namely, McDade et al. have tested two crosslinkers, EDC and glutaraldehyde, and found glutaraldehyde very toxic, while for EDC cytotoxicity was not observed [28]. Furthermore, also our previous investigation of HUVECs (human umbilical vein endothelial cells) and HMVECs (human microvascular endothelial cells) adhesion on surfaces, where EDC was used as a crosslinker to bind heparin, showed very good cell proliferation [8].

4. Conclusions

Samples of PET polymer were pretreated with neutral reactive particles present in the afterglow of nonequilibrium plasma of oxygen and nitrogen, incubated with heparin, and the haemostatic response has been determined by monitoring the density of adhered blood platelets as well as their morphological properties. Flowing afterglow of gaseous plasma has been selected instead of glowing plasma in order to

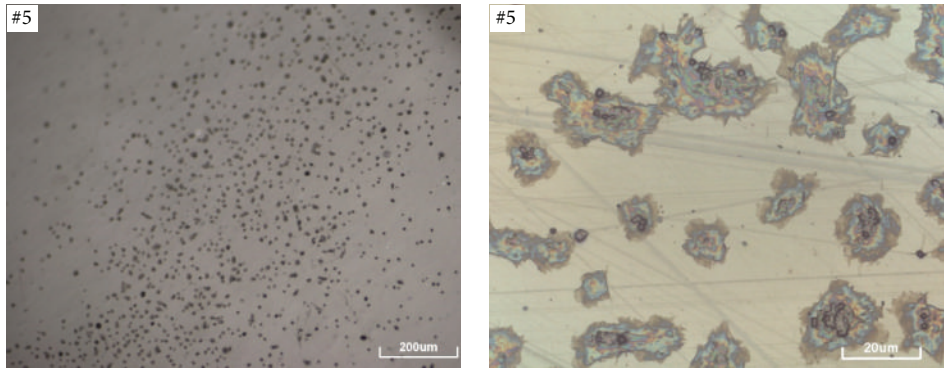

(a) (b)

Figure 7: Optical image of platelets on surface of PET polymer treated in nitrogen plasma and coated with heparin (#5) after incubation with fresh blood at two different magnifications ((a) and (b)).

avoid any modification of polymer surface film by UV/VUV radiation arising from gaseous plasma. The density of neutral reactive particles in the treatment chamber was large enough to assure saturation of any surface functionality that is formed on the polymer surface upon the treatment. The fluence of neutral atoms (either oxygen or nitrogen) was approximately 10^{24} m^{-2} that is about five orders of magnitude larger than the surface density of atoms in solid materials so even probabilities for interaction as low as 10^{-5} should be high enough to saturate surface functionalities. Materials treated in afterglow were tested for haemocompatibility and the results were as good as for materials treated by glowing plasma, if not better. Some differences between samples treated by O- and N-atoms were observed. The density of adhered blood platelets on O-atom treated samples was somehow smaller than on N-atom treated ones. The minimization of blood platelet adhesion was explained by appropriate conformation of blood proteins on polymer surface rich in polar functional groups. The polarity of oxygen groups was even higher than nitrogen; thus the antithrombogenic character of O-treated samples was somehow better than that of Natom treated ones.

Incubation of polymer samples with heparin using the standard technique does not cause substantial effects indicating nonadequate immobilization. The XPS analyses confirmed presence of a thin heparin film on the samples of PET polymer pretreated with O- or N-atoms, however, not on the untreated polymer samples. The covalent bonding was not achieved in either case, though. The heparin on the surface of samples treated by oxygen or nitrogen plasma afterglow was likely washed away from the polymer surface upon incubation with fresh blood.

Although the treatments described in this paper led to important improvement of polymer biocompatibility when in contact with human blood, the surface finish using this method was not as good as in the case of covalently bonded heparin [8]. The immobilization of such an antithrombogenic polysaccharide coating on the polyethylene surface therefore remains a difficult task.

Conflict of Interests

The authors declare that there is no conflict of interests regarding the publication of this paper.

Acknowledgment

This research was financially supported by the Slovenian Research Agency ARRS (Project P2-0082).

References

[1] J. Jagur-Grodzinski, "Polymers for tissue engineering, medical devices, and regenerative medicine. Concise general review of recent studies," *Polymers for Advanced Technologies*, vol. 17, no. 6, pp. 395–418, 2006.

[2] T. Holland and A. Mikos, "Review: biodegradable polymeric scaffolds. Improvements in bone tissue engineering through controlled drug delivery," in *Tissue Engineering I*, K. Lee and D. Kaplan, Eds., vol. 102 of *Advances in Biochemical Engineering/Biotechnology*, pp. 161–185, Springer, Berlin, Germany, 2006.

[3] S. K. Jaganathan, A. Balaji, M. V. Vellayappan et al., "Review: radiation-induced surface modification of polymers for biomaterial application," *Journal of Materials Science*, vol. 50, no. 5, pp. 2007–2018, 2015.

[4] A. A. John, A. P. Subramanian, M. V. Vellayappan et al., "Review: physico-chemical modification as a versatile strategy for the biocompatibility enhancement of biomaterials," *RSC Advances*, vol. 5, no. 49, pp. 39232–39244, 2015.

[5] L. Pinchuk, "A review of the biostability and carcinogenicity of polyurethanes in medicine and the new generation of 'biostable' polyurethanes," *Journal of Biomaterials Science—Polymer Edition*, vol. 6, no. 3, pp. 225–267, 1994.

[6] R. J. Linhardt, S. Murugesan, and J. Xie, "Immobilization of heparin: approaches and applications," *Current Topics in Medicinal Chemistry*, vol. 8, no. 2, pp. 80–100, 2008.

[7] S. W. Jordan and E. L. Chaikof, "Novel thromboresistant materials," *Journal of Vascular Surgery*, vol. 45, no. 6, pp. A104–A115, 2007.

[8] M. Kolar, M. Mozetič, K. Stana-Kleinschek, M. Fröhlich, B. Turk, and A. Vesel, "Covalent binding of heparin to functionalized pet materials for improved haemocompatibility," *Materials*, vol. 8, no. 4, pp. 1526–1544, 2015.

[9] S. Abou Rich, T. Dufour, P. Leroy, F. Reniers, L. Nittler, and J.-J. Pireaux, "LDPE surface modifications induced by atmospheric plasma torches with linear and showerhead configurations," *Plasma Processes and Polymers*, vol. 12, no. 8, pp. 771–785, 2015.

[10] M. Gołda, M. Brzychczy-Włoch, M. Faryna, K. Engvall, and A. Kotarba, "Oxygen plasma functionalization of parylene C coating for implants surface: nanotopography and active sites for drug anchoring," *Materials Science and Engineering C*, vol. 33, no. 7, pp. 4221–4227, 2013.

[11] J. A. Barish and J. M. Goddard, "Topographical and chemical characterization of polymer surfaces modified by physical and chemical processes," *Journal of Applied Polymer Science*, vol. 120, no. 5, pp. 2863–2871, 2011.

[12] P. Slepicka, N. S. Kasalkova, J. Siegel, Z. Kolska, L. Bacakova, and V. Svorcik, "Nano-structured and functionalized surfaces for cytocompatibility improvement and bactericidal action," *Biotechnology Advances*, vol. 33, no. 6, pp. 1120–1129, 2015.

[13] S. de Valence, J.-C. Tille, C. Chaabane et al., "Plasma treatment for improving cell biocompatibility of a biodegradable polymer scaffold for vascular graft applications," *European Journal of Pharmaceutics and Biopharmaceutics*, vol. 85, no. 1, pp. 78–86, 2013.

[14] P. Ferreira, P. Alves, P. Coimbra, and M. H. Gil, "Improving polymeric surfaces for biomedical applications: a review," *Journal of Coatings Technology and Research*, vol. 12, no. 3, pp. 463–475, 2015.

[15] A. Vesel, K. Eleršic, M. Modic, I. Junkar, and M. Mozetic, "Formation of nanocones on highly oriented pyrolytic graphite by oxygen plasma," *Materials*, vol. 7, no. 3, pp. 2014–2029, 2014.

[16] A. Vesel, I. Junkar, U. Cvelbar, J. Kovac, and M. Mozetic, "Surface modification of polyester by oxygen- and nitrogen-plasma treatment," *Surface and Interface Analysis*, vol. 40, no. 11, pp. 1444–1453, 2008.

[17] K. Kutasi, V. Guerra, and P. A. Sá, "Active species downstream of an Ar-O_2 surface-wave microwave discharge for biomedicine, surface treatment and nanostructuring," *Plasma Sources Science and Technology*, vol. 20, no. 3, Article ID 035006, 2011.

[18] M. R. Wertheimer, A. C. Fozza, and A. Holländer, "Industrial processing of polymers by low-pressure plasmas: the role of VUV radiation," *Nuclear Instruments and Methods in Physics Research Section B*, vol. 151, no. 1–4, pp. 65–75, 1999.

[19] A. Vesel, M. Kolar, N. Recek, K. Kutasi, K. Stana-Kleinschek, and M. Mozetic, "Etching of blood proteins in the early and late flowing afterglow of oxygen plasma," *Plasma Processes and Polymers*, vol. 11, no. 1, pp. 12–23, 2014.

[20] S. Gore, J. Andersson, R. Biran, C. Underwood, and J. Riesenfeld, "Heparin surfaces: impact of immobilization chemistry on hemocompatibility and protein adsorption," *Journal of Biomedical Materials Research. Part B Applied Biomaterials*, vol. 102, no. 8, pp. 1817–1824, 2014.

[21] S. Murugesan, J. Xie, and R. J. Linhardt, "Immobilization of heparin: approaches and applications," *Current Topics in Medicinal Chemistry*, vol. 8, no. 2, pp. 80–100, 2008.

[22] J. Izdebska and T. Sabu, *Printing on Polymers: Fundamentals and Applications*, Elsevier Science, Waltham, Mass, USA, 2016.

[23] S. L. Goodman, T. G. Grasel, S. L. Cooper, and R. M. Albrecht, "Platelet shape change and cytoskeletal reorganization on polyurethaneureas," *Journal of Biomedical Materials Research*, vol. 23, no. 1, pp. 105–123, 1989.

[24] M. Modic, I. Junkar, K. Stana-Kleinschek, R. Kostanjšek, and M. Mozetič, "Morphology transformations of platelets on plasma activated surfaces," *Plasma Processes and Polymers*, vol. 11, no. 6, pp. 596–605, 2014.

[25] M. Modic, I. Junkar, A. Vesel, and M. Mozetic, "Aging of plasma treated surfaces and their effects on platelet adhesion and activation," *Surface and Coatings Technology*, vol. 213, pp. 98–104, 2012.

[26] N. Recek, M. Jaganjac, M. Kolar et al., "Protein adsorption on various plasma-treated polyethylene terephthalate substrates," *Molecules*, vol. 18, no. 10, pp. 12441–12463, 2013.

[27] A. B. Moshnikova, V. N. Afanasyev, O. V. Proussakova, S. Chernyshov, V. Gogvadze, and I. P. Beletsky, "Cytotoxic activity of 1-ethyl-3-(3-dimethylaminopropyl)-carbodiimide is underlain by DNA interchain cross-linking," *Cellular and Molecular Life Sciences*, vol. 63, no. 2, pp. 229–234, 2006.

[28] J. K. McDade, E. P. Brennan-Pierce, M. B. Ariganello, R. S. Labow, and J. Michael Lee, "Interactions of U937 macrophage-like cells with decellularized pericardial matrix materials: influence of crosslinking treatment," *Acta Biomaterialia*, vol. 9, no. 7, pp. 7191–7199, 2013.

Hindawi Publishing Corporation
International Journal of Polymer Science
Volume 2016, Article ID 6594960, 10 pages
http://dx.doi.org/10.1155/2016/6594960

Research Article

Antiepileptic Effects of Lacosamide Loaded Polymers Implanted Subdurally in GAERS

Sebastien H. Bauquier,[1] Jonathan L. Jiang,[2] Zhilian Yue,[3] Alan Lai,[2] Yu Chen,[3] Simon E. Moulton,[3,4] Karen J. McLean,[2] Sara Vogrin,[2] Amy J. Halliday,[2] Gordon Wallace,[3] and Mark J. Cook[2]

[1] *Faculty of Veterinary Science, University of Melbourne, 250 Princes Highway, Werribee, VIC 3030, Australia*
[2] *Centre for Clinical Neurosciences and Neurological Research, St. Vincent's Hospital Melbourne, P.O. Box 2900, Fitzroy, VIC 3065, Australia*
[3] *Intelligent Polymer Research Institute and ARC Centre of Excellence for Electromaterials Science, AIIM Facility, University of Wollongong, Innovation Campus, Wollongong, NSW 2522, Australia*
[4] *Faculty of Science, Engineering and Technology, Swinburne University of Technology, Hawthorn, VIC 3122, Australia*

Correspondence should be addressed to Sebastien H. Bauquier; bauquier@unimelb.edu.au
and Simon E. Moulton; smoulton@swin.edu.au

Received 30 September 2015; Revised 18 December 2015; Accepted 22 December 2015

Academic Editor: Alenka Vesel

The current experiment investigated the ability of coaxial electrospun poly(D,L-lactide-co-glycolide) (PLGA) biodegradable polymer implants loaded with the antiepileptic drugs (AED) lacosamide to reduce seizures following implantation above the motor cortex in the Genetic Absence Epilepsy Rat from Strasbourg (GAERS). In this prospective, randomized, masked experiments, GAERS underwent surgery for implantation of skull electrodes ($n = 6$), skull electrodes and blank polymers ($n = 6$), or skull electrodes and lacosamide loaded polymers ($n = 6$). Thirty-minute electroencephalogram (EEG) recordings were started at day 7 after surgery and continued for eight weeks. The number of SWDs and mean duration of one SWD were compared week-by-week between the three groups. There was no difference in the number of SWDs between any of the groups. However, the mean duration of one SWD was significantly lower in the lacosamide polymer group for up to 7 weeks when compared to the control group ($0.004 < p < 0.038$). The mean duration of one seizure was also lower at weeks 3, 5, 6, and 7 when compared to the blank polymer group ($p = 0.016$, 0.037, 0.025, and 0.025, resp.). We have demonstrated that AED loaded PLGA polymer sheets implanted on the surface of the cortex could affect seizure activity in GAERS for a sustained period.

1. Introduction

Epilepsy is a chronic neurological condition characterized by recurrent seizures. The incidence of epilepsy in most developed countries is between 50 and 100 cases per 100,000 population per year although it is estimated that up to 5% of a population will experience nonfebrile seizures at some point in life [1, 2]. Individuals with medically untreatable epilepsy often have impaired ability to work or function socially (e.g., inability to drive, difficulty at attending school, losing jobs and friends, and anxiety regarding the possibility of having seizure in potentially hazardous conditions) [3]. Treatment with conventional antiepileptic drugs (AEDs, e.g., phenytoin and lacosamide administered orally) results in only 33% of the patients having no seizure recurrence [1, 2]. Alternatively, neurostimulation based therapy has also been shown to reduce seizure activity but has typical reductions of seizure frequency of approximately 40% acutely and 50–69% after several years [4]. Surgical resection of the seizure focus can be performed in the case of focal seizures; however, this procedure can only be applied on selected patients depending on the localization of the epileptic foci [5]. Indeed, the success

of inducing long-lasting seizure remission from epilepsy surgery ranges from a low of 25% for patients exhibiting extrahippocampal seizure origin to 70% in appropriately selected candidates [5].

The mechanisms by which resistance to AEDs treatment develops are not fully understood; some evidence suggests that this may be due to a lack of effective penetration into the brain parenchyma; however, the drug side effects prevent large increase in the posology [6]. Alternative therapies aiming at improving the availability of AEDs such as the intracranial implantation of polymer-based drug delivery systems are being investigated [7, 8]. This targeted drug delivery approach has shown some success in the treatment of animal models of several neurological disorders such as Parkinson's disease, Huntington's disease, and Alzheimer's disease [9]. Also, Halliday et al. used Levetiracetam loaded biodegradable polymer implants in the tetanus toxin model of temporal lobe epilepsy in rats; the results of this study indicated that drug-eluting polymer implants represent a promising evolving treatment option for intractable epilepsy; however, important limitations of the study were that the effects could only be seen for a week and only a single group of control animals were investigated. These animals received an injection of tetanus toxin and a sham craniotomy, without the implantation of a polymer sheet [8].

Poly(D,L-lactide-*co*-glycolide) (PLGA) is the most commonly used biodegradable polymer as it is highly biocompatible and easily engineered and has been approved for drug delivery purposes by the United States Food and Drug Administration [10]. It has been used in numerous applications including bone and skin tissue engineering, ocular treatment, vaccine, cancer therapy, and nerve regeneration [11–15]. PLGA polymers have also been successfully used for intracranial drug delivery in animal models of neurological disorders, showing no evidence of toxic injury or immune-mediated inflammation when implanted subdurally above the motor cortex in rats [10].

Genetic Absent Epilepsy Rat from Strasbourg (GAERS) is a strain of rats where 100% of the animals present with recurrent generalized nonconvulsive seizures [16]. This animal model has become the gold standard to study the mechanisms underlying absence epilepsy [16]. In the present investigation, PLGA sheets loaded with the commonly used AED lacosamide were developed and their ability to decrease seizure activity was investigated in the GAERS. Lacosamide stabilizes neuronal membranes through enhancing slow inactivation of voltage-gated sodium channel and is effective in different rodent seizure models including generalized seizure [17].

The aim of the study is to investigate the effect of subdural implantation of biodegradable polymers (PLGA) loaded with lacosamide on seizure activity in an animal model of epilepsy (GAERS); the hypothesis is that subdural implantation of lacosamide loaded PLGA polymers can decrease seizure activity of the GAERS. Our results demonstrated that focal delivery of lacosamide can achieve partial sustained antiepileptic effect in an animal model of generalized epilepsy.

2. Materials and Methods

The study was designed as a randomized controlled masked experiment. The experiment was approved by St. Vincent's Hospital (Melbourne) Animal Ethics Committee and conducted in accordance with the Australian Code of Practice for the Care and Use of Animals for Scientific Purposes (2004).

2.1. PLGA Polymer Mat Production. Lacosamide-laden polymer mats were produced using a coaxial electrospinning method [18], with the core composed of lacosamide and 75 : 25 PLGA (lactide/glycolide = 75 : 25) and the shell composed of 85 : 15 PLGA (lactide/glycolide = 85 : 15). The core solution was prepared at 17% w/v 75 : 25 PLGA in dimethylformamide (DMF), to which lacosamide was added to give a range of final concentration of 2.5, 12.5, or 20% w/w relative to the polymer. The shell solution was prepared at 20% w/v 85 : 15 PLGA in a binary solvent system comprising dichloromethane and DMF (dichloromethane/DMF = 7/3). Coaxial electrospinning was conducted using a nanoelectrospinning system (NANON-01A, MECC Co. Ltd.) at an applied DC voltage of 23 kV. A coaxial spinneret with a diameter of 0.2 mm for the core and 0.8 mm for the sheath nozzles was connected to the core and shell solutions and a feed rate of 5 μL min^{-1} and 20 μL min^{-1} for the core and shell solutions, respectively. Fiber mats were collected on a grounded plate collector that was set 15 cm away from the spinneret tip. The drug-free, coaxially spun polymer mats were also prepared using the above procedure.

Depending on lacosamide loading in the core, the as-prepared, coaxially electrospun polymer mats were denoted as PLGA-2.5%, PLGA-12.5%, and PLGA-20%. The drug-free mats are denoted as blank polymers. All the samples were finally dried in a vacuum oven at 40°C for 72 h to remove residual solvent and were stored at −20°C prior to subsequent physiochemical characterization and animal studies.

2.2. Morphology Study. The morphology of the electrospun mats (with and without drug) was examined using a field emission scanning electron microscope (FESEM, JEOL JSM-7500FA). The samples were sputter-coated with gold prior to FESEM to avoid sample charging.

2.3. Determination of Drug Loading in Polymer Mats. An extraction method was used to determine the drug loading in the electrospun mats. Briefly, each sample (1 cm × 1 cm) was weighed and placed into 1 mL methanol for 12 hours after which the methanol was removed and replenished with 1 mL of fresh methanol. This extraction procedure was repeated four times with each methanol sample allowed to evaporate to leave residual drug behind which was reconstituted in methanol (1 mL), diluted 20 times with the HPLC mobile phase (see below), and filtered through a 0.2 μm syringe filter. The fourth reconstituted sample showed no presence of drug indicating that the entire drug had been extracted from the electrojetted sample.

2.4. In Vitro Drug Release. The lacosamide loaded polymers (1 cm × 1 cm) were suspended in 1 mL of aCSF, and the release experiment was conducted at 37°C in a shaker water bath (Julabo Pty. Ltd.). The aCSF contained NaCl (0.866% w/v), KCl (0.224% w/v), $CaCl_2$-$2H_2O$; (0.0206% w/v), and $MgCl_2$-$6H_2O$ (0.0164% w/v) in 1 mM phosphate buffer (pH 7.4) [8]. For each sample, the release medium solution was collected and replenished with fresh aCSF at various time points and stored at −20°C prior to HPLC analysis being undertaken. The eluted samples were analyzed by HPLC using a modified method on an Agilent 1260 Infinity HPLC system [19]. An Atlantis® T3 C18 column (250 mm × 4.6 mm, 5 μm) was employed as the analytic column and set at 40°C. The mobile phase was composed of water, acetonitrile, and methanol (65 : 26.2 : 8.8, v/v/v), and the injection volume was 10 μL with the flow rate of 0.8 mL/min. The eluting lacosamide was detected using a UV-vis detector set at a wavelength of 230 nm (λ_{max} of lacosamide). To convert the UV-vis absorbance to drug concentration a standard curve was established by plotting in triplicate the UV-vis peak areas against respective concentrations of standard solutions (10, 20, 50, 100, 200, and 500 μM lacosamide).

2.5. Animals. Adult female GAERS were obtained from the University of Melbourne (Parkville, Victoria, Australia) and housed individually in inverted 12-hour light/dark cycles (the light was turned off between 6 am and 6 pm) with ad libitum access to food and water. Six-month-old rats were randomly allocated to a control group (no implant; $n = 6$), blank polymer group (bilateral implantation of blank PLGA polymers not containing lacosamide; $n = 6$), or treatment group (bilateral implantation of lacosamide loaded PLGA polymers; $n = 6$). The randomization was performed using the random function in Microsoft Excel 2007. The group attribution list was kept concealed from the researchers performing the EEG analysis.

2.5.1. Implantation Surgery. Immediately prior to surgery, rats were weighted and anaesthetized using a balanced anesthesia protocol including an intraperitoneal injection of ketamine (75 mg/kg) and xylazine (10 mg/kg). Following anesthesia induction rats were placed in a stereotaxic apparatus, given isoflurane (0.5 to 1% in oxygen, 1 L/min) via a nose-cone as needed, and given subcutaneous (SQ) carprofen (5 mg/kg) for pain relief and 0.9% sodium chloride (2 mL) for cardiovascular support.

Rats from the control group underwent surgery for EEG recording electrode implantation whereas surgeries for the rats from the blank polymer group, the treatment group, and the silicone group also included bilateral craniotomies for subdural placement of two identical implants. Over the scalp of all rats, the hair was clipped and the skin was aseptically prepared. A single incision was made down the midline, the skull cleared of tissue, and the exposed bone dried with 3% hydrogen peroxide. Five extradural electrodes, consisting of small jeweller's screws, were implanted caudal to the intended polymer implantation sites through burr holes. Four were implanted cranially to the interaural line (two on each side of the sagittal suture) and one was implanted caudally to the interaural line on the right side of the sagittal suture (Figures 1(a) and 1(b)). The electrodes were then connected to an adaptor and secured with dental cement.

Implants measuring 3 mm by 4 mm were cut from the polymer sheets described above. Placements of the implants were performed after 5 mm by 4 mm craniotomies were created bilaterally at the level of the coronal suture (over the motor cortices) and after excising the dura to expose the brain surface (Figures 1(a) and 1(b)). Following implant placements, the skull removed from craniotomy sites was replaced. The craniotomy sites were then sealed with an alginate-based hydrogel, the entire surgical site was covered with dental cement, and the skin was sutured leaving exposed only part of the dental cement. The animals were placed on heat pads for recovery. Postoperative treatment included SQ buprenorphine every twelve hours (0.03 mg/kg, twice a day), saline (2 mL, once a day), and carprophen SID (5 mg/kg, once a day) for up to 3 days.

2.5.2. Electroencephalograph Recording and Analysis. At day 7 or 8 after surgery and at least 3 days per week for the following 7 weeks, rats were monitored for one hour (half an hour anesthesia recovery/acclimation time and half an hour recording time) (Figure 1(c)). At each monitoring session, rats were briefly anaesthetized in an induction cage with isoflurane (4% in oxygen, 2 L/min, for 2 to 3 minutes), and shielded cables were used to connect the recording electrodes to the EEG acquisition system, which consisted of TDT processors and high impedance head stages driven by custom-designed software (Tucker Davis Technologies, USA). The rats were allowed to recover from the anesthetic before recordings began. The EEGs were visualized using a custom-designed MATLAB program (The MathWorks, Inc., USA). During EEG recording, if the rats were perceived as being asleep, and after confirmation of no seizure activity on the EEG, a noise stimulus between 94 and 98 decibels was applied. At the end of a recording session, the rats were again briefly anaesthetized with isoflurane (4% in oxygen, 2 L/min) to be disconnected from the shielded cable. The researcher performing EEG analysis was masked to the treatment and used a GAERS specific automated spike-and-wave discharges (SWDs) detection algorithm [20].

2.6. Primary Outcome: Epileptic Activity. For each rat, the median value and interquartile range for number of SWDs, duration of one SWD, and cumulative duration of SWDs over 30 min were calculated for eight recording blocks, each block representing 1 week of recording. The first block only included one recording at day 6 or 7 after surgery (total of 30 minutes of EEG recording) whereas the following 7 blocks included 3 recordings per week (total of 90 minutes of EEG recording per week) (Figure 1(c)).

2.7. Secondary Outcome: Postoperative Health Monitoring. For a minimum of three days after surgery and until full recovery from the surgery, the rats were monitored for weight loss once a day and for mobility and grooming twice

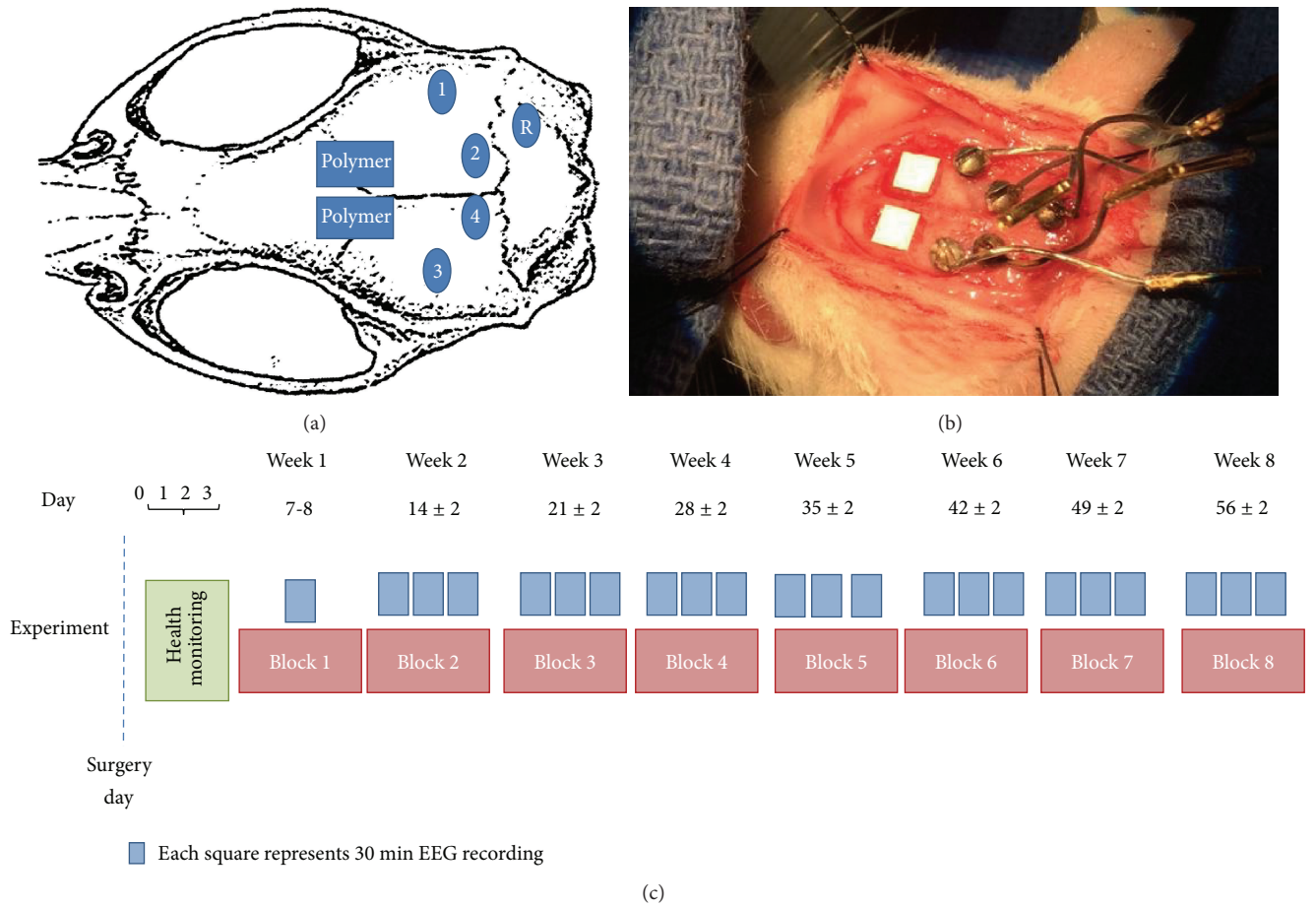

Figure 1: Schematic diagram illustrating the positioning of epidural recording screw electrodes (1–4), reference electrode (R) and polymer (a); picture of the actual surgery (b); timeline of the study design: for a minimum of three days after surgery the rats were monitored for weight loss once a day and for mobility and grooming twice a day. Thirty-minute electroencephalogram recording began at day 7 or 8 after surgery and for the following 7 weeks on 3 days per week. For each rat, the mean desired values (number of SWDs, duration of one SWD, or cumulative duration of SWDs over 30 min) were calculated for eight recording blocks, each block being 1 week of duration.

a day. Those observations were given scores (Table 1). For each day a debilitation score was calculated by cumulating the highest grooming and mobility scores with the weight loss score (Table 1). A debilitation score of 0, 1 to 3, 4 to 6, and 7 to 9 meant that the rat health was not affected, mildly affected, moderately affected, and severely affected by the surgery/polymer implantation, respectively. The highest debilitation score of each rat over the postoperative period is reported.

2.8. Statistical Analysis. Data analysis was performed using a commercially available software (IBM SPSS Statistic 22; Stata 13.0; StataCorp, 2013). The number of SWDs, mean duration of one SWD, and cumulative duration of SWDs were compared between the three groups using individual Kruskal-Wallis tests for each block of the study. When significant values were found, post hoc pairwise comparisons were conducted for this block, comparing the control versus lacosamide polymer and blank polymer versus lacosamide polymer conditions using the Mann-Whitney U test. The debilitation scores of group lacosamide were compared to group control and group blank polymer using a 2-tailed Mann-Whitney exact test. Significance level was set at 5%.

3. Results

The FESEM images obtained from the PLGA mats without lacosamide (Figure 2(a)) show a smooth and regular morphology characteristic of PLGA electrospun fibers. However, when lacosamide was incorporated into the PLGA the fibers within the mats demonstrated a mixture of porous and nonporous morphology when examined under FESEM (Figure 2(b)). Measured by visual inspection of the FESEM images, the fiber diameter ranged between 2 μm and 5 μm. These observations of the PLGA-12.5% samples shown in Figure 2(c) were also observed in the other PLGA-2.5% and PLGA-20.0% samples.

The in vitro release results for the PLGA-lacosamide mats are presented in Figure 2(c). The polymer containing 20% lacosamide showed a cumulative drug release above 40% after only 7 days. The polymers containing 2.5 and 12.5% lacosamide both had a reduction in release after around 42

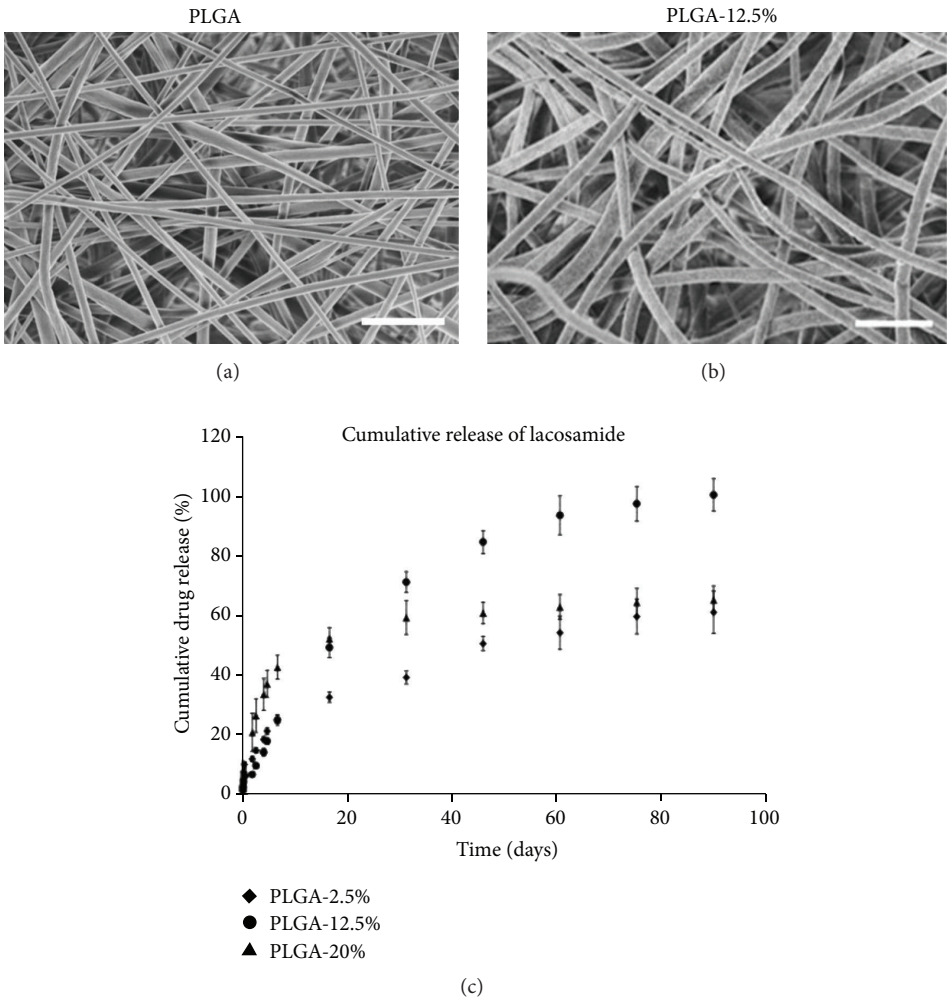

Figure 2: Scanning electron micrographs of coaxially electrospun polymer mats of PLGA Blank (a) and PLGA-12.5% lacosamide (b) (scale bar represents 10 μm). In vitro release data of lacosamide polymers with final core lacosamide concentration of 2.5, 12.5, and 20% w/w relative to the polymer (c). Bars are representing standard deviation.

days (6 weeks); however, the total drug release was higher for 12.5% lacosamide polymer. In consequence, the polymer containing 12.5% lacosamide was chosen to be implanted for the in vivo experiment.

The results for the postoperative debilitation score are presented in Figure 3. One rat from the blank polymer group and 3 rats from the lacosamide had a debilitation score which were classified as moderate. One rat from the blank polymer group and 3 rats from the lacosamide group had a debilitation score which were classified as severe. The debilitation scores were significantly increased for the lacosamide polymer group when compared to the control and blank polymer groups ($p = 0.002$ and $p = 0.041$, resp.).

The results of the measurements performed to evaluate the epileptic activity for the groups control, blank polymer, and lacosamide polymer are presented in Figure 4. The difference in the number of SWDs between the groups was not statistically significant. However, the mean duration of one SWD was significantly lower in the lacosamide polymer group for up to 7 weeks when compared to the control group

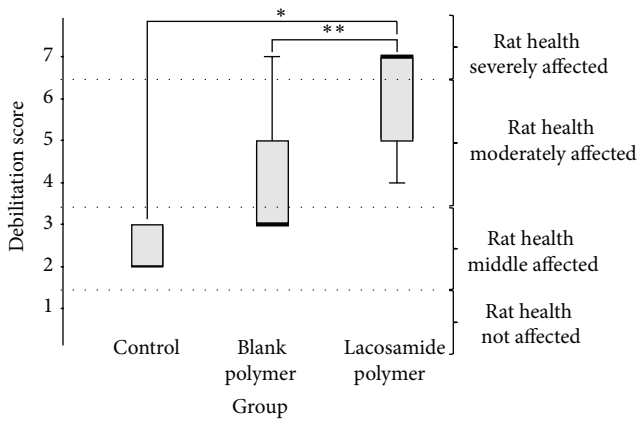

Figure 3: Postoperative debilitation scores obtained for groups control ($n = 6$), blank polymer ($n = 6$), and lacosamide polymer ($n = 6$). Rats from the lacosamide polymer group had debilitation scores that were higher when compared to the 2 other groups ($^{*}p = 0.002$; $^{**}p = 0.041$). The box indicates the interquartile range (25th to 75th percentile), and the whiskers indicate the range.

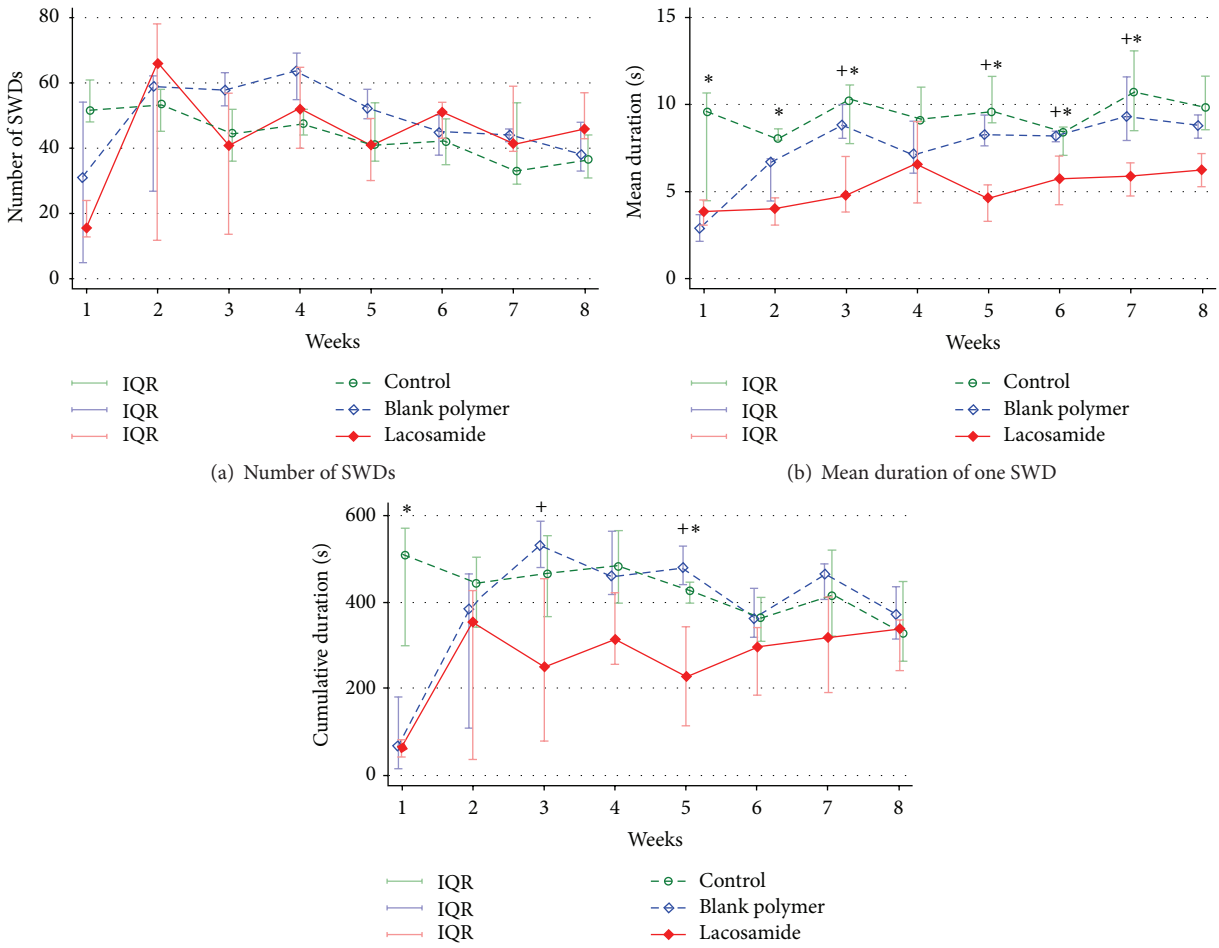

(a) Number of SWDs

(b) Mean duration of one SWD

(c) Cumulative duration of SWDs

FIGURE 4: Comparison of the measurements obtained to evaluate the epileptic activity of groups control ($n = 6$), blank polymer ($n = 6$), and lacosamide polymer ($n = 6$). SWD: spike-and-wave discharge; IQR: interquartile range; results are reported as median. $*$ and $+$ represent the time points at which the results from the lacosamide polymer group were significantly different to the control and blank polymer groups, respectively ($p < 0.05$).

($p = 0.037$, 0.004, 0.01, 0.025, 0.037, and 0.016 for weeks 1, 2, 3, 4, 6, and 7, resp.). The mean duration of one seizure was also lower at weeks 3, 5, 6, and 7 when compared to the blank polymer group ($p = 0.016$, 0.037, 0.025, and 0.025, resp.). The cumulative duration of SWDs of the lacosamide group was significantly lower when compared to the control group at weeks 1 and 5 ($p = 0.010$ and $p = 0.055$, resp.) and when compared to the blank polymer group at weeks 3 and 5 ($p = 0.010$ and $p = 0.055$, resp.). Examples of EEG recordings are presented in Figure 5.

4. Discussion

Drug release from electrospun polymeric structures typically follows zero-order kinetics [18]. Zero-order kinetics implies a homogeneous drug distribution and a release profile governed by the wetting properties of the material and encapsulation of hydrophilic and neutrally charged drugs of low molecular weight can be problematic for these types of structures [21–24]. The interaction of these types of drug molecules with the polymer is usually very poor and their rate of diffusion is often faster than the rate of polymer erosion. This fast rate of diffusion has detrimental effects on drug release from electrospun polymer structures.

Several factors are responsible for the variations in the release profiles of AEDs, namely, the solubility of the drug in the mat, the morphology of the fibers within the mat, and the distribution of the drug throughout the fibers (i.e., the degree of drug encapsulation within the core of the coaxial spun mats). The solubility of lacosamide (465 mg/L) contributes to the relatively fast elution of that drug from the polymer. Also, the morphology of the fibers within the electrospun mats shows a porous nature for the PLGA-lacosamide structures which increases the rate at which the release media (aCSF) can infuse into the internal region of the fibers and promote the elution of the drug.

The initial rapid drug release observed in the in vitro experiment for the polymer mats tested with a final core lacosamide concentration of 12.5% (Figure 2(c)) coincided

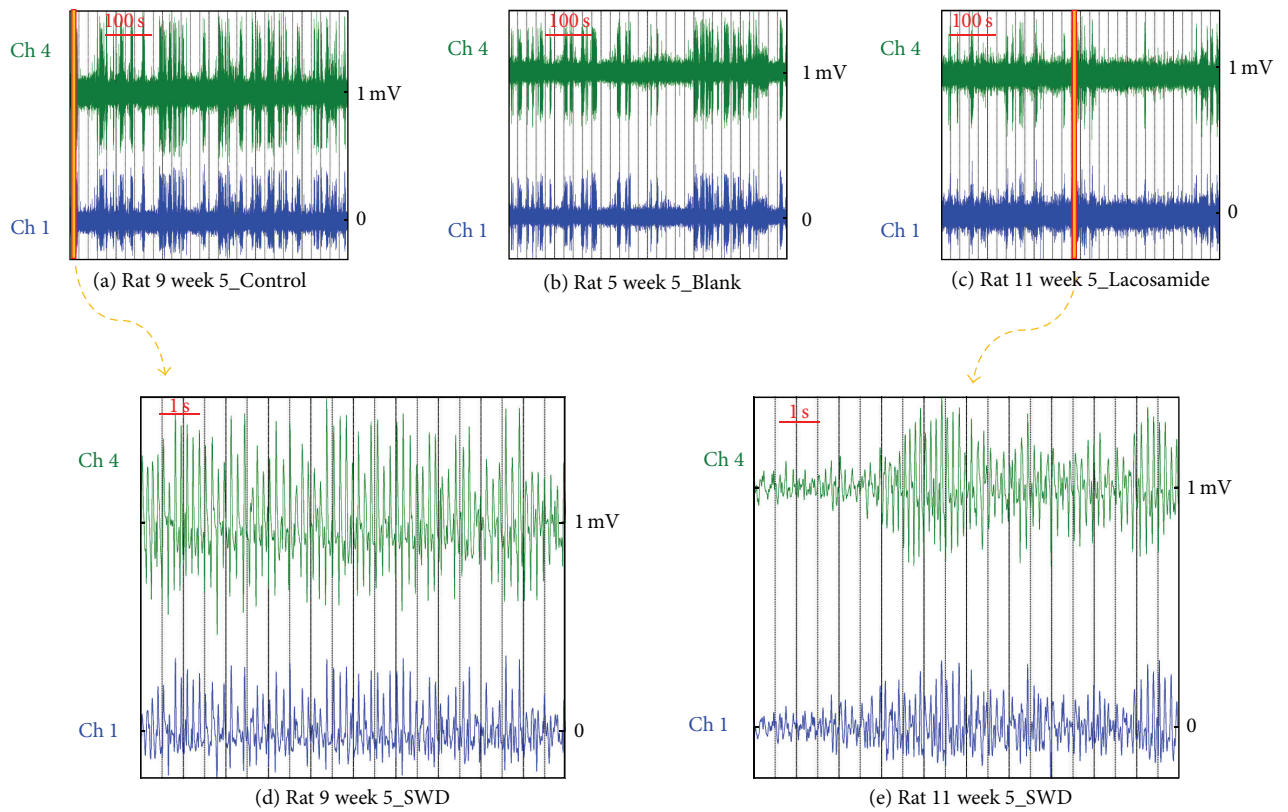

Figure 5: Example of EEG recording from 3 rats belonging to group control (a), blank polymer (b), and lacosamide polymer (c). Figures (d) and (e) are amplifications of spike-and-wave discharges observed during the recording shown and Figures (a) and (c), respectively.

with the postsurgical debilitation seen in most animals of the lacosamide polymer group. It is unlikely that the surgery alone was responsible for these adverse events as this debilitation was not observed to such extent in the blank polymer group. Debilitated rats were treated with fluid therapy and analgesic administration and they all recovered well. Looking at the results retrospectively, one could argue that implanting the PLGA-2.5% may have been a better choice as the initial release of drug is not as abrupt and the constant lacosamide release seems to last longer. Indeed the lack of effect of lacosamide after 7 weeks correlates with the almost absence of release of the lacosamide from the polymer. Variations in the release profiles observed in Figure 2(a) from the samples prepared with varying amounts of lacosamide indicate that the interaction of the drug with the polymer (and hence its propensity to be released from the structures) is influenced by the drug loading. It has previously been shown that the amount of drug loaded into electrospun fibers and drug-polymer-electrospinning solvent interactions has an effect on the release profiles [25–28].

Biodegradable PLGA polymer sheets containing a large amount of lacosamide were implanted above the motor cortices of GAERS. In the GAERS model of epilepsy, the rats present recurrent generalized nonconvulsive seizures characterized by bilateral and synchronous SWD accompanied with behavioral arrest, staring, and sometimes twitching of the vibrissae [16]. Furthermore, the GAERS were at least 6 months old, time at which 100% of the GAERS should present SWDs and at which the numbers of SWDs are at their maximum [16]. Although depth EEG recordings and lesion experiments show that SWDs in GAERS depend on cortical and thalamic structures with a possible rhythmic triggering by the lateral thalamus, more recent studies indicate a seizure initiation site within the perioral region of the somatosensory cortex (S1po) as well as the somatosensory cortex forelimb region (S1FL) [16, 29, 30]. Neurophysiological, behavioral, pharmacological, and genetic studies have demonstrated that spontaneous SWDs in GAERS fulfill all the requirements for an experimental model of absence epilepsy [16]. Although twenty-minute recordings were used by the original paper describing GAERS EEGs, to try to improve the performance of the EEG analysis 30 min recordings were used during the present experiment [16].

Although spontaneous SWDs start and end abruptly on a normal background EEG and are quite easy to isolate, the EEG patterns seen during sleep make it more difficult to differentiate start and stop of SWD [20]. In previous experiments, rats were stimulated when seen sleeping to improve seizure detection [20]. This intervention was reduced during the present experiment by inverting the light cycle of the rats. The EEG recordings of those diurnal animals were then recorded during the time of maximal activity reducing sleep time EEG interferences. SWDs usually occur at a mean frequency of 1.5 per min when the animals are in a state of

Table 1: Postoperative health monitoring chart. For a minimum of three days after surgery and until full recovery from the surgery, the rats were monitored for weight loss once a day and for mobility and grooming twice a day. For each day a debilitation score was calculated by cumulating the highest grooming and mobility scores with the weight loss score. A debilitation score of 0, 1 to 3, 4 to 6, and 7 to 9 meant that the rat health was not affected, middle affected, moderately affected, and severely affected by the surgery/polymer implantation, respectively.

Postoperative health monitoring chart	Score
Percentage of weight loss	
No weight loss	0
Less than 10% weight loss	1
10% to less than 20% weight loss	2
20% or more weight loss	3
Mobility score	
Rat moving normally	0
Rat ataxic moving at a normal speed	1
Rat ataxic and moving slowly	2
Rat recumbent	3
Grooming score	
No decrease in grooming activity	0
Middle decrease in grooming activity	1
Moderate decrease in grooming activity	2
No grooming activity	3
Total score = debilitation score	0–9

quiet wakefulness and have duration ranging from 0.5 to 75 s [16].

Isoflurane was used for a short period to connect and disconnect the recording apparatus before and after each recording. The authors found in previous experiments that during that setup without the use of anaesthesia some rats were showing stress behaviour (like crying) and in consequence the authors opted for a short general anaesthesia/sedation to improve animal welfare. Isoflurane was chosen for its low blood:gas solubility (1.4) allowing quick elimination. Indeed, rats recovered quickly from those short anaesthesia episodes and, although it cannot be excluded, it is unlikely that after 30 minutes isoflurane could still be interfering with their epileptic activity [31].

Implantation of the lacosamide sheets led to shorter seizures for up to seven weeks after implantation compared to rats that did not receive the implant.

During the first 2 weeks of the experiment, the blank polymer group also demonstrated decrease duration of SWDs when compared to the control group and to better understand the effect seen, silicon sheets were implanted in four older GAERS from the same colony (unpublished data). Although the SWD activity in GAERS is age dependent, preventing statistical comparison with the present experiment, the post-surgical transient decrease in SWD's duration was observed again. We could assume that the PLGA sheets were not themselves responsible for the decreased duration of SWDs seen in the control blank polymer group but could be attributed to brain injuries resulting from the surgery. This assumption is in agreement with previous publication reporting that PLGA-based implants are very well tolerated by the brain in animal models of other neurological disorders [32–37].

Only one EEG recording per rat was performed during the first week at day 6 or 7 while there were three recordings per week performed during the following seven weeks. This study design allowed time for good surgical wound healing before some traction could be applied to the electrodes "adaptor."

The lacosamide was chosen for its lipophilic properties allowing easy drug loading within the polymer and its proven efficacy in treating absence epilepsy [38]. Knowing that the polymer mats were implanted over the motor cortex and that previous investigations have shown that substances released from intraparenchymally implanted polymers are able to penetrate around 3 mm, it is possible that the lacosamide released from the sheets in our study may not have reached the seizure triggering focus in high enough concentration to stop seizure from happening [39–42]. However, lacosamide reduces the ability of epileptic neurons to endure extended firing burst by enhancing slow inactivation of voltage-gated sodium channel [43]. This would explain the unchanged number of SWDs but significant decrease in SWDs duration. The total duration of SWDs during the recording of SWD reflects the arithmetic product of the number of seizures and the mean duration of SWDs. Another AED alternative could have been the use of valproic acid which is one of the drugs of choice for the treatment of absence seizure. Its use could have provided additional support for the validity of the novel delivery method. Lastly, now that it has been shown that lacosamide loaded PLGA polymer sheets implanted on the surface of the cortex could affect the duration of the individual SWDs in GAERS, performing dose-response experiments in order to determine optimal concentrations of the drug in PLGA would be required to effectively improve the treatment and the novel delivery method.

From the statistical perspective, Bender and Lange recommended that data of exploratory studies be analyzed without multiplicity adjustment [44]. However, the lack of adjustment for multiple comparisons as well as the pilot nature of our study means that caution needs to be exercised when interpreting the results of this exploratory study. A larger study is needed to confirm these findings.

Although temporary side effects were seen, we have demonstrated that lacosamide loaded PLGA polymer sheets implanted on the surface of the cortex could affect seizure activity in GAERS by decreasing the mean duration of the SWDs events for a sustained period of up to 7 weeks. With improvements in polymer technologies and episodic release offering potentially much longer lasting release durations, intracranial polymer-based drug delivery systems may provide an effective therapeutic strategy for chronic epilepsy.

Conflict of Interests

The authors declare that they have no financial or other conflict of interests in relation to this research and its publication.

Acknowledgments

The authors gratefully acknowledge the sponsorship of the Victorian Government through its Science Technology and Innovation Initiative administered by the Department of Industry, Innovation and Regional Development. The authors thank the Australian Research Council (ARC) for continuing financial support. Gordon Wallace thanks the ARC for his Laureate Fellowships. The authors also acknowledge use of the facilities and the assistance of Mr. Tony Romeo at the UOW Electron Microscopy Centre. The authors are grateful for access to materials synthesis and characterization equipment made available through the Australian National Fabrication Facility (ANFF).

References

[1] J. W. Sander, "The epidemiology of epilepsy revisited," *Current Opinion in Neurology*, vol. 16, no. 2, pp. 165–170, 2003.

[2] S. D. Shorvon, "The epidemiology and treatment of chronic and refractory epilepsy," *Epilepsia*, vol. 37, supplement 2, pp. S1–S3, 1996.

[3] K. Swarztrauber, S. Dewar, and J. Engel Jr., "Patient attitudes about treatments for intractable epilepsy," *Epilepsy and Behavior*, vol. 4, no. 1, pp. 19–25, 2003.

[4] R. S. Fisher and A. L. Velasco, "Electrical brain stimulation for epilepsy," *Nature Reviews Neurology*, vol. 10, no. 5, pp. 261–270, 2014.

[5] P. Kwan and M. R. Sperling, "Refractory seizures: try additional antiepileptic drugs (after two have failed) or go directly to early surgery evaluation?" *Epilepsia*, vol. 50, supplement 8, pp. 57–62, 2009.

[6] W. Löscher, "Mechanisms of drug resistance," *Epileptic Disorders*, vol. 7, supplement 1, pp. S3–S9, 2005.

[7] A. J. Halliday, S. E. Moulton, G. G. Wallace, and M. J. Cook, "Novel methods of antiepileptic drug delivery—Polymer-based implants," *Advanced Drug Delivery Reviews*, vol. 64, no. 10, pp. 953–964, 2012.

[8] A. J. Halliday, T. E. Campbell, T. S. Nelson, K. J. McLean, G. G. Wallace, and M. J. Cook, "Levetiracetam-loaded biodegradable polymer implants in the tetanus toxin model of temporal lobe epilepsy in rats," *Journal of Clinical Neuroscience*, vol. 20, no. 1, pp. 148–152, 2013.

[9] A. J. Halliday and M. J. Cook, "Polymer-based drug delivery devices for neurological disorders," *CNS & Neurological Disorders—Drug Targets*, vol. 8, no. 3, pp. 205–221, 2009.

[10] A. J. Halliday, T. E. Campbell, J. M. Razal et al., "In vivo biocompatibility and in vitro characterization of poly-lactide-co-glycolide structures containing levetiracetam, for the treatment of epilepsy," *Journal of Biomedical Materials Research—Part A*, vol. 100, no. 2, pp. 424–431, 2012.

[11] R. Groynom, E. Shoffstall, L. S. Wu, R. H. Kramer, and E. B. Lavik, "Controlled release of photoswitch drugs by degradable polymer microspheres," *Journal of Drug Targeting*, vol. 23, no. 7-8, pp. 710–715, 2015.

[12] M. Allahyari and E. Mohit, "Peptide/protein vaccine delivery system based on PLGA particles," *Human Vaccines & Immunotherapeutics*, 2015.

[13] F. Zhang, Q. Song, X. Huang et al., "A novel high mechanical property PLGA composite matrix loaded with nanodiamond-phospholipid compound for bone tissue engineering," *ACS Appl Mater Interfaces*, vol. 8, no. 2, pp. 1087–1097, 2016.

[14] H. Cao, M. M. Chen, Y. Liu et al., "Fish collagen-based scaffold containing PLGA microspheres for controlled growth factor delivery in skin tissue engineering," *Colloids and Surfaces B: Biointerfaces*, vol. 136, pp. 1098–1106, 2015.

[15] K. Yu, J. Zhao, Z. Zhang et al., "Enhanced delivery of Paclitaxel using electrostatically-conjugated Herceptin-bearing PEI/PLGA nanoparticles against HER-positive breast cancer cells," *International Journal of Pharmaceutics*, vol. 497, no. 1-2, pp. 78–87, 2016.

[16] C. Marescaux, M. Vergnes, and A. Depaulis, "Genetic absence epilepsy in rats from Strasbourg—a review," *Journal of Neural Transmission, Supplement*, vol. 35, pp. 37–69, 1992.

[17] B. K. Beyreuther, J. Freitag, C. Heers, N. Krebsfänger, U. Scharfenecker, and T. Stöhr, "Lacosamide: a review of preclinical properties," *CNS Drug Reviews*, vol. 13, no. 1, pp. 21–42, 2007.

[18] L. Viry, S. E. Moulton, T. Romeo et al., "Emulsion-coaxial electrospinning: designing novel architectures for sustained release of highly soluble low molecular weight drugs," *Journal of Materials Chemistry*, vol. 22, no. 22, pp. 11347–11353, 2012.

[19] P.-C. Lin, Y.-H. Hsieh, F.-F. Liao, and S.-H. Chen, "Determination of free and total levels of phenytoin in human plasma from patients with epilepsy by MEKC: an adequate alternative to HPLC," *Electrophoresis*, vol. 31, no. 9, pp. 1572–1582, 2010.

[20] S. H. Bauquier, A. Lai, J. L. Jiang, Y. Sui, and M. J. Cook, "Evaluation of an automated spike-and-wave complex detection algorithm in the EEG from a rat model of absence epilepsy," *Neuroscience Bulletin*, vol. 31, no. 5, pp. 601–610, 2015.

[21] T. Ishihara and T. Mizushima, "Techniques for efficient entrapment of pharmaceuticals in biodegradable solid micro/nanoparticles," *Expert Opinion on Drug Delivery*, vol. 7, no. 5, pp. 565–575, 2010.

[22] N. V. N. Jyothi, P. M. Prasanna, S. N. Sakarkar, K. S. Prabha, P. S. Ramaiah, and G. Y. Srawan, "Microencapsulation techniques, factors influencing encapsulation efficiency," *Journal of Microencapsulation*, vol. 27, no. 3, pp. 187–197, 2010.

[23] J. Kluge, M. Mazzotti, and G. Muhrer, "Solubility of Ketoprofen in colloidal PLGA," *International Journal of Pharmaceutics*, vol. 399, no. 1-2, pp. 163–172, 2010.

[24] S. K. Tiwari, R. Tzezana, E. Zussman, and S. S. Venkatraman, "Optimizing partition-controlled drug release from electrospun core-shell fibers," *International Journal of Pharmaceutics*, vol. 392, no. 1-2, pp. 209–217, 2010.

[25] S. Y. Chew, J. Wen, E. K. F. Yim, and K. W. Leong, "Sustained release of proteins from electrospun biodegradable fibers," *Biomacromolecules*, vol. 6, no. 4, pp. 2017–2024, 2005.

[26] W. Cui, X. Li, X. Zhu, G. Yu, S. Zhou, and J. Weng, "Investigation of drug release and matrix degradation of electrospun poly(DL-lactide) fibers with paracetanol inoculation," *Biomacromolecules*, vol. 7, no. 5, pp. 1623–1629, 2006.

[27] J. Zeng, L. Yang, Q. Liang et al., "Influence of the drug compatibility with polymer solution on the release kinetics of electrospun fiber formulation," *Journal of Controlled Release*, vol. 105, no. 1-2, pp. 43–51, 2005.

[28] Z. Xie and G. Buschle-Diller, "Electrospun poly(D,L-lactide) fibers for drug delivery: the influence of cosolvent and the mechanism of drug release," *Journal of Applied Polymer Science*, vol. 115, no. 1, pp. 1–8, 2010.

[29] J.-P. A. Manning, D. A. Richards, N. Leresche, V. Crunelli, and N. G. Bowery, "Cortical-area specific block of genetically determined absence seizures by ethosuximide," *Neuroscience*, vol. 123, no. 1, pp. 5–9, 2004.

[30] A. A. Gurbanova, R. Aker, K. Berkman, F. Y. Onat, C. M. van Rijn, and G. van Luijtelaar, "Effect of systemic and intracortical administration of phenytoin in two genetic models of absence epilepsy," *British Journal of Pharmacology*, vol. 148, no. 8, pp. 1076–1082, 2006.

[31] S. H. Bauquier, A. Lai, J. L. Jiang, and M. J. Cook, "Clonic seizures induced by oral administration of enrofloxacin in GAERS," *Comparative Medicine*, In press.

[32] A. McRae, S. Hjorth, D. W. Mason, L. Dillon, and T. R. Tice, "Microencapsulated dopamine (DA)-induced restitution of function in 6-OHDA-denervated rat striatum in vivo: comparison between two microsphere excipients," *Journal of Neural Transplantation and Plasticity*, vol. 2, no. 3-4, pp. 165–173, 1991.

[33] A. McRae and A. Dahlström, "Transmitter-loaded polymeric microspheres induce regrowth of dopaminergic nerve terminals in striata of rats with 6-OH-DA induced parkinsonism," *Neurochemistry International*, vol. 25, no. 1, pp. 27–33, 1994.

[34] C. Gouhier, S. Chalon, M.-C. Venier-Julienne et al., "Neuroprotection of nerve growth factor-loaded microspheres on the D2 dopaminergic receptor positive-striatal neurones in quinolinic acid-lesioned rats: a quantitative autoradiographic assessment with iodobenzamide," *Neuroscience Letters*, vol. 288, no. 1, pp. 71–75, 2000.

[35] P. Menei, J. M. Pean, V. Nerrière-Daguin, C. Jollivet, P. Brachet, and J. P. Benoit, "Intracerebral implantation of NGF-releasing biodegradable microspheres protects striatum against excitotoxic damage," *Experimental Neurology*, vol. 161, no. 1, pp. 259–272, 2000.

[36] J.-M. Péan, P. Menei, O. Morel, C. N. Montero-Menei, and J.-P. Benoit, "Intraseptal implantation of NGF-releasing microspheres promote the survival of axotomized cholinergic neurons," *Biomaterials*, vol. 21, no. 20, pp. 2097–2101, 2000.

[37] B. Arica, H. S. Kaş, A. Moghdam, N. Akalan, and A. A. Hincal, "Carbidopa/levodopa-loaded biodegradable microspheres: in vivo evaluation on experimental Parkinsonism in rats," *Journal of Controlled Release*, vol. 102, no. 3, pp. 689–697, 2005.

[38] U. Sodemann, H. S. Møller, M. Blaabjerg, and C. P. Beier, "Successful treatment of refractory absence status epilepticus with lacosamide," *Journal of Neurology*, vol. 261, no. 1, pp. 2025–2027, 2014.

[39] C. E. Krewson, R. Dause, M. Mak, and W. M. Saltzman, "Stabilization of nerve growth factor in controlled release polymers and in tissue," *Journal of Biomaterials Science, Polymer Edition*, vol. 8, no. 2, pp. 103–117, 1996.

[40] C. E. Krewson, M. L. Klarman, and W. M. Saltzman, "Distribution of nerve growth factor following direct delivery to brain interstitium," *Brain Research*, vol. 680, no. 1-2, pp. 196–206, 1995.

[41] W. M. Saltzman, M. W. Mak, M. J. Mahoney, E. T. Duenas, and J. L. Cleland, "Intracranial delivery of recombinant nerve growth factor: release kinetics and protein distribution for three delivery systems," *Pharmaceutical Research*, vol. 16, no. 2, pp. 232–240, 1999.

[42] J.-C. Bensadoun, L. P. De Almeida, E. G. Fine, J. L. Tseng, N. Déglon, and P. Aebischer, "Comparative study of GDNF delivery systems for the CNS: polymer rods, encapsulated cells, and lentiviral vectors," *Journal of Controlled Release*, vol. 87, no. 1–3, pp. 107–115, 2003.

[43] C. Kellinghaus, "Lacosamide as treatment for partial epilepsy: mechanisms of action, pharmacology, effects, and safety," *Therapeutics and Clinical Risk Management*, vol. 5, no. 1, pp. 757–766, 2009.

[44] R. Bender and S. Lange, "Adjusting for multiple testing—when and how?" *Journal of Clinical Epidemiology*, vol. 54, no. 4, pp. 343–349, 2001.

Hindawi Publishing Corporation
International Journal of Polymer Science
Volume 2015, Article ID 731690, 10 pages
http://dx.doi.org/10.1155/2015/731690

Research Article

Designing of Collagen Based Poly(3-hydroxybutyrate-*co*-4-hydroxybutyrate) Scaffolds for Tissue Engineering

S. Vigneswari,[1,2] H. P. S. Abdul Khalil,[3] and A. A. Amirul[4,5]

[1] *Malaysian Institute of Pharmaceuticals and Nutraceuticals, NIBM, MOSTI, 11700 Penang, Malaysia*
[2] *Institute of Marine Biotechnology, Universiti Malaysia Terengganu, 21030 Kuala Terengganu, Malaysia*
[3] *School of Industrial Technology, Universiti Sains Malaysia, 11800 Penang, Malaysia*
[4] *School of Biological Sciences, Universiti Sains Malaysia, 11800 Penang, Malaysia*
[5] *Centre for Chemical Biology, Universiti Sains Malaysia, 11900 Penang, Malaysia*

Correspondence should be addressed to A. A. Amirul; amirul@usm.my

Received 14 September 2015; Revised 17 November 2015; Accepted 17 November 2015

Academic Editor: Yakai Feng

P(3HB-*co*-4HB) copolymer was modified using collagen by adapting dual solvent system. The surface properties of samples were characterized by Fourier transform infrared spectroscopy (FTIR), scanning electron microscopy (SEM), organic elemental analysis (CHN analysis), and water contact angle measurements. The effects of collagen concentration, scaffold thickness, and 4HB molar fraction on the hydrophilicity were optimized by the Taguchi method. The orthogonal array experiment was conducted to obtain the response for a hydrophilic scaffold. Analysis of variance (ANOVA) was used to determine the significant parameters and determine the optimal level for each parameter. The results also showed that the hydrophilicity of P(3HB-*co*-4HB)/collagen blend scaffolds increased as the collagen concentration increased up to 15 wt% with a molar fraction of 50 mol% at 0.1 mm scaffold thickness. The biocompatibility of the P(3HB-*co*-4HB)/collagen blend surface was evaluated by fibroblast cell (L929) culture. The collagen blend scaffold surfaces showed significant cell adhesion and growth as compared to P(3HB-*co*-4HB) copolymer scaffolds.

1. Introduction

Over the years, considerable effort has been channeled in developing scaffolds for tissue engineering using biodegradable and biocompatible polymeric materials. Ideally, a scaffold should mimic the structure and biological function of native extracellular matrix (ECM) proteins, which regulate cellular activities [1].

Biopolymers which are nontoxic, noncarcinogen, nongenotoxic, and biocompatible are favoured and have been widely studied for applications in tissue engineering [2]. Among the variety of biopolymers tested, poly(3-hydroxybutyrate-*co*-4-hydroxybutyrate) [P(3HB-*co*-4HB)]P(3HB-*co*-4HB) derived from microorganisms is a biocompatible material that has gained attention [3, 4]. Despite possessing desirable mechanical and physical properties, these materials have one major drawback whereby the surface of P(3HB-*co*-4HB) is hydrophobic with no recognition sites for cell attachment that limits the applicability in the tissue engineering field [5, 6]. Therefore, surface modifications by blending collagen to further enhance cell adhesion have been studied.

Collagen has been considered as a biomaterial for medical applications as it exhibits biodegradability, low antigenicity, negligible cytotoxicity, and the ability to support cell growth [7]. Collagen contains the peptide sequence Arg-Gly-Asp [RGD] that can be recognized by the cell surface and allows the attachment of native tissue cells to ECM that are composed of fibril proteins [8]. Blending collagen with other polymer materials may result in better properties that are more favourable for medical applications. The RGD peptide sequence found in collagen is the minimal cell-recognizable sequence found abundantly in ECM [8, 9].

In the present work, P(3HB-*co*-4HB)/collagen blend scaffold was prepared by facile blending via solvent casting adapting a dual solvent system to improve the hydrophilicity of P(3HB-*co*-4HB). The dual solvent system prevents the use of toxic solvents which are commonly used in polymer blending [10]. The effects of collagen concentration, scaffold thickness, and 4HB molar fraction on the hydrophilicity were optimized by the Taguchi method and significant parameters and optimal level for each parameter determined. In order to assay the cytocompatibility and cell behavior of P(3HB-*co*-4HB)/collagen scaffold, murine fibroblast cells, L929, were used to evaluate the cell attachment. Incorporating collagen onto the surface of P(3HB-*co*-4HB) may give new and interesting properties for applications in tissue engineering.

2. Experimental

2.1. Materials. The P(3HB-*co*-4HB) copolymers (20, 35, 50, and 82 mol%) used in this study were synthesized using wild-type and transformant strains of *Cupriavidus* sp. USM1020 isolated from Lake Kulim, Malaysia, in a 20 L fermenter as previously described [11]. Collagen powder from Tilapia fish skin (Hainan Zhongxin Chemical Co., Ltd., China) with high purity (95%) and molecular weight of less than 3000 Da was used. Solvents, chloroform and glacial acetic acid, were bought from R&M Chemicals, United Kingdom.

2.2. Removal of Endotoxins Using Oxidizing Agents. Inactivation and removal of endotoxins were achieved by using hydrogen peroxide, as stated previously [12]. The copolymer P(3HB-*co*-4HB) produced was dissolved in chloroform 2% (w/v) at 60°C. Three aliquots of 55 μL/g of hydrogen peroxide solution (30% in water) were added to the solution at intervals of 20 minutes at 60°C. The polymer solution was cooled and the copolymer was precipitated using methanol. The endotoxin levels were tested using E-TOXATE Kits (Sigma-Aldrich).

2.3. Fabrication of P(3HB-co-4HB)/Collagen Blend Scaffolds by Facile Blending. Collagen powder of different weight ratios (5, 10, and 15 wt%) was dissolved in glacial acetic acid solution (8 wt%). An amount of 0.42 g or 0.83 g which was previously optimized weight of P(3HB-*co*-4HB) copolymer was dissolved in 15 or 20 mL of chloroform and collagen solution was added under vigorous stirring. The solution was poured into glass Petri dish (diameter of 5 cm) as a casting surface. The scaffolds were then air-dried (24 h) and later vacuum-dried for 48 h using BINDER GmbH VD 23 (BINDER GmbH, Germany) to remove any remaining solvent. The thickness of the scaffolds was measured using Teclock dial thickness gauge (Teclock, Japan). Scaffolds in thickness of 0.1 mm (prepared using 0.42 g) and 0.2 mm (prepared using 0.83 g) were formed.

2.4. Fourier Transform Infrared (FTIR) Spectroscopy. The FTIR spectroscope (Perkin Elmer Spectrum GX) was used to analyze the functional groups present in the P(3HB-*co*-4HB) copolymer, collagen, and blend scaffolds. The spectra of each sample were obtained in the range of 4000–500 cm^{-1} at a resolution of 4 cm^{-1}. The spectral outputs were recorded in transmittance as a function of wave number.

2.5. Determination of Amino Groups Using Ninhydrin. The collagen density on the P(3HB-*co*-4HB)/collagen scaffolds was determined using ninhydrin. Ninhydrin was used as an indicator to qualitatively and quantitatively detect the presence of NH_2 groups on the P(3HB-*co*-4HB)/collagen scaffolds. The scaffolds fabricated were cut into 10 mm × 10 mm and immersed in 1.0 mol/L ninhydrin/ethanol solution. The pieces of scaffolds were later placed in glass tubes and heated at 80°C using Memmert water baths (Memmert GmbH, Germany) for 10 mins for accelerating the reaction between ninhydrin and amino groups. Later, 5 mL of chloroform was quickly added to the tube to dissolve the scaffolds. When the scaffolds displayed purple, 2-propanol (5 mL) was added to stabilize the blue compound. The OD was measured at 560 nm. A calibration curve using known concentration of 1,6-hexanediamine in chloroform/2-propanol (1/1, v/v) was obtained.

2.6. Organic Elemental Analysis (CHN). The organic elemental analysis is conducted to measure the C, H, and N content in the scaffolds fabricated using the CHN Elemental Analyzer 2400 Series II with AD-6 Autobalance (PerkinElmer, USA). The elemental analyzer was operated with constant helium flow as the carrier gas. The heating temperature was maintained constant at 925 for the combustion column and 640°C for the reduction column. Approximately 2 mg of sample is used for each measurement. The samples are weighed using AD-6 Autobalance (PerkinElmer, USA). Cystine was used as the standard.

2.7. Water Contact Angle Determination. The contact angles of the fabricated scaffolds were measured using KSV CAM 101 Series Drop Shape Analysis Contact Angle Meter. The scaffolds were placed flat and a droplet of distilled water was placed on the scaffold by pressing the dropper. The drop was observed on the computer screen and the value of the contact angle was calculated using the computer.

2.8. Scanning Electron Microscopy (SEM). The morphologies of the films and scaffolds were also observed using scanning electron microscopy (SEM) (Leo Supra 50 VP Field Mission SEM, Carl-Ziess SMT, Oberkochen, Germany). The dried samples were mounted on aluminium stumps coated with gold in a sputtering device before viewing under the SEM.

2.9. In Vitro Cytotoxicity Evaluation. Various P(3HB-*co*-4HB)/collagen blend scaffolds were cut in size (6 mm in diameter) fitting the 96-well flat bottom culture plate and sterilized under GERMICIDE UV Steriliser (CA-MI, Italy) for 1 hour. The scaffolds were then placed in the 96-well flat bottom culture plate. Cells were seeded at 5×10^4 cells/mL and were incubated in a 5% CO_2 incubator at 37°C for 24 and 72 h. The cells viability and proliferation were assayed with MTS (3-(4,5-dimethylthiazol-2-yl)-5-(3-carboxymethoxyphenyl)-2-(4-sulfophenyl)-2H-tetrazolium)/PMS(phenazine methosulfate).

Table 1: Endotoxin levels present in the P(3HB-*co*-4HB) scaffolds recovered by the chloroform extraction method before and after pyrogen removal.

Polymer	Endotoxin before pyrogen removal (EU/g)	Endotoxin after pyrogen removal (EU/g)
P(3HB-*co*-20% 4HB)	16 ± 2	0.5 ± 0.1
P(3HB-*co*-35% 4HB)	16 ± 1	1.0 ± 0.2
P(3HB-*co*-50% 4HB)	32 ± 2	1.0 ± 0.3
P(3HB-*co*-82% 4HB)	16 ± 1	0.5 ± 0.1

3. Results and Discussion

3.1. Pyrogen Removal. Pyrogen removal was required since PHA polymers produced by Gram-negative bacteria are known to exhibit the presence of endotoxins [12]. The endotoxin levels of the copolymers before and after pyrogen removal are shown in Table 1. The copolymers recovered by the chloroform extraction method recorded endotoxin levels in the range of 16–32 EU/g. Rapid decrease in endotoxin value was seen after pyrogen removal (0.5–1 EU/g). According to the US Food and Drug Administration guideline, the range of endotoxin permitted in PHA used for medical applications should possess 4-5 EU/g [13]. Therefore, the P(3HB-*co*-4HB) copolymers produced here were suitable for *in vivo* applications after endotoxin removal.

3.2. Fabrication of P(3HB-co-4HB)/Collagen Blend by Simple Blending. The fabrication of P(3HB-*co*-4HB)/collagen blend scaffold was carried out by facile blending combining two different solvents. This method was modified from previous work carried out [14]. Conversely, in another study, a single common solvent was used to dissolve both P(3HB-*co*-4HB) and collagen using 1,1,3,3,3-hexafluoro-2-propanol (HFIP) to fabricate P(3HB-*co*-4HB)/collagen blend by simple blending technique [12]. In fabricating blends, these solvents present a challenge to be completely removed from the scaffolds as strong hydrogen bonds can be formed with the blend. Moreover, recent research has suggested that collagen fibers from HFIP lack native ultrastructure [15]. Thus, a judicious choice of using these two different solvents which could mimic the nature of toxic solvents such as HFIP was used.

Here, two different solvents were combined in the solution processing to fabricate the P(3HB-*co*-4HB)/collagen blend. The P(3HB-*co*-4HB) copolymer was dissolved in chloroform whereas the collagen which was soluble in acidic solvents was dissolved in glacial acetic acid (3 mL). Since the organic solvent chloroform was used to dissolve P(3HB-*co*-4HB), the presence of water was prevented to avoid phase separation in the blend. The volume of acetic acid to chloroform was maintained at 2 : 13 in all the blending process in order to obtain a homogenous solution. The collagen content in the blend scaffold was only up to 15 wt% as further increment left large holes on the scaffold. This could be due to the fast evaporation rate of P(3HB-*co*-4HB) in chloroform as compared to collagen in acetic acid leaving behind large holes as the amount of collagen increases in the scaffold.

Table 2: CHN analysis of P(3HB-*co*-50 mol% 4HB)/collagen blends.

Polymer	Carbon (%)	Hydrogen (%)	Nitrogen (%)
P(3HB-*co*-4HB)[a]	56.24	7.25	0.0
P(3HB-*co*-4HB)/5 wt% collagen	17.54	7.16	63.71
P(3HB-*co*-4HB)/10 wt% collagen	15.47	6.78	68.16
P(3HB-*co*-4HB)/15 wt% collagen	13.65	5.43	73.87
Cysteine[b]	30.54	5.02	12.05

[a]P(3HB-*co*-50 mol% 4HB) was used as control.
[b]Standard.

3.3. Determination of Surface Chemical Composition on the P(3HB-co-4HB)/Collagen Blend. The elemental analysis of C, H, and N is used to further determine the presence of N element present in the P(3HB-*co*-4HB)/collagen blend scaffolds. As it is, collagen which is a protein contains N element, whereas P(3HB-*co*-4HB) does not naturally contain N. Therefore, blending of collagen with P(3HB-*co*-4HB) will result in the presence of N in P(3HB-*co*-4HB)/collagen blends. Based on Table 2, the incorporation of collagen onto the P(3HB-*co*-4HB) by simple blending technique was evident by observing the presence of N element through C, H, and N analysis. The copolymer without the incorporation of collagen did not have the additional nitrogen group. The analysis clearly shows the composition enhancement of N element in P(3HB-*co*-4HB)/5 wt% collagen blend scaffolds of 63.71% as compared to P(3HB-*co*-4HB) copolymer scaffold. Besides that, it was also observed that P(3HB-*co*-4HB)/collagen blend scaffolds recorded an increase in percentage of N element as the collagen concentration increased to 15 wt% recording an increase of 1.15-fold. Similar C, H, and N elemental analysis was carried out previously to determine the presence of N element on modified silica surface blended with mercaptopropyl [16].

FTIR studies were carried out to monitor chemical modifications on the P(3HB-*co*-4HB)/collagen blend scaffolds. All peaks corresponding to P(3HB-*co*-4HB) and collagen were observed. Based on the FTIR spectrum in Figure 1(a), collagen was identified based on the presence of amide I band at 1634 cm^{-1} and amide II band at 1526 cm^{-1}. The broad band at 3300 in collagen is due to N-H stretching [17]. In the natural P(3HB-*co*-4HB) polymer (Figure 1(b)), the characteristic absorption band at 1720 cm^{-1} was mainly due to ester carbonyl group [18, 19]. In P(3HB-*co*-4HB)/collagen blends, both amides I and II and ester carbonyl group were observed. The spectra of P(3HB-*co*-4HB)/collagen blends with different collagen concentration of 5–15 wt% (Figures 1(c)–1(e)) were quite similar to each other but the changes in the content of collagen from 5, 10, and 15 wt% were revealed in the spectra with the changing proportion of collagen. Prominent change was the change in the amide I and amide II intensity as the collagen intensity increased.

3.4. Hydrophilicity of P(3HB-co-4HB)/Collagen Blend Using Taguchi Method. The hydrophilicity was measured using water contact angle meter. Water contact angle was used to

Table 3: The variables for P(3HB-*co*-4HB)/collagen blend fabrication using Taguchi method.

Symbol	Scaffold parameters	Level 1	Level 2	Level 3	Level 4
A	Scaffold thickness	0.1	0.2	—	—
B	4HB molar fraction	20	35	50	82
C	Collagen concentration	5	10	15	—

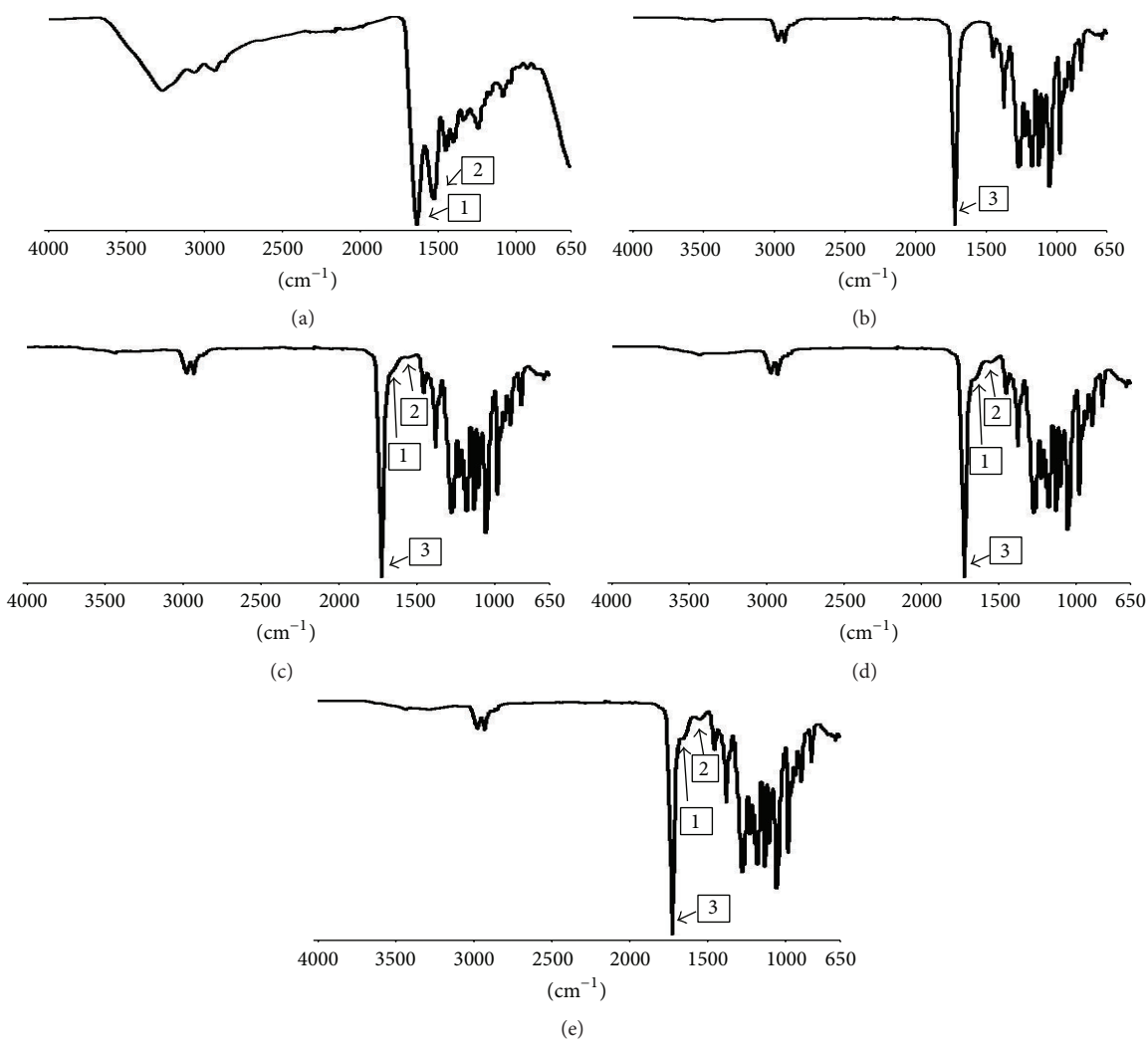

Figure 1: FTIR spectra of simple blend scaffolds: (a) collagen, (b) P(3HB-*co*-4HB), (c) P(3HB-*co*-4HB)/5 wt% collagen, (d) P(3HB-*co*-4HB)/10 wt% collagen, and (e) P(3HB-*co*-4HB)/15 wt% collagen. Arrows 1, 2, and 3 indicate amide I, amide II, and ester group, respectively.

characterize interfacial wetting phenomena which directly relates to the hydrophilicity of a biomaterial [20]. Studies have shown that increase in hydrophilicity is attributed to the possibility of improving the biocompatibility of a biomaterial scaffold [20]. The hydrophilicity of the P(3HB-*co*-4HB)/collagen blend scaffold was determined using water contact angle analysis. A number of research efforts have shown that comonomer composition [14] and collagen concentration [17] were investigated as potential factors affecting scaffold hydrophilicity. As shown in Table 3, 4HB composition, collagen concentrations, and scaffold thickness were investigated. The scaffold thickness was also considered because a previous study using collagen-chitosan porous scaffold as wound dressing demonstrated scaffold thickness as potential factors improving wound healing [21].

Taguchi method is efficient in designing optimizing parameters over a variety of conditions [22]. Here, Taguchi design of L_{32} ($2^1 \times 4^9$ orthogonal array) was used to analyze the optimum scaffold fabrication parameters to get lowest water contact angle. The dependent variable is water contact angle which denotes hydrophilicity. A total of 32 responses (water contact angle) based on the designed parameters are shown in Table 4. According to the ANOVA results (Table 5), the parameters 4HB molar fraction and collagen concentration were found to be statistically significant at a confidence level of 95%.

Table 4: Variables of P(3HB-*co*-4HB)/collagen blend scaffold fabrication and response.

Run	Scaffold thickness (mm) *A*	4HB molar fraction (mol%) *B*	Collagen concentration (5 mg/mL) *C*	Water contact angle (°)
1	0.1	35	10	57.2 ± 1.7
2	0.1	50	0	73.2 ± 1.2
3	0.2	35	15	51.3 ± 0.9
4	0.1	20	5	80.1 ± 1.1
5	0.2	20	15	64.0 ± 1.3
6	0.2	50	5	68.3 ± 0.5
7	0.1	20	15	62.3 ± 1.6
8	0.1	20	0	81.2 ± 1.3
9	0.2	82	0	53.2 ± 1.0
10	0.1	50	5	68.9 ± 1.2
11	0.1	50	15	44.5 ± 1.1
12	0.1	35	15	52.4 ± 1.3
13	0.2	50	15	61.3 ± 1.7
14	0.1	82	10	49.2 ± 1.6
15	0.2	20	10	74.1 ± 0.8
16	0.2	82	15	48.1 ± 1.3
17	0.2	50	0	69.8 ± 1.4
18	0.2	20	0	79.8 ± 1.1
19	0.2	20	5	77.5 ± 1.2
20	0.2	82	10	53.0 ± 1.8
21	0.1	50	10	64.6 ± 1.3
22	0.2	35	5	73.3 ± 1.7
23	0.2	35	0	76.6 ± 0.6
24	0.2	35	10	64.3 ± 0.9
25	0.2	82	5	51.9 ± 0.6
26	0.1	35	5	63.3 ± 1.1
27	0.1	82	5	55.2 ± 1.3
28	0.2	50	10	68.7 ± 1.6
29	0.1	82	0	56.7 ± 1.9
30	0.1	82	15	45.4 ± 1.3
31	0.1	35	0	78.4 ± 1.5
32	0.1	20	10	73.6 ± 1.7

Table 5: ANOVA for P(3HB-*co*-4HB)/collagen blend fabrication.

	SS[a]	d.f.	MS[b]	*F* value	Prob. > *F*	Contribution %	
Model	4009.49	22	182.25	8.91	0.0010	—	Significant
A	64.70	1	64.70	3.16	0.1091	1.61	
B	2041.94	3	680.65	33.27	<0.0001	50.93	
C	1476.01	3	492.00	24.05	0.0001	36.81	
AB	98.95	3	32.98	1.61	0.2541	2.47	
AC	119.57	3	39.86	1.95	0.1925	2.98	
BC	208.32	9	23.15	1.13	0.4285	5.2	
Residual	184.12	9	20.46				
Cor. total	4193.61	31					

[a]Sum square.
[b]Mean square.
% contribution = SS/total of SS.

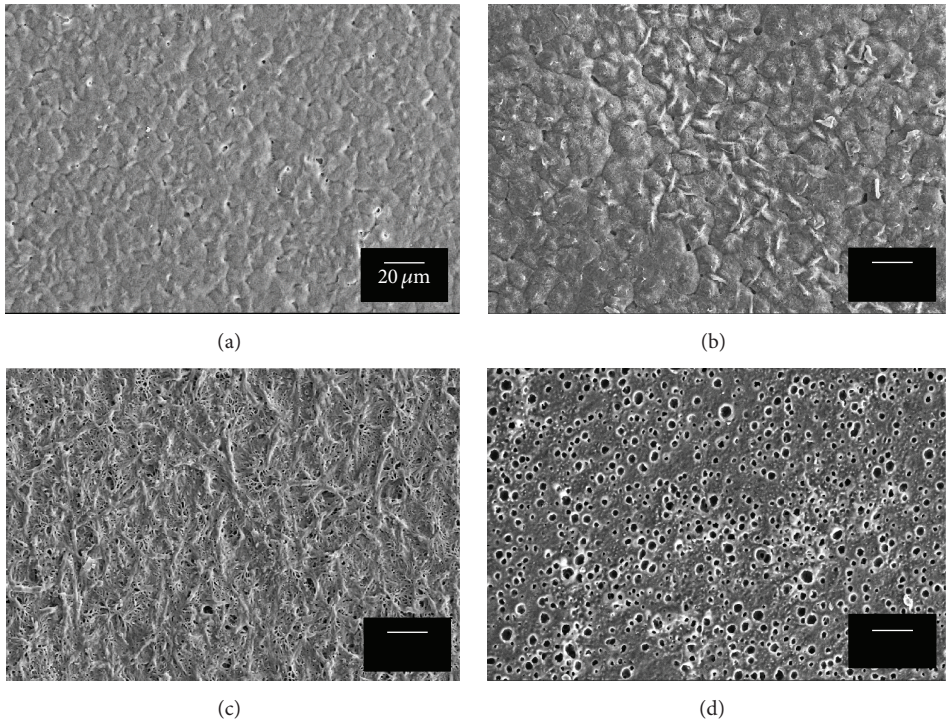

Figure 2: SEM images of surface morphology of (a) P(3HB-*co*-50 mol% 4HB), (b) P(3HB-*co*-50 mol% 4HB)/5 wt% collagen, (c) P(3HB-*co*-50 mol% 4HB)/10 wt% collagen, and (d) P(3HB-*co*-50 mol% 4HB)/15 wt% collagen.

However, it is evident that 4HB molar fraction contributes the highest with 50.93% to the water contact angle of the scaffold. The collagen concentration is the next contributing factor having 36.81% on water contact angle. Nevertheless, the result showed there were no significant interactions between the parameters tested.

The factorial analysis gave a predictive model which formed as an equation obtained by the Taguchi method shown as

$$\begin{aligned}\text{Water contact angle} = {} & +64.16 + 0.54 * A + 9.92 \\ & * B[1] + 0.44 * B[2] + 2.21 \\ & * B[3] + 6.96 * C[1] + 3.56 \\ & * C[2] - 1.07 * C[3] - 0.77 \\ & * AB[1] + 1.23 * AB[2] \\ & + 0.12 * AB[3] - 1.81 \\ & * AC[1] - 0.51 * AC[2] \\ & + 1.39 * AC[3] - 0.53 \\ & * B[1]C[1] + 5.94 \\ & * B[2]C[1] - 1.82 \\ & * B[3]C[1] + 1.17 \\ & * B[1]C[2] + 0.14 \\ & * B[2]C[2] + 0.28 \\ & * B[3]C[2] + 0.84 \\ & * B[1]C[3] - 2.78 \\ & * B[2]C[3] + 1.36 \\ & * B[3]C[3]. \end{aligned} \quad (1)$$

Based on the results generated using the Taguchi method, P(3HB-*co*-50 mol% 4HB)/15 wt% collagen with 0.1 mm thickness recorded the lowest water contact angle of 44.5°. This was further proved by the SEM analysis carried out to determine the surface morphologies of the scaffolds. It was observed that the P(3HB-*co*-50 mol% 4HB)/15 wt% collagen blend surface (Figure 2(d)) has more irregular large open pores with rougher surfaces as compared to the other P(3HB-*co*-4HB)/collagen blend surface (Figures 2(a)–2(c)). The P(3HB-*co*-50 mol% 4HB)/5 wt% and P(3HB-*co*-50 mol% 4HB)/10 wt% collagen blend surfaces were wave-like with small closed-pores probably resulting from the evaporation of solvent during the fabrication of the scaffold. However, it was evident that P(3HB-*co*-4HB) scaffold surface becomes more porous after blending. Rougher surface was observed as the collagen concentration increased from 5 to 15 wt% as compared to P(3HB-*co*-4HB) scaffold without collagen (Figures 2(a)–2(d)). Previous research exhibited porous P(3HB-*co*-4HB) scaffolds with improved wettability after blending with collagen [12]. Thus, the surface porosity increases and at the same time increases the surface area of the scaffolds which contributes to enclosing large amount of water on the surface. However, the fast evaporation of chloroform as compared to

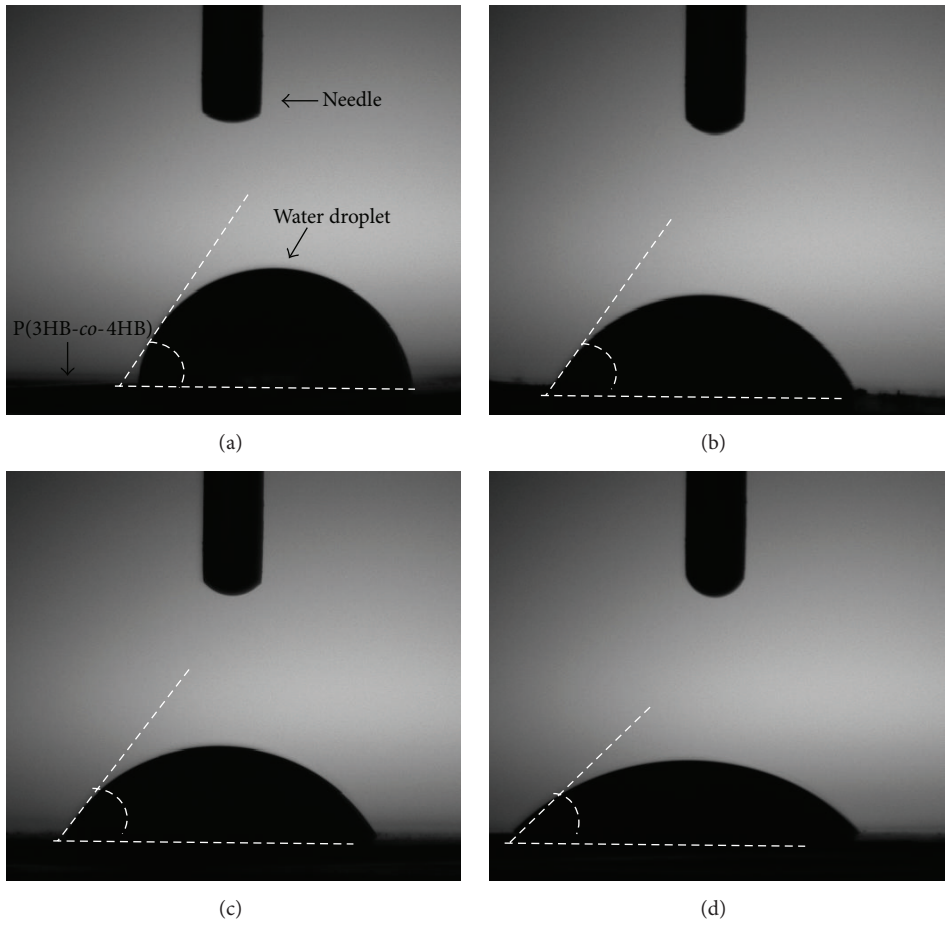

Figure 3: Sessile drops for static water contact angle measurement of 0.1 mm thick (a) P(3HB-*co*-50 mol% 4HB) (control) [73.2°], (b) P(3HB-*co*-50 mol% 4HB)/5 mg collagen [68.9°], (c) P(3HB-*co*-50 mol% 4HB)/10 mg collagen [64.6°], and (d) P(3HB-*co*-50 mol% 4HB)/15 mg collagen [44.5°].

the acetic acid used in fabricating the blend left large visible holes on the scaffold blends.

Figures 3(a)–3(d) show the static contact angles for water drops on 0.1 mm thick P(3HB-*co*-50 mol% 4HB), P(3HB-*co*-50 mol% 4HB)/5 wt% collagen, P(3HB-*co*-50 mol% 4HB)/10 wt% collagen, and P(3HB-*co*-50 mol% 4HB)/15 wt% collagen blends. The static water contact angles of water for the various substrates were measured in various sample locations. The decrease in contact angle from P(3HB-*co*-50 mol% 4HB) to P(3HB-*co*-50 mol% 4HB)/15 wt% collagen was evident. The contact angle is quantified as the angle formed by the intersection of the liquid-solid interface. Figure 3(d) shows the smallest contact angle (44.5°) as the water droplet spreads on the surface as compared to the large contact angle observed in Figure 3(a) [73.2°] when the water droplet beaded on the surface. It can be seen that as the collagen concentration increases, the water contact angle decreases.

3.5. Biocompatibility and Cytotoxicity of P(3HB-co-4HB)/Collagen Blend Scaffolds via In Vitro Cell Proliferation. The ability to support attachment and promote proliferation of cultured cells is a prerequisite of a functional biomedical scaffold. In order to evaluate cellular behavior or cell growth, L929 fibroblasts cells were seeded onto the various P(3HB-*co*-4HB)/collagen blend scaffolds fabricated. In general L929 cell numbers increased on all scaffolds over the time period of 3 days as compared to the initial seeding. Incorporation of collagen was found to further improve cytocompatibility. Cell counts on collagen blends improved greatly compared with those without collagen (Figure 4). This was also evident with increasing collagen concentration recording highest proliferation rate of cells with scaffolds blend of 15 wt% collagen. This can be attributed to the fact that collagen has high water affinity, low antigenicity, and a key element in extracellular matrix (ECM) which contributes to the good cell compatibility [23]. This was further supported by previous research which reported collagen to stimulate differentiation of cartilage tissue [24]. The P(3HB-*co*-50 mol% 4HB)/collagen blend scaffold showed significantly higher proliferation rate with various collagen concentration than other scaffold blends. At 15 wt% collagen concentration, 0.1 mm thick and 0.2 mm P(3HB-*co*-50 mol% 4HB)/collagen blend scaffold measured a significantly higher cell number (>1.62-fold and >1.38-fold, resp.) than the initial seeding for the L929.

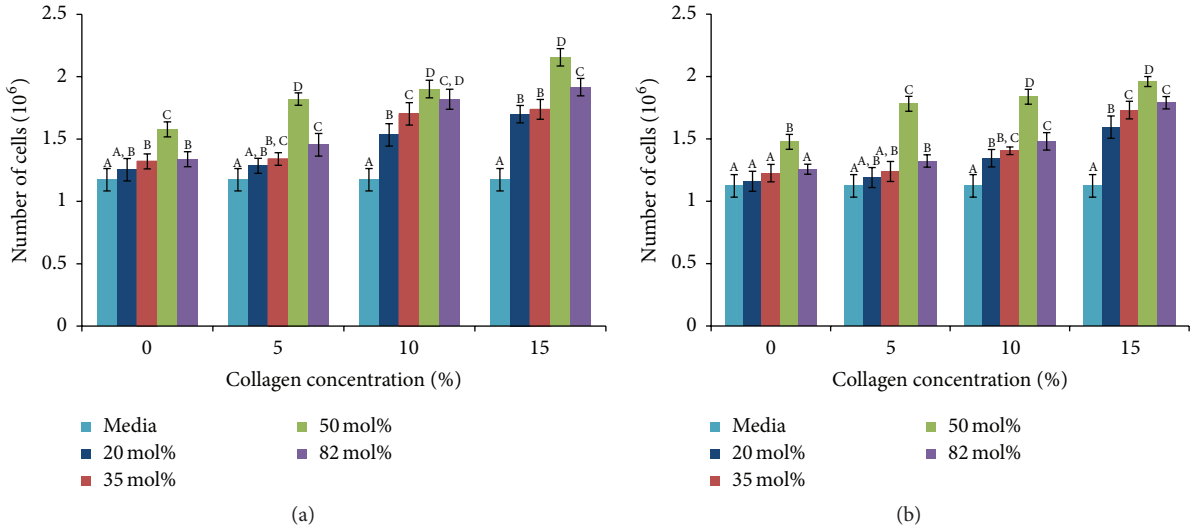

Figure 4: (a) Proliferation of L929 cells on day 3 seeded on the various P(3HB-*co*-4HB)/collagen blend scaffold of varying collagen concentration with 0.1 mm thickness. Values are mean of four replicates. Mean data accompanied by different alphabets indicates significant difference within the group (Tukey's HSD test, $p < 0.05$). (b) Proliferation of L929 cells on day 3 seeded on the various P(3HB-*co*-4HB)/collagen blend scaffold of varying collagen concentration with 0.2 mm thickness. Values are mean of four replicates. Mean data accompanied by different alphabets indicates significant difference within the group (Tukey's HSD test, $p < 0.05$).

Proliferation of cells on the PHA scaffolds increased in the order of P(3HB-*co*-20 mol% 4HB) < P(3HB-*co*-35% 4HB) < P(3HB-*co*-82 mol% 4HB) < P(3HB-*co*-50 mol% 4HB) for both 0.1 and 0.2 mm scaffold thickness. The results correlate with the similar pattern of increase in hydrophilicity. The highest hydrophilicity of 44.5° (Figure 3(d)) is recorded by P(3HB-*co*-50 mol% 4HB)/15 mg collagen blend scaffold. Interestingly, the fibroblast cell proliferation was also found to be influenced by the thickness of the scaffolds. It can be observed that 0.1 mm thick P(3HB-*co*-4HB)/collagen blend scaffold showed an increase in proliferation rate as compared to 0.2 mm collagen scaffolds for L929 fibroblast cells (Figures 4(a) and 4(b)). The results indicate that optimization of film thickness could produce significant enhancements in initial adhesion and subsequent growth of the L929 cells. Similar observation has been reported earlier where growth rate of human aortic endothelial cells (HAEC) on poly(vinylacetic acid) scaffold was dependent on film thickness and cell proliferation increased as the film thickness decreased to 0.2×10^{-3} mm [25]. It has been reported that degree of roughness could increase protein adsorption and cell attachment, hence providing anchorage as well as space for cell growth [26]. Notably, surface roughness greatly influences the interactions between cells and materials [27]. The surface morphology observed with SEM analysis also indicated a rough and porous surface of P(3HB-*co*-50 mol% 4HB)/15 mg collagen blend scaffold (Figure 2(d)) which explains the highest hydrophilicity, thus contributing to the highest proliferation rate on this collagen blend scaffold (Figure 5).

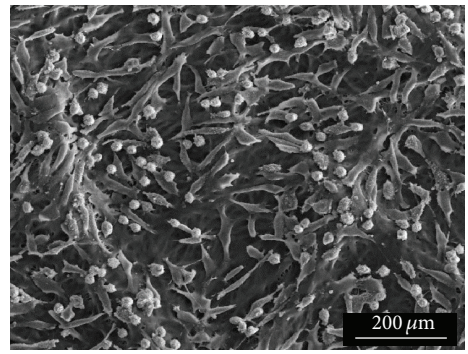

Figure 5: SEM micrographs of proliferation of L929 cells on P(3HB-*co*-50 mol% 4HB)/15 mg collagen.

4. Conclusion

Collagen was incorporated onto the P(3HB-*co*-4HB) copolymer to enhance the hydrophilicity for application in tissue engineering. Dual solvent system was adapted to minimize the use of toxic solvents. FTIR, CHN analysis, and SEM analysis were carried out to further confirm the modification process. Various parameters such as collagen concentration, thickness of the scaffold, and 4HB molar fraction were investigated in fabricating a scaffold with increases of hydrophilicity as an ideal scaffold material in tissue engineering. The parameters were optimized using Taguchi method. It can be deduced that the P(3HB-*co*-4HB)/collagen blend scaffold with increased collagen concentration of up to 15 wt%, with molar fraction of 50 mol% and thickness of 0.1 mm, increased hydrophilicity and thus increased the L929 cell proliferation on the surface. This study shows that surface modification by blending biomacromolecules can enhance the biocompatibility of a polymeric material.

Conflict of Interests

The authors declare that there is no conflict of interests regarding the publication of this paper.

Acknowledgment

The authors thank Ministry of Science, Technology and Innovation (MOSTI) for the e-science fund financial support (Grant no. 02-05-23-SF0003).

References

[1] Y. P. Jiao and F. Z. S. Cui, "Surface modification of polyester biomaterials for tissue engineering," *Biomedical Materials*, vol. 2, no. 4, pp. 24–37, 2007.

[2] S. F. Williams, D. P. Martin, D. M. Horowitz, and O. P. Peoples, "PHA applications: addressing the price performance issue I. Tissue engineering," *International Journal of Biological Macromolecules*, vol. 25, no. 1–3, pp. 111–121, 1999.

[3] T. H. Ying, D. Ishii, A. Mahara et al., "Scaffolds from electrospun polyhydroxyalkanoate copolymers: fabrication, characterization, bioabsorption and tissue response," *Biomaterials*, vol. 29, no. 10, pp. 1307–1317, 2008.

[4] D. P. Martin and S. F. Williams, "Medical applications of poly-4-hydroxybutyrate: a strong flexible absorbable biomaterial," *Biochemical Engineering Journal*, vol. 16, no. 2, pp. 97–105, 2003.

[5] S. Rathbone, P. Furrer, J. Lübben, M. Zinn, and S. Cartmell, "Biocompatibility of polyhydroxyalkanoate as a potential material for ligament and tendon scaffold material," *Journal of Biomedical Materials Research Part A*, vol. 93, no. 4, pp. 1391–1403, 2010.

[6] F. J. O. Brien, "Biomaterials & scaffolds for tissue engineering," *Materials Today*, vol. 14, no. 3, pp. 88–95, 2011.

[7] S. M. Rezaei and Z. A. Mohd Ishak, "Grafting of collagen onto interpenetrating polymer networks of poly(2-hydroxyethyl methacrylate) and poly(dimethyl siloxane) polymer films for biomedical applications," *Express Polymer Letters*, vol. 8, no. 1, pp. 39–49, 2014.

[8] S. D. Gorham, S. Srivastava, D. A. French, and R. Scott, "The effect of gamma-ray and ethylene oxide sterilization on collagen-based wound-repair materials," *Journal of Materials Science: Materials in Medicine*, vol. 4, no. 1, pp. 40–49, 1993.

[9] Y.-Y. Wang, L.-X. Lü, J.-C. Shi, H.-F. Wang, Z.-D. Xiao, and N.-P. Huang, "Introducing RGD peptides on PHBV films through PEG-containing cross-linkers to improve the biocompatibility," *Biomacromolecules*, vol. 12, no. 3, pp. 551–559, 2011.

[10] D. I. Zeugolis, S. T. Khew, E. S. Y. Yew et al., "Electro-spinning of pure collagen nano-fibres—just an expensive way to make gelatin?" *Biomaterials*, vol. 29, no. 15, pp. 2293–2305, 2008.

[11] A. A. Amirul, A. R. M. Yahya, K. Sudesh, M. N. M. Azizan, and M. I. A. Majid, "Biosynthesis of poly(3-hydroxybutyrate-*co*-4-hydroxybutyrate) copolymer by *Cupriavidus* sp. USMAA1020 isolated from Lake Kulim, Malaysia," *Bioresource Technology*, vol. 99, no. 11, pp. 4903–4909, 2008.

[12] U. Rao, R. Kumar, S. Balaji, and P. K. Sehgal, "A novel biocompatible poly(3-hydroxy-*co*-4-hydroxybutyrate) blend as a potential biomaterial for tissue engineering," *Journal of Bioactive and Compatible Polymers*, vol. 26, pp. 452–463, 2011.

[13] S. Y. Lee, J.-I. Choi, K. Han, and J. Y. Song, "Removal of endotoxin during purification of poly(3-hydroxybutyrate) from gram-negative bacteria," *Applied and Environmental Microbiology*, vol. 65, no. 6, pp. 2762–2764, 1999.

[14] M. Rennukka and A. A. Amirul, "Fabrication of poly(3-hydroxybutyrate-*co*-4-hydroxybutyrate)/chitosan blend material: synergistic effects on physical, chemical, thermal and biological properties," *Polymer Bulletin*, vol. 70, no. 6, pp. 1937–1957, 2013.

[15] B. Dong, O. Arnoult, M. E. Smith, and G. E. Wnek, "Electrospinning of collagen nanofiber scaffolds from benign solvents," *Macromolecular Rapid Communications*, vol. 30, no. 7, pp. 539–542, 2009.

[16] N. H. Khdary, M. A. Ghanem, M. G. Merajuddine, and F. M. Bin Manie, "Incorporation of Cu, Fe, Ag, and Au nanoparticles in mercapto-silica (MOS) and their CO_2 adsorption capacities," *Journal of CO_2 Utilization*, vol. 5, pp. 17–23, 2014.

[17] L.-Y. Wang, Y.-J. Wang, and D.-R. Cao, "Surface modification of poly(3-hydroxybutyrate-*co*-3-hydroxyvalerate) membrane by combining surface aminolysis treatment with collagen immobilization," *Journal of Macromolecular Science, Part A: Pure and Applied Chemistry*, vol. 46, no. 8, pp. 765–773, 2009.

[18] N. Nagiah, L. Madhavi, R. Anitha, N. T. Srinivasan, and U. T. Sivagnanam, "Electrospinning of poly(3-hydroxybutyric acid) and gelatin blended thin films: fabrication, characterization, and application in skin regeneration," *Polymer Bulletin*, vol. 70, no. 8, pp. 2337–2358, 2013.

[19] K. Kansiz, H. Billman-Jacobe, and D. McNaughton, "Quantitative determination of the biodegradable polymer poly(β-hydroxybutyrate) in a recombinant *Escherichia coli* strain by use of mid-infrared spectroscopy and multivariative statistics," *Applied and Environmental Microbiology*, vol. 66, no. 8, pp. 3415–3420, 2000.

[20] H. P. S. Abdul Khalil and N. L. Suraya, "Anhydride modification of cultivated kenaf bast fibers: morphological, spectroscopic, and thermal studies," *BioResources*, vol. 6, no. 2, pp. 1122–1135, 2011.

[21] S. Haifei, W. Xingang, W. Shoucheng, M. Zhengwei, Y. Chuangang, and H. Chunmao, "The effect of collagen—chitosan porous scaffold thickness on dermal regeneration in a one-stage grafting procedure," *Journal of the Mechanical Behavior of Biomedical Materials*, vol. 29, pp. 114–125, 2014.

[22] A. Canakci, F. Erdemir, T. Varol, and A. Patir, "Determining the effect of process parameters on particle size in mechanical milling using the Taguchi method: measurement and analysis," *Measurement*, vol. 46, no. 9, pp. 3532–3540, 2013.

[23] S. A. Sell, M. J. McClure, K. Garg, P. S. Wolfe, and G. L. Bowlin, "Electrospinning of collagen/biopolymers for regenerative medicine and cardiovascular tissue engineering," *Advanced Drug Delivery Reviews*, vol. 61, no. 12, pp. 1007–1019, 2009.

[24] J. Glowacki and S. Mizuno, "Collagen scaffolds for tissue engineering," *Biopolymers*, vol. 89, no. 5, pp. 338–344, 2008.

[25] D. Bhattacharyya, H. Xu, R. R. Deshmukh, R. B. Timmons, and K. T. Nguyen, "Surface chemistry and polymer film thickness effects on endothelial cell adhesion and proliferation," *Journal of Biomedical Materials Research Part A*, vol. 94, no. 2, pp. 640–648, 2010.

[26] Y.-J. Hu, X. Wei, W. Zhao, Y.-S. Liu, and G.-Q. Chen, "Biocompatibility of poly(3-hydroxybutyrate-*co*-3-hydroxyvalerate-*co*-3-hydroxyhexanoate) with bone marrow mesenchymal stem cells," *Acta Biomaterialia*, vol. 5, no. 4, pp. 1115–1125, 2009.

[27] Y.-S. Liang, W. Zhao, and G.-Q. Chen, "Study on the biocompatibility of novel terpolyester poly(3-hydroxybutyrate-*co*-3-hydroxyvalerate-*co*-3-hydroxyhexanoate)," *Journal of Biomedical Materials Research Part A*, vol. 87, no. 2, pp. 441–449, 2008.

Hindawi Publishing Corporation
International Journal of Polymer Science
Volume 2015, Article ID 231059, 7 pages
http://dx.doi.org/10.1155/2015/231059

Research Article

Direct Synthesis of Hyperbranched Poly(acrylic acid-co-3-hydroxypropionate)

Efkan Çatıker and Tahsin Filik

Department of Chemistry, Faculty of Art & Science, Ordu University, 52200 Ordu, Turkey

Correspondence should be addressed to Efkan Çatıker; ecatiker@gmail.com

Received 29 July 2015; Revised 18 October 2015; Accepted 25 October 2015

Academic Editor: Vitor Sencadas

Hyperbranched poly(acrylic acid-co-3-hydroxypropionate) (PAcHP) was synthesized by base-catalyzed hydrogen transfer polymerization of acrylic acid through one step. The copolymers obtained through solution and bulk polymerization were insoluble in water and all organic solvents tried. Structural and compositional characterizations of hyperbranched PAcHP were performed by using FTIR, solid ^{13}C-NMR, TGA, and titrimetric analysis. Acrylate fraction of the hyperbranched PAcHP obtained via bulk polymerization was determined as 60–65% by comparing TGA curves of hyperbranched PAcHP and pure poly(3-hydroxy propionate) (PHP). However, analytical titration of the same sample revealed that acrylic acid units were about 47.3%. The results obtained from TGA and analytical titration were used to evaluate the chemical structure of the copolymer. Hyperbranched PAcHP exhibited hydrogel properties. Swelling behavior of the copolymer was investigated at a wide pH range and ionic strength. The dynamic swelling profiles of hyperbranched PAcHP exhibited a fast swelling behavior in the first hour and achieved the equilibrium state within 12 h in PBS. Depending on the conditions, the copolymers exhibited swelling ratios up to 2100%. As the copolymer has easily biodegradable propionate and versatile functional acrylic acid units, it can be used as not only biodegradable material in medical applications but also raw material in personal care commodities.

1. Introduction

Base-catalyzed hydrogen transfer polymerization (HTP) is an anionic polymerization route applied to vinyl monomers containing loose hydrogen atom(s). Strong bases as an initiator, a radical polymerization inhibitor, and an aprotic solvent (in case of solution polymerization) are used to perform the polymerization. Base-catalyzed HTP was reported for the first time by Breslow et al. [1] to obtain poly-β-alanine from acrylamide. Breslow et al. [1] revealed that base-catalyzed HTP of acrylamide, methacrylamide, crotonamide, and so forth resulted in the corresponding aliphatic polyamides. Then, many scientists reported kinetics [2, 3], mechanism [4–6], and application of base-catalyzed HTP to various acrylamide derivatives [7–11]. Base-catalyzed HTP was not interesting for scientists possibly due to the low degree of polymerization (DP) [2–8], uncontrolled branching [12, 13], sometimes low yield [7, 8], and applicability to limited monomers.

Saegusa et al. [14] reported that base-catalyzed HTP of acrylic acid yielded oligomeric poly(3-hydroxy propionate) which is a biodegradable thermoplastic polyester. Yamada et al. [15] reported that poly(3-hydroxy propionate) with higher molecular weight might be synthesized by HTP of acrylic acid in the presence of crown ether as a cocatalyst. In the study, Yamada et al. [15] fractionated the polymerization products as firstly ether-soluble and ether-insoluble (chloroform soluble) and then ether-insoluble fraction as water-soluble and water-insoluble. Yamada et al. [15] have isolated an insoluble fraction in all organic solvents as a product of HTP for long reaction times and attributed it to vinyl polymerization product (polyacrylic acid). But some points still remained unclear. Rozenberg et al. [3, 16] have recently published many detailed studies on mechanism and kinetics of base-catalyzed HTP of hydroxyethyl (met) acrylate [16] and some acrylamide derivatives [3]. Rozenberg et al. elicited complex mechanism of HTP and well-characterized the structures of the hyperbranched products.

Table 1: Base-catalyzed HTP of acrylic acid at different experimental conditions.

[M] moles	[I] moles	Temperature (°C)	Time (h)	Solvent	$f1$ %	$f2$ %	$f3$ %	$f4$ %
0.1	0.001	60	72	N/A	79.4	20.3	0.3	—
0.1	0.001	100	240	N/A	3.2	13.2	2.1	81.5
0.1	0.001	100	240	Pyridine	1.7	16.0	5.5	76.8
0.1	0.001	60	240	Pyridine	58.6	34.6	0.9	5.9

Our study aims to reveal the structure and swelling properties of insoluble fraction obtained HTP of acrylic acid and to propose possible application field(s). In this study, HTP of acrylic acid was carried out in bulk and solution phase for long reaction times. Chemically distinct fractions of both (bulk and solution) polymerization products were isolated successfully. Insoluble fraction of bulk polymerization product was characterized by using spectroscopic, thermal, and analytical methods. Swelling behavior of the insoluble fraction was investigated at a wide PH range and ionic strength.

2. Materials and Methods

2.1. Polymerization. Anhydrous acrylic acid (99%, Sigma), potassium tert-butoxide (≥99.0%, Aldrich), and anhydrous pyridine (99% Acros Organics) were purchased commercially and used as obtained. Polymerization reactions were tabulated in Table 1. Reaction mixtures in Schlenk flask were stirred under argon atmosphere in dark. Reaction mixture was poured into excess amount of diethyl ether to precipitate out. Ether-soluble fractions (fraction 1) were isolated by evaporation of ether using rotary evaporator. Ether-insoluble white crystals were then treated with chloroform to extract poly(3-hydroxy propionate) (PHP) which is named as fraction 2. Chloroform insoluble part was then filtrated, dried, and treated with methanol to extract polyacrylic acid (fraction 3). Methanol insoluble fraction (fraction 4), which is insoluble in water and all organic solvents tried, was dried at 60°C in vacuum oven.

2.2. Characterization. Polymerization products were characterized using FTIR, ^{1}H-NMR, ^{13}C-NMR, solid ^{13}C-NMR, TGA, and titrimetric method. FTIR spectra of PHP and PAcHP samples were recorded using Shimadzu IRAffinity-1. FTIR data processing was carried out using Shimadzu IRSolution 1.50 provided by Shimadzu Corporation. ^{1}H-NMR and ^{13}C-NMR spectra of PHP in $CDCl_3$ were recorded using 500 MHz Varian NMR spectrometer. Solid ^{13}C-NMR spectra of insoluble products were recorded using Varian Mercury 300. NMR data was processed using MestReNova 6.0.2-5475 software. TGA thermograms of polymer samples were obtained using TA instrument Hi-Res TGA 2950 with 10°C min^{-1} heating rate under nitrogen flux. Insoluble fraction (PAcHP) samples were titrated using standardized 0.05 N NaOH to determine the degree of acrylic acid units in the copolymer samples.

2.3. Swelling Ratios of Hydrogels. Swelling behavior of the hyperbranched PAcHP copolymer obtained from bulk polymerization was investigated in phosphate-buffered saline (PBS) solutions with different pH values (4, 6, 7, 8, 10, and 12). Completely dry, irregular shaped hydrogels were weighed and then immersed in 25 mL of PBS solutions with different pH at room temperature. At a predetermined time point, the hydrogel was removed from the solution and weighed after wiping with a filter paper for the removal of the free solution on the surface. After each weighing, the samples were returned to the containers with refreshed buffer solution. All experiments were performed in triplicate.

Swelling ratios (SRs) of samples were calculated as follows:

$$\mathrm{SR} = \left(W_t - W_d\right) * \frac{100}{W_d}, \tag{1}$$

where W_d is the weight of dry samples and W_t is the weight of wet samples at time t.

Na_2SO_4 solutions with different ionic strengths (0.025, 0.010, 0.25, and 1.000 M) were used to evaluate the salt effect on the swelling of PAcHP hydrogels at room temperature. The same swelling protocol and calculation route were applied as mentioned above.

2.4. Swelling-Deswelling Behavior of the Hydrogels. Swelling-deswelling behavior of the PAcHP hydrogels was examined using pH = 2.0 and pH = 12.0 buffer solutions. Swelling ratios of the hydrogels were determined according to (1) at consecutive time intervals. The experiments were performed in triplicate and the average of results was reported.

3. Results

3.1. Base-Catalyzed Hydrogen Transfer Polymerization of Acrylic Acid. As shown in Table 1, hyperbranched polymer was not formed at the first stage (in a few days) of the polymerization. At this stage, HTP and uncontrolled radical vinyl polymerization occurred. One of the most important results is formation of hyperbranched polymers at elevated temperature and in longer reaction time. This may be due to (i) conversion of living PHP chains to hyperbranched PAcHP through addition of new monomers to the propagating PHP chains as acrylic acid units and then branching and (ii) viscous reaction medium hindering proton transfers to carbanion atom and thus carbanion atom getting involved in anionic vinyl polymerization instead of proton transfer.

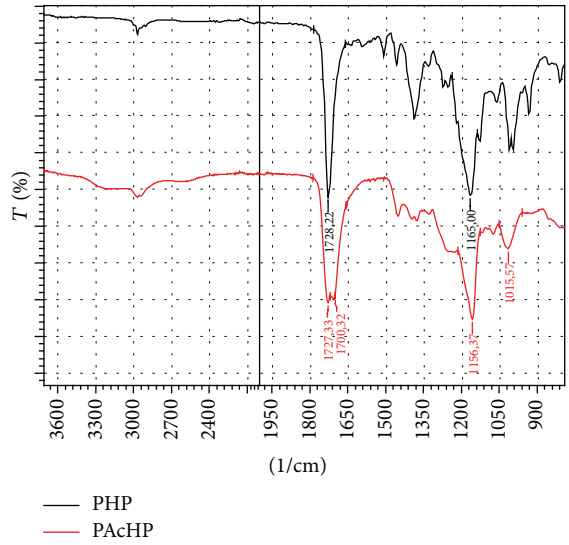

Figure 1: FTIR spectra of PHP (black line, upper) and PAcHP (red line, bottom) obtained from bulk polymerization.

Pyridine, which was the best solvent for HTP of acrylamide [1], exhibited positive effect on formation of PHP (an increment from 13.2% to 16.0%). This may be due to contribution of the basic solvent to the hydrogen transfer from monomers or propagating chain-ends.

3.2. Characterization of Polymerization Products

3.2.1. FTIR Spectroscopy. FTIR spectra of fraction 2 and fraction 4 obtained from bulk polymerization were recorded to understand the differences in functional groups in both fractions 2 and 4. Although spectrum (a) in Figure 1 has only a characteristic ester carbonyl stretching band at about 1728 cm^{-1}, spectrum (b) has two carbonyl stretching bands at about 1727 and 1700 cm^{-1}. The band at about 1700 cm^{-1} may be attributed to acid carbonyl which is commonly seen in the 1690–1720 cm^{-1} range. Furthermore, broad band at asymmetric OH stretching region (3000–3500 cm^{-1}) in spectrum (b) intensifies the existence of carboxylic acid units in fraction 4. This approach may be outlined as follows: fraction 2 is a polyester (PHP) and fraction 4 has both ester units and carboxylic acid units.

3.2.2. NMR Spectroscopy. ^{1}H-NMR spectrum of fraction 2 in Figure 2 was recorded to ensure that it was a linear homopolymer of 3-hydroxypropionate (PHP). Two triplets at 2.9 and 4.6 ppm belong to methylene protons next to the oxygen atom and carbonyl group, respectively. Peak groups at about 6.2 ppm were attributed to the olefinic end-group protons shown in Figure 2. Considering the peak intensities belonging to chain-ends, it may be concluded that fraction 2 consisted of oligomeric PHP.

Since fraction 4 was not soluble in water and all organic solvents tried, solid ^{13}C-NMR spectrum of fraction 4 was recorded and compared to ^{13}C-NMR spectrum of fraction 2

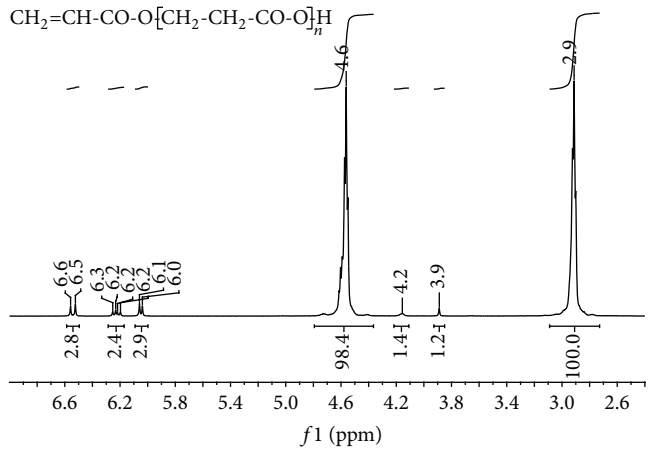

Figure 2: ^{1}H-NMR spectrum of PHP.

(oligomeric PHP) as shown in Figure 3. Considering that the ^{13}C-NMR spectrum of polyacrylic acid [17] reported previously has three peaks for CH_2 (32 ppm), CH (39 ppm), and COOH (184 ppm), ^{13}C-NMR spectrum of fraction 4 may be attributed to combination of acrylic acid and 3-hydroxypropionate units. The peak with low intensity at about 94.5 ppm corresponds to olefinic carbons at chain-ends.

3.2.3. TG Analysis. Figure 4 shows derivative curves of TG thermograms for fraction 2 and fraction 4. Although fraction 2 (PHP) decomposes at temperature interval of 150–275°C through one step, fraction 4 begins to decompose at about 150°C through two steps. First step is completed at about 300°C by a mass loss of 51.9%. Second step takes place at a temperature range of 325–475°C by a mass loss of 31.9%. As easily shown, first step overlaps completely with the decomposition of fraction 2 (PHP).

As is well known, poly(acrylic acid) decomposes through two steps [18]. At the first step, 27.4% of poly(acrylic acid) decomposes at a temperature interval of 142–301°C. At the second step, 55.2% of poly(acrylic acid) decomposes at a temperature interval of 335–425°C. In the light of the literature, at first step in the DTG curve of fraction 4 is related to both complete ester (PHP) units and partial acrylic acid units. Considering the peak areas in the DTG curve, acrylate ratio in fraction 4 may be estimated roughly as 60–65% by a simple calculation.

3.2.4. Titrimetric Analysis. The relative amount of acrylic acid units was determined as 47.3% by titration of fraction 4 samples with standardized NaOH solution. Considering that the result obtained from titration was lower than that of DTG (60–65%), structure of fraction 4 (hyperbranched PAcHP) was proposed as shown in Figure 5. The hyperbranched structure consists of four types of units: (1) acrylic acid units shown by red color, (2) acrylate units as branching points shown by green color, (3) propionate units shown by black color, and (4) propionic acid units at chain-ends shown by

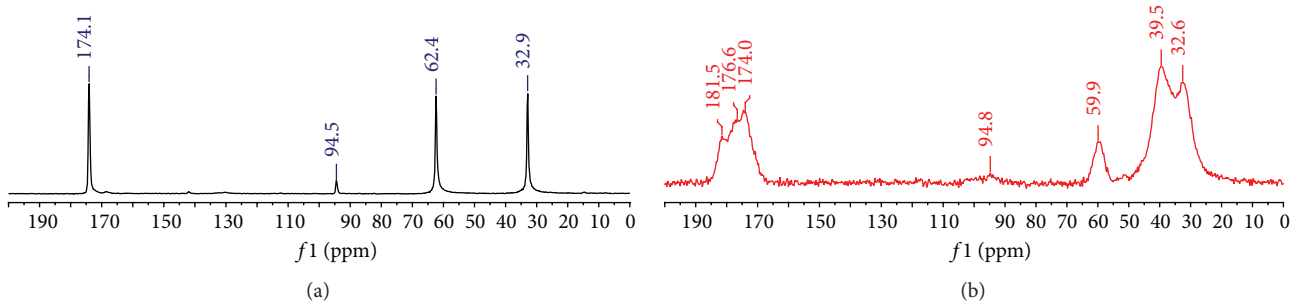

Figure 3: ^{13}C-NMR spectra of (a) PHP and (b) PAcHP obtained from bulk polymerization.

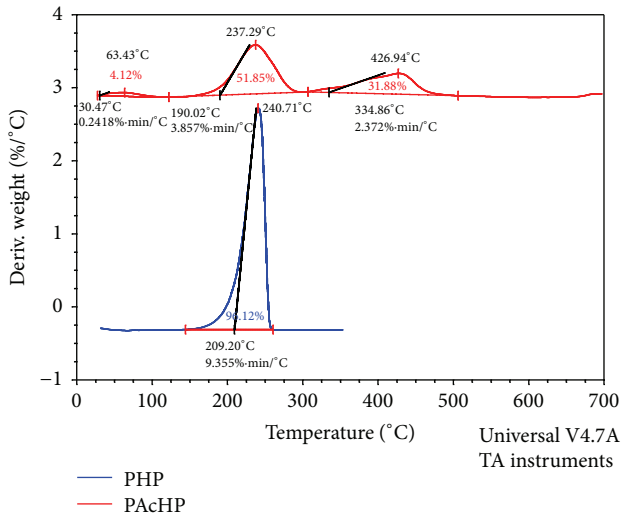

Figure 4: TGA curves of PHP (blue line, bottom) and PAcHP (red line, upper) obtained from bulk polymerization.

blue color. Units 1 and 4 contribute to the result obtained from titration (47.3%) since they contain acidic protons. Similarly, units 1 and 2 contribute to the result obtained from DTG (60–65%).

3.3. Swelling Study of Hyperbranched PAcHP Samples

3.3.1. pH Effect. The swelling behavior of the hyperbranched PAcHP was investigated over a period of 5-6 days in PBS with pH ranging from 4.0 to 12.0 at room temperature. The dynamic swelling profiles of hyperbranched PAcHP exhibited a fast swelling behavior in the first hour and achieved the equilibrium state within 12 h in PBS as shown in Figure 6. The initial fast swelling of hydrogels was due to the osmotic pressure difference. Since the copolymer was composed of acrylic acid groups which can dissociate or get protonated at suitable pH of the swelling media, swelling ratio of the copolymer underwent appreciable change with external pH. At pH of 4.0, a slight swelling capacity of the copolymer was observed due to the protonation of carboxylic groups. The carboxylic groups on the hyperbranched structure were converted to the protonated acid form which resulted in the decreased swelling ratio of the copolymer. As pH exceeded 6.0, some carboxylate groups were ionized and the electrostatic repulsion between the carboxylate groups resulted in an enhancement of the swelling ratio [19]. Moreover, the ionization also causes an increase in ion osmotic pressure. These two factors were thus responsible for a higher degree of swelling in the medium of pH range from 6 to 12.

3.3.2. Ionic Strength Effect. The effect of the ionic strength on the swelling ratios of the hyperbranched copolymer is shown in Figure 7. It shows that an increase in the ionic strength within the range of 0.025–1.000 M yields a significant decrease in the swelling ratio of the copolymer. This is because of the "salting-out" effect, which is a characteristic of the aqueous solutions of many polymers [20]. The addition of salts in polymer aqueous solutions results in a partial dehydration of polymer chains and decreases the hydrophilicity of the polymer chains [21]. Thus, the presence of salt reduces the hydrophilicity and equilibrium swelling ratio of PAcHP hydrogels.

3.3.3. Swelling-Deswelling Behavior. To investigate the time-dependent swelling behavior of PAcHP hydrogels, dynamic swelling studies were performed. The hydrogels were tested in buffer solutions with pH values of 12.0 and 2.0. Figure 8 presents the swelling ratios of hydrogels in buffer solutions with pH values of 12.0 and 2.0 at ambient temperature as a function of time. The reversible swelling-deswelling behavior of the hydrogel was observed. At pH 12.0, the hydrogel swells within 150 minutes up to 2700% due to anion-anion repulsive electrostatic forces, while at pH 2.0 it shrinks within 90 minutes due to protonation of the carboxylate groups. This pH-dependent reversible swelling behavior (on-off switching behavior) of the hydrogel makes it possible candidate for controlled drug delivery systems.

4. Discussion

HTP of acrylic acid at elevated temperature and in longer reaction times yields an insoluble product. The study revealed that the product has hyperbranched structure composed of hydrophobic ester (3-hydroxy propionate) and hydrophilic acid (acrylic acid) units. PHP is known to be easily biodegradable [22, 23] and poly(acrylic acid) is one of the most popular components used for controlled drug delivery [24–26] and

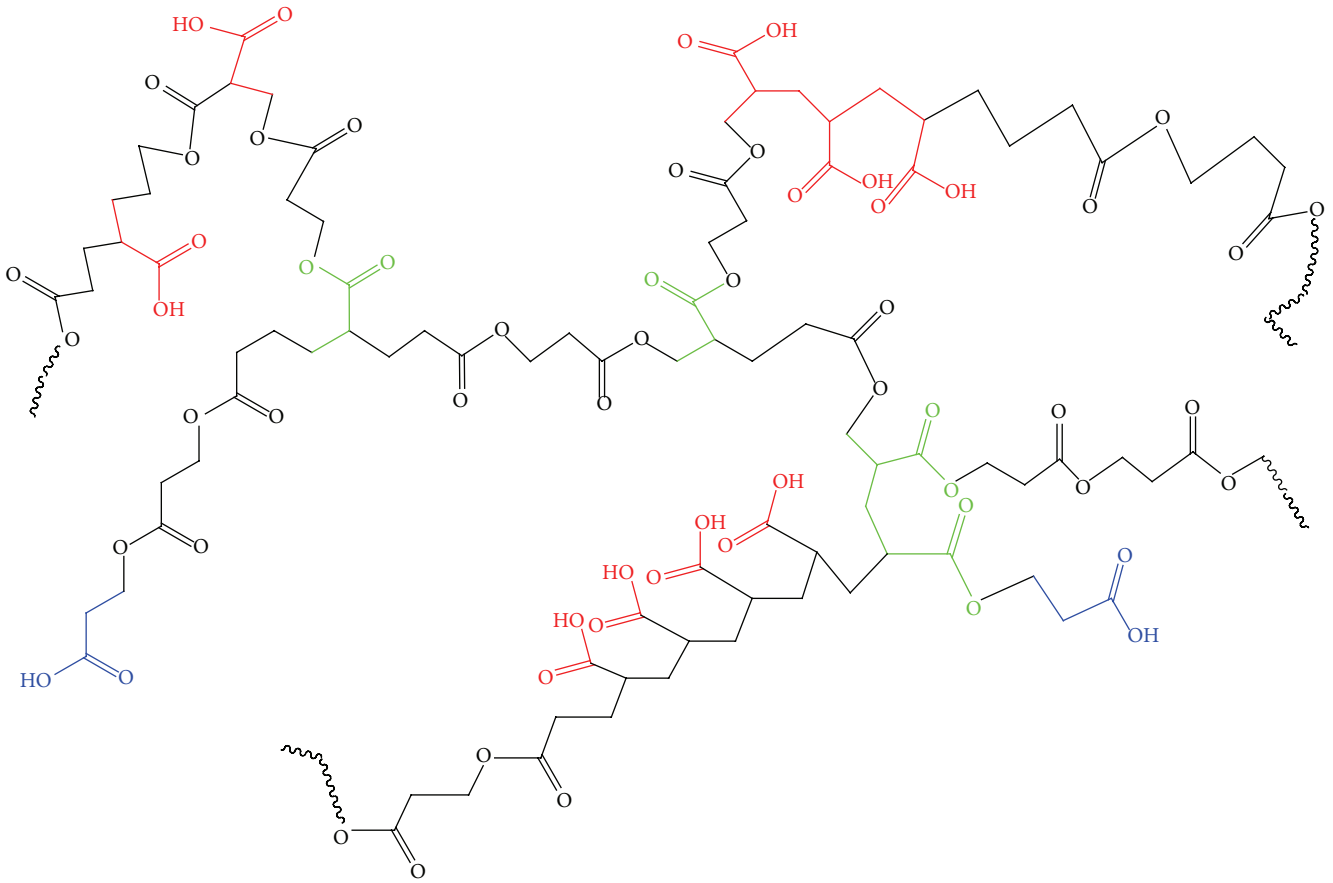

Figure 5: Chemical structure of hyperbranched PAcHP.

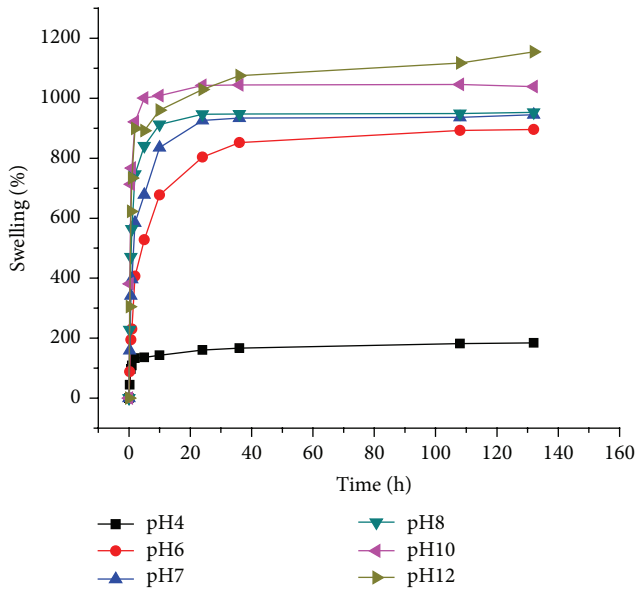

Figure 6: Time dependence of swelling ratio for hyperbranched PAcHP obtained from bulk polymerization at a wide range of pH.

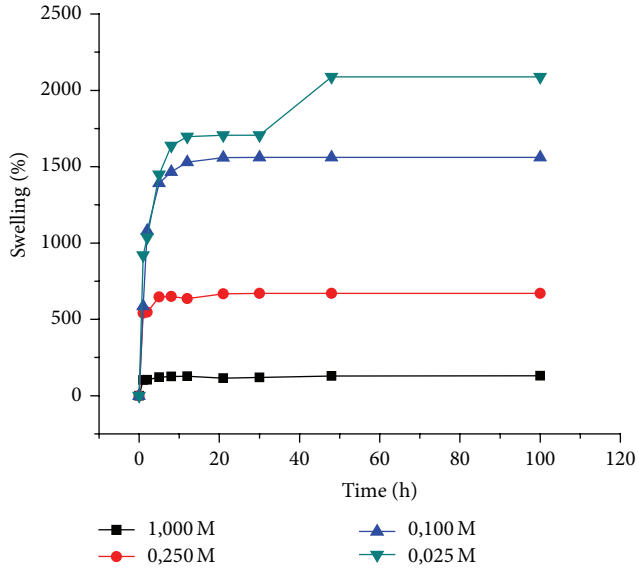

Figure 7: Time dependence of swelling ratio for hyperbranched PAcHP obtained from bulk polymerization (ionic strength).

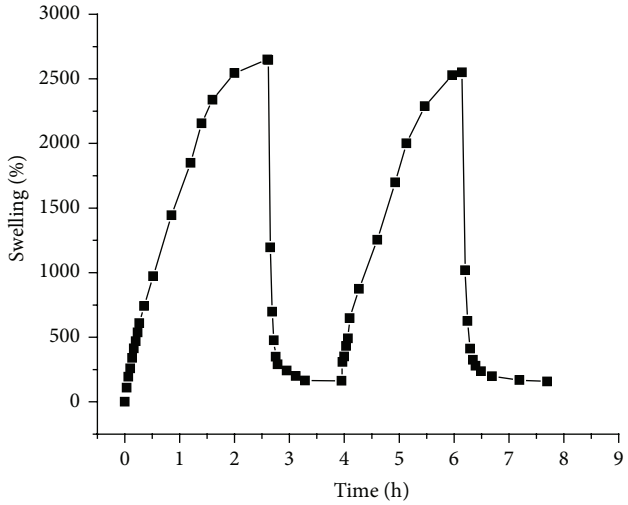

Figure 8: Dynamic swelling (pH 12.0)/deswelling (pH 2.0) behavior of PAcHP hydrogels obtained from bulk polymerization.

tissue scaffolding [24]. Our study shows that hyperbranched PAcHP exhibits hydrogel properties and hence may be considered biodegradable polymer matrix for drug delivery and (or) hydrogel scaffold for tissue engineering applications.

Conflict of Interests

The authors declare that there is no conflict of interests regarding the publication of this paper.

References

[1] D. S. Breslow, G. E. Hulse, and A. S. Matlack, "Synthesis of poly-β-alanine from acrylamide. A novel synthesis of β-alanine," *Journal of the American Chemical Society*, vol. 79, no. 14, pp. 3760–3763, 1957.

[2] H. Nakayama, T. Higashimura, and S. Okamura, "Base-catalyzed polymerization of vinyl acetamide and allyl cyanide," *Journal of Macromolecular Science Part A—Chemistry*, vol. 2, no. 1, pp. 53–68, 1968.

[3] L. L. Gur'eva, A. I. Tkachuk, E. A. Dzhavadyan et al., "Kinetics and mechanism of the anionic polymerization of acrylamide monomers," *Polymer Science—Series A*, vol. 49, no. 9, pp. 987–999, 2007.

[4] L. Trossarelli, M. Guaita, and G. Camino, "Research on the mechanism of base-catalyzed hydrogen-transfer polymerization," *Journal of Polymer Science Part C: Polymer Symposia*, vol. 22, no. 2, pp. 721–727, 1969.

[5] H. Tani, N. Oguni, and T. Araki, "Initiation reaction in the strong base catalyzed polymerization of acrylamide," *Macromolecular Chemistry and Physics*, vol. 76, no. 1, pp. 82–88, 1969.

[6] G. Camino, M. Guaita, and L. Trossarelli, "Chain growth in the base catalyzed hydrogen transfer polymerization of acrylamide to poly-β-alanine," *Macromolecular Chemistry and Physics*, vol. 136, no. 1, pp. 155–159, 1970.

[7] K. Yokota, M. Shimizu, Y. Yamashita, and Y. Ishii, "Hydrogen migration polymerization of N-substituted acrylamides," *Die Makromolekulare Chemie*, vol. 77, no. 1, pp. 1–6, 1963.

[8] Y. Iwakura, N. Nakabayashi, K. Sagara, and Y. Ichikura, "Hydrogen-transfer polymerization of Cinnamide," *Journal of Polymer Science Part A-1: Polymer Chemistry*, vol. 5, no. 3, pp. 675–676, 1967.

[9] T. Iwamura, I. Tomita, M. Suzuki, and T. Endo, "Hydrogen-transfer polymerization of vinyl monomers derived from p-tolyl isocyanate and acrylamide derivatives," *Reactive & Functional Polymers*, vol. 40, no. 2, pp. 115–122, 1999.

[10] T. Iwamura, I. Tomita, M. Suzuki, and T. Endo, "Hydrogen-transfer polymerization behavior of N-acylacrylamide," *Journal of Polymer Science Part A: Polymer Chemistry*, vol. 38, no. 3, pp. 430–435, 2000.

[11] T. Iwamura, I. Tomita, M. Suzuki, and T. Endo, "Novel hydrogen-transfer polymerization of vinyl monomer derived from p-toluenesulfonyl isocyanate and acrylamide," *Journal of Polymer Science. Part A. Polymer Chemistry*, vol. 36, no. 9, pp. 1491–1494, 1998.

[12] Y. Iwakura, F. Toda, Y. Torii, and R. Sedii, "Base-catalyzed polymerization of acryloyl-and methacryloyl-alpha-amino acid amides," *Journal of Polymer Science. Part A-1, Polymer Chemistry*, vol. 5, no. 7, pp. 1585–1597, 1967.

[13] J. D. Glickson and J. Applequist, "Chain branching in poly-β-alanine," *Macromolecules*, vol. 2, no. 6, pp. 628–634, 1969.

[14] T. Saegusa, S. Kobayashi, and Y. Kimura, "Hydrogen-transfer polymerization of acrylic acid to poly(β-propiolactone)," *Macromolecules*, vol. 7, no. 2, pp. 256–258, 1974.

[15] B. Yamada, Y. Yasuda, T. Matsushita, and T. Otsu, "Preparation of polyester from acrylic acid in the presence of crown ether," *Journal of Polymer Science: Polymer Letters Edition*, vol. 14, no. 5, pp. 277–281, 1976.

[16] B. A. Rozenberg, Y. I. Estrin, and G. A. Estrina, "Reactions of functional end group redistribution over macromolecules and their characterization by liquid chromatography under

critical conditions," *International Journal of Polymer Analysis and Characterization*, vol. 9, no. 4, pp. 197–212, 2004.

[17] A. S. Vasilescu and C. C. Ponta, "A ^{13}C-NMR study of polyacrylic acid gels as radioactive ion sorbents," *Progress in Colloid & Polymer Science*, vol. 102, pp. 98–100, 1996.

[18] S. Dubinsky, G. S. Grader, G. E. Shter, and M. S. Silverstein, "Thermal degradation of poly(acrylic acid) containing copper nitrate," *Polymer Degradation and Stability*, vol. 86, no. 1, pp. 171–178, 2004.

[19] H. K. Ju, S. Y. Kim, and Y. M. Lee, "pH/temperature-responsive behaviors of semi-IPN and comb-type graft hydrogels composed of alginate and poly(N-isopropylacrylamide)," *Polymer*, vol. 42, no. 16, pp. 6851–6857, 2001.

[20] T. G. Park and A. S. Hoffman, "Sodium chloride-induced phase transition in nonionic poly(N-isopropylacrylamide) gel," *Macromolecules*, vol. 26, no. 19, pp. 5045–5048, 1993.

[21] J. Wang and M. Satoh, "Novel PVA-based polymers showing an anti-Hofmeister series property," *Polymer*, vol. 50, no. 15, pp. 3680–3685, 2009.

[22] Y. Furuhashi, T. Iwata, Y. Kimura, and Y. Doi, "Structural characterization and enzymatic degradation of α-, β-, and γ-crystalline forms for poly (β-propiolactone)," *Macromolecular Bioscience*, vol. 3, no. 9, pp. 462–470, 2003.

[23] M. S. Cortizo, M. S. Molinuevo, and A. M. Cortizo, "Biocompatibility and biodegradation of polyester and polyfumarate based-scaffolds for bone tissue engineering," *Journal of Tissue Engineering and Regenerative Medicine*, vol. 2, no. 1, pp. 33–42, 2008.

[24] M. Larsson, A. Bergstrand, L. Mesiah, C. Van Vooren, and A. Larsson, "Nanocomposites of polyacrylic acid nanogels and biodegradable polyhydroxybutyrate for bone regeneration and drug delivery," *Journal of Nanomaterials*, vol. 2014, Article ID 371307, 9 pages, 2014.

[25] S. M. H. Bukhari, S. Khan, M. Rehanullah, and N. M. Ranjha, "Synthesis and characterization of chemically cross-linked acrylic acid/gelatin hydrogels: effect of pH and composition on swelling and drug release," *International Journal of Polymer Science*, vol. 2015, Article ID 187961, 15 pages, 2015.

[26] Y. Chen, Y. Qi, and B. Liu, "Polyacrylic acid functionalized nanographene as a nanocarrier for loading and controlled release of doxorubicin hydrochloride," *Journal of Nanomaterials*, vol. 2013, Article ID 345738, 8 pages, 2013.